UNIVERSIDAD DE CHILE
FACULTAD DE CIENCIAS FÍSICAS Y MATEMÁTICAS
ESCUELA DE POSTGRADO

Sedimentation of polydisperse particles at low Reynolds numbers in inclined geometries

Numerical and laboratory experiments

TESIS PARA OPTAR AL GRADO DE DOCTOR EN CIENCIAS DE LA INGENIERÍA
MENCIÓN FLUIDODINÁMICA

Sergio Andrés Palma Moya

PROFESOR GUÍA:
Dr. Christian Ihle Bascuñan

MIEMBROS DE LA COMISIÓN:
Dr. Aldo Tamburrino Tavantzis
Dr. Stuart Bruce Dalziel
Dr. Rodrigo Soto Bertrán
Dr. Francisco Santibañez Calderón

Esta tesis ha sido parcialmente financiada por CONICYT
Beca de Doctorado Nacional N° 21110766

SANTIAGO DE CHILE
2016

Abstract

RESUMEN DE TESIS
PARA OPTAR AL GRADO DE DOCTOR EN
CIENCIAS DE LA INGENIERÍA
MENCIÓN FLUIDODINÁMICA
POR: SERGIO PALMA M.
PROF. GUÍA: CHRISTIAN IHLE B.

Sedimentation of polydisperse particles at low Reynolds numbers in inclined geometries Numerical and laboratory experiments

Hydraulic transport of particles at high concentrations in the industry is a widely used technique to deliver different sorts of granular materials by carrying them mixed with fluid, water in most cases. In the first chapter of this thesis, we will discuss the most important aspects of the dynamics of suspensions. In particular, we will explain the physics of dilute suspensions, semi dilute suspensions and concentrated suspensions. Additionally, a review of sedimentation of particles will be presented. Sedimentation is a process by which solid particles are separated from a fluid, usually under the action of gravitational forces. Sedimentation is one of the oldest known techniques used in industry to clean fluids or, alternatively, to recover particles. In the second chapter, we will show the results of a numerical-experimental work of sedimentation of quasi-monodisperse particles. A series of sedimentation experiments and numerical simulations have been conducted to understand the factors that control the final angle of a static sediment layer formed by quasi-monodisperse particles settling in an inclined container. The set of experiments includes several combinations of fluid viscosity, container angle and solids concentration. A comparison between the experiments and a set of two-dimensional numerical simulations shows that the physical mechanism responsible for the energy dissipation in the system are the collisions between the particles. The present results provide new insights into the mechanism that sets the morphology of the sediment layer formed by the settling of quasi-monodisperse particles onto the bottom of an inclined container. Tracking the interface between the suspension solids and the clear fluid zone reveals that the final angle adopted by the sediment layer shows strong dependencies on the initial particle concentration and the container inclination, but not the fluid viscosity within the small particle Reynolds number range tested. It is concluded that (1) the hindrance function plays an important role on the sediment bed angle, (2) the relation between the friction effect and the slope may be explained as quasi linear function of the projected velocity along the container bottom, and (3) prior to the end of settling there is a significant interparticle interaction through the fluid affecting to the final bed organization. We can express the sediment bed slope as a function of two dimensionless numbers, a version of the inertial number and the particle concentration. The present experiments confirm some previous results on the role of the interstitial fluid on low Stokes number flows of particulate matter. Finally, we will show the results of a numerical work. Here, we have used a continuum mixture model to solve numerically the momentum and continuity equations associated with the sedimentation dynamics of highly concentrated fluid-solid mixtures in tilted duct at low Reynolds numbers. The set of numerical simulations included several combinations of fluid viscosity, duct angle and solid concentration of particles. This research aims to show the phenomenology and dynamics associated with the sedimentation of monodisperse particles under different physical conditions and the characterization of the final stage of the sediment layer in two kinds of inclined geometries, with and without a horizontal section. Using scaling arguments, a mathematical expression formed by three dimensionless groups including the inertial number, particle concentration and the ratio between the sedimentation Grashof number to the Reynolds number is proposed to explain the height of the sediment layer in the slope change zone of a duct. Additionally, we have found that the initial particle concentration is a very relevant variable for knowing under what conditions the duct could get obstructed. In combination with some system angles, they might represent a risk of duct plug. Imposing a condition of obstruction, we have found dimensionless parameters that result in the blockage of the duct in the slope change zone. . The main results of the thesis were submitted in two scientific articles, the first one published in the Journal Physics of Fluids, and the second has been submitted to the International Journal of Multiphase Flow.

Resumen

RESUMEN DE TESIS
PARA OPTAR AL GRADO DE DOCTOR EN
CIENCIAS DE LA INGENIERÍA
MENCIÓN FLUIDODINÁMICA
POR: SERGIO PALMA M.
PROF. GUÍA: CHRISTIAN IHLE B.

Sedimentación de partículas polidispersas a bajos números de Reynolds en geometrías inclinadas Experimentos numéricos y de laboratorio

El transporte hidráulico de partículas a altas concentraciones es una tecnología ampliamente utilizada en la industria para transportar diferentes tipos de materiales granulares mediante la mezcla con fluidos, agua en la mayoría de los casos. En el primer capítulo de esta tesis, vamos a discutir los aspectos más importantes de la dinámica de las suspensiones. En particular, vamos a explicar la física de las suspensiones diluidas, suspensiones semi-diluidas y suspensiones concentradas. Adicionalmente, una revisión de la sedimentación de partículas será mostrada. La sedimentación es un proceso por el cual las partículas sólidas se separan de un líquido, generalmente bajo la acción de fuerzas gravitacionales. La sedimentación es una de las técnicas más antiguas conocidas utilizadas en la industria para limpiar fluidos o, alternativamente, para recuperar partículas. En el segundo capítulo, vamos a mostrar los resultados de un trabajo numérico experimental de sedimentación de partículas ligeramente polidispersas. Una serie de simulaciones numéricas y experimentos de sedimentación se han realizado para comprender los factores que controlan el ángulo final de una capa de sedimento estática formada por partículas cuasi-monodispersas que sedimentan en un contenedor inclinado. El conjunto de experimentos incluye varias combinaciones de la viscosidad del fluido, ángulo del contenedor y concentración de sólidos. Una comparación entre los experimentos y un conjunto de simulaciones numéricas en dos dimensiones muestra que el mecanismo físico responsable de la disipación de energía en el sistema son las colisiones entre las partículas. Los resultados proporcionan nuevos conocimientos sobre el mecanismo que establece la morfología de la capa de sedimento formada por la sedimentación de las partículas en el fondo de un contenedor inclinado. El seguimiento de la interfaz entre los sólidos de la suspensión y la zona clara de fluido revela que el ángulo final adoptada por la capa de sedimento muestra fuertes dependencias de la concentración inicial de partículas y la inclinación del recipiente, pero no la viscosidad del fluido dentro de un rago de números de Reynolds de partículas pequeños. Se concluye que (1) la función de escondimiento juega un papel importante en el ángulo de la capa de sedimentos, (2) la relación entre el efecto de fricción y la pendiente puede ser explicado como una función casi lineal de la velocidad proyectada a lo largo del fondo del contenedor, y (3) antes de la finalización de la sedimentación hay una interacción entre partículas significativa a través del fluido que afecta a la organización de la capa final. Podemos expresar la pendiente del lecho de sedimentos como una funci|ón de dos números adimensionales, una versión del número inercial y la concentración de partículas. Los presentes experimentos confirman algunos resultados anteriores sobre el papel del fluido intersticial en los flujos a bajos número de Stokes de partículas. Por último, vamos a mostrar los resultados de un trabajo numérico. Aquí, hemos utilizado un modelo de mezcla continuo para resolver numéricamente las ecuaciones de momento y continuidad asociadas con la dinámica de sedimentación de mezclas de líquido y sólido altamente concentradas en un conducto inclinado a bajos números de Reynolds. El conjunto de simulaciones numéricas incluye varias combinaciones de la viscosidad del fluido, ángulo de conducto y concentración de partículas. Esta investigación tiene como objetivo mostrar la fenomenología y dinámica asociada a la sedimentación de partículas monodispersas bajo diferentes condiciones físicas y la caracterización de la etapa final de la capa de sedimento en dos tipos de geometrías inclinadas, con y sin una sección horizontal. Usando argumentos de escala, una expresión matemática formada por tres grupos adimensionales, incluyendo el número inercial, la concentración de partículas y la relación entre el número de sedimentación Grashof para el número de Reynolds se propone para explicar la altura de la capa de sedimento en la zona de cambio de pendiente de un conducto. Además, encontramos que la concentración inicial es una variable muy importante para saber bajo qué condiciones el conducto podría obstruirse.Los principales resultados de esta tesis se presentaron como dos artículos científicos, el primero publicado en el Journal Physics of Fluids, y el segundo trabajo bajo revisión en el International Journal of Multiphase Flow.

A mi familia

Alicia, Sergio y Javiera

Thinking is easy, acting is difficult, and to put one's thoughts into action is the most difficult thing in the world.

Johann Wolfgang von Goethe

Learn from yesterday, live for today, hope for tomorrow. The important thing is not to stop questioning.

Albert Einstein

Acknowledgment

Firstly, I would like to thank to my supervisors Dr. Christian Ihle and Dr. Aldo Tamburrino for the opportunity of doing this PhD in their group. Although I did not want to do more experiments in my life, working in experimental fluid dynamics has been an amazing experience (and sometimes frustrating), but quite interesting and rewarding. Thanks very much for your patience and support during this PhD. I am also very grateful for the collaboration with Dr. Stuart Dalziel of The University of Cambridge for accepting me in his group. Doing experiments and numerical simulations in the G.K. Batchelor Laboratory at the Department of Applied Mathematics and Theoretical Physics has been a very rewarding and motivating experience from a personal and professional point of view.

I would like to thank the support of the National Commission for Scientific and Technological Research of Chile, CONICYT, Grant N° 21110766, Fondecyt Projects N° 11110201 and N° 1130910, the Department of Civil Engineering, the Department of Mining Engineering and the Advanced Mining Technology Center of the University of Chile, as well the staff of the G.K. Batchelor Laboratory.

I want to thank my friends Hugo Ulloa, Juvenal Letelier, Tomas Trewhela, Javier Osorio, Jocelyn Dunstan, Jorge Casanova, Francisca Guzman, Jaime Cotroneo, Gonzalo Montserrat, Sergio Mercado, Francisca Coddou, Asieh Hekmat and Adeline Delonca. You guys have been a very essential part of my life during this very long (and unending!) process in Cambridge and Santiago. It has been great for me to share so many good moments with you. Finally, I would like to thank to my dear family **Alicia**, **Sergio** and **Javiera** who gave me all the support that I needed to successfully complete this PhD thesis. I love you.

Main objective

The main objective of this PhD thesis is to study the sedimentation of mono and bi-disperse particles under different physical conditions and the characterization of the final stage of a sediment layer in open and closed inclined geometries.

Specific objectives

- To design, build and operate an experimental set-up to study the process of sedimentation of particles in open and closed inclined geometries.

- To implement the optical light transmission technique for tracking the interface between the particle suspension and the clear fluid zone.

- To implement and solve a continuum mixture model in COMSOL Multiphysics with the CFD package to investigate particle sedimentation processes.

- To employ the dimensional analysis theory to characterize the slope of a sediment layer in tilted containers and, the height of the sediment layer of inclined ducts.

Table of Contents

List of Figures

List of Tables

Chapter 1

An introduction to suspension dynamics

1.1 Introduction

The suspensions of solid particles in a viscous fluid are very common in all areas of daily life, from biological systems, such as blood, household cleaning products, paints and industrial processes such as the transport of concentrates ores and the concentrates of organic waste, as well as chemical pharmaceutical processes, among many others, Figure 1.1.1, (Davis & Acrivos, 1985; Guazzelli & Hinch, 2011). Suspensions are a class of fluids, called complex fluids, which can be differentiated according to the physical and chemical nature of the solid particles in suspension. In most investigations related to suspensions, it is considered that the particles do not agglomerate, they are chemically stable and solid particles in the fluid, which can be either Newtonian or non-Newtonian. In general, the solid particles are considered spherical because of the simplicity to model the phenomenon from a mathematical point of view. The research for the dynamics of suspensions is relatively recent, being of particular interest the dense or highly concentrated suspensions, for applications within the chemical industry, mining and oil.

When we speak of suspensions and the focus is on length scales of the order of a particle, the mechanics of these physical systems is controlled by the Navier-Stokes equations. Although it is possible to search theoretical solutions of these equations for each of the particles, however, due to the complicated nature of the phenomenon, there are numerous interactions between many particles simultaneously and between the particles and the fluid; and thus the mathematics becomes extraordinarily complicated, even at small particle volume fractions. For much larger scales, sizes of 100 particles radii, it is more appropriate to consider the suspension as a fluid, i.e., as a continuous medium (Duran, 2012; Guazzelli & Morris, 2012). The mechanics for the suspension of low concentrations (diluted) was studied in detail by Einstein (1906) and intermediate concentrations (semi-dilute) in the work of Batchelor (1977, 1970) and Batchelor & Green (1972b,a). However, due to the complexity of the problem there are no known constitutive relations between the stress and strain rate for highly concentrated suspensions, or hyper concentrated, and therefore the rheology is equally little understood, which accordingly means it is an area with considerable projection research (Shapley *et al.* , 2004).

Experiments of suspensions in complex fluids in the last two decades have revealed very interesting findings. These include: shear-thinning, thixotropy, shear-thickening, rheopexy and yield stresses (Barnes *et al.* , 1989; Barnes, 2000; Tanner, 2000), which are detailed below. Shear-thinning is a term used to describe rheology suspensions for the non-Newtonian fluids that suffer a decrease in viscosity when the fluid is subjected to shear stress. Many authors believe that it is a synonym of pseudo

plastic behaviour. Furthermore, thixotropy is a special case of shear-thinning, which features the time dependence. On the other hand, shear-thickening is a term used to explain the fluids which increase their viscosity with an increasing strain rate. Additionally, rheopexy is a property of non-Newtonian fluids, showing an increase in viscosity as time passes. Finally, yield stress is the stress level at which a material ceases to behave elastically. Many experiments in recent decades have focused on studying the viscosity of fluids with a high concentration of particles, however, the complexity of their physics has prevented the unification of a single theoretical model for description. It is not only experiments that have played an important role in the study of suspensions but the development of ever-faster computers and better numerical techniques that have contributed greatly to the understanding of the rheology and physical suspension (Prosperetti & Tryggvason, 2009; Yeoh & Tu, 2009).

From the perspective of numerical simulations, it is possible to find in literature diverse mathematical models to represent the behaviour of particles, fluids, and mixing between particles and fluids (suspensions); which have advantages and disadvantages. In the case of dry granular media, the most used techniques at present are molecular dynamics, event-driven molecular dynamics, direct simulation Monte Carlo and Rigid-body dynamics. A detailed review of each of these models can be found in the books written by Poschel & Schwager (2005) and Thornton (2015). These models are known to be computationally very expensive, because for each time step, the model requires calculating the interaction forces between particles. On the other hand, the most commonly used technique for simulating suspensions at low Reynolds numbers and a wide range of Peclet numbers, is the Stokesian dynamics (Brady & Bossis, 1988; Sierou & Brady, 2002). In the Stokesian dynamics the equations modeling Stokes flow are simultaneously solved at discrete time steps for all the particles (Sierou & Brady, 2002).

1.2 Sedimentation in vertical containers

Sedimentation is the process by which solid particles immersed in a fluid are deposited on the bottom of a container by the action of gravity. The sedimentation process is frequently used in the chemical and pharmaceutical industry, in the mining and oil industries as well as the wastewater and treatment plants. This physical mechanism has been widely used for separating solids from fluids (Burger *et al.* , 2011). Due to the importance of sedimentation in several areas of engineering, extensive research has been conducted as much experimental and theoretical-numerical in recent decades. One of the early works was that of Stokes, who studied the motion of a rigid spherical particle immersed in a Newtonian fluid by gravity, albeit descending by a very low Reynolds number. Stokes proposed the following equation (see Lamb (1932) and references therein),

$$u_{\mathrm{st}} = \frac{2a^2(\rho_s - \rho_f)g}{9\eta}, \tag{1.2.1}$$

where u_{st} is the sedimentation velocity of the particle, a is the particle radius, ρ_s is the particle density and ρ_f is the fluid density, η is the viscosity of the fluid and g is the acceleration of gravity. Since the work of Stokes, investigations have focused on studying the generalization of Stokes' law considering particles for different sizes, different shapes (spherical and non-spherical), drops and bubbles, in

Figure 1.1.1: Different types of granular media. The first and second rows show different types of granular materials in nature and engineering and, the last row shows the application of some suspensions (mixture of granular material and fluid) in engineering, copper concentrates and mine waste transport (Nedderman, 2005; Burger *et al.* , 2011; Duran, 2012).

Newtonian fluids and non-Newtonian. In the 70s, Batchelor (1974) investigated the transportation properties of two-phase materials, as well as sedimentation of particles at low concentrations in viscous fluids. Leal (1980) found that the Brownian mechanics is only relevant for sufficiently small particles in the sedimentation process due to gravity, but there will be occasions when these statistical effects are very important. Subsequently, the stability and coagulation of suspensions under shear flows was study by Schowalter (1984). In particular, he studied the Van der Waals forces and forces of electrical attraction.

Most of the investigations carried out consider a suspension consisting of rigid spherical particles of the same shape and size, immersed in a Newtonian fluid and very small particle Reynolds numbers, corresponding to the range of Stokes, $Re \ll 1$. Furthermore, it is assumed that the particle suspension is stable, i.e., that Brownian motion of particles and attractive forces such as Van der Waals are very small, so that the particles do not clump with each other. A suspension of particles immersed in a fluid housed in a container, which is initially homogeneously mixed, is generally divided into three regions when the settling process begins. A clear fluid layer will form on the top of the container and its thickness increases with time, as the particles begin to accumulate in the bottom of the container. Therein, under this layer is the suspension area and the sediment layer.

This area is characterized by the containment by all zero speed particles that were initially suspended. If the particle suspension is diluted, i.e., it has a very low concentration of particles, the particles sediment at the speed defined by Stokes using equation (1.2.1). We can be generalize the sedimentation velocity for many particles. This can be done by multiplying the speed by a function of Stokes concealment that depends on particle concentration $f(\phi)$ (Davis & Acrivos, 1985). This function models the interaction of particles in a fluid medium. Thus, the velocity of sedimentation for the suspension, is commonly written as $u = u_{\text{st}} f(\phi)$. The function $f(\phi)$ depends only on the particle concentration and is a decreasing monotonously function that has a maximum at $f(0)$ and a minimum in $f(1)$. However, it only makes physical sense for the maximum value of particle packing, $f(\phi_{max} = 0.62)$. In general, this correction to Stokes' law works very well when the suspensions are non-colloidal. For colloidal suspensions, the function will depend on the concentration and interactions between particles, $f(\phi, F)$. Here, F is a function that describes interactions between particles (Davis & Acrivos, 1985). As mentioned above, the third region corresponds to a layer of sediment that is formed on the bottom of the container. This region is assumed that the concentration of particles is both a constant (only present in non-cohesive media) and maximum value of particle packing, which is about 0.60. The latter area is also called the thickening layer. Dixon (1979), who worked with mathematical thickening models, found that the rate of sedimentation and the compaction of particles in the background depended on the concentration of particles in the sediment layer, the gradient concentration of the forces between particles and the depth of the sediment layer. There are discontinuities of the particle concentration along the three regions; these occur in the interfaces between certain areas: the layer of sediment-suspension between the suspension and the fluid layer-clear. The first theory that described discontinuities between areas was obtained by Kynch (1952). It is imperative to find a function $f(\phi)$ allowing us to correctly model the interaction between many particles in a sedimentation process in order to obtain a correct physical understanding of the phenomenon. During last century, several models of $f(\phi)$ have been proposed. We summarize below the most widely used models. Steinour (1944) proposed an empirical equation,

$$f(\phi) = (1 - \phi)\exp(-4.19\phi). \tag{1.2.2}$$

Some years after, Hawksley (1951) published a model slightly different,

$$f(\phi) = (1 - \phi)\exp\left(\frac{-2.5\phi}{1 - 0.609\phi}\right). \tag{1.2.3}$$

Three years later, Richardson & Zaki (1954a) published a model widely used in physics and engineering. Here, this equation is valid for low Reynolds numbers.

$$f(\phi) = (1 - \phi)^{4.65}. \tag{1.2.4}$$

On the other hand, Oliver (1961) proposed another empirical model. However, this model has some limitations for high concentration values, as can be seen in Figure 1.2.1,

$$f(\phi) = \frac{1}{(1-\phi)}\left[(1-2.15\phi)(1-0.75\phi^{1/3})\right]. \tag{1.2.5}$$

In the 70s, Barnea & Mizrahi (1973) proposed the following exponential model,

$$f(\phi) = \frac{(1-\phi)}{(1+\phi^{1/3})\exp\left(\frac{5\phi}{3(1-\phi)}\right)}. \tag{1.2.6}$$

Figure 1.2.1 shows these models. Here, we can see that the behaviour is very different at low particle concentrations. The models presented above are empirical. Ideally, it would be appropriate to have models that come from the first principles of physics. Here, we present some of the work done by this approach. One approach is the cell model, which involves solving the equations of the fluid and the suspension within an imaginary cell (Prosperetti & Tryggvason, 2009). The relationship between cell volume and the particle volume is set equal to the concentration of particles in suspension. Once calculated $f(\phi) \sim 1 - \alpha\phi^{1/3}$, the value of the constant α depends on the appropriate choice of the cell and the conditions around it. This model gives acceptable results although not very reliable. Therefore,

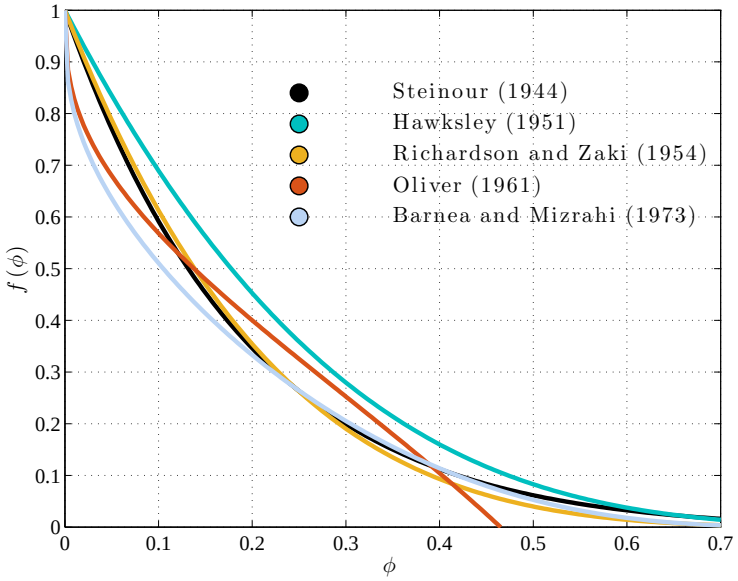

Figure 1.2.1: Different hindered functions proposed by Steinour (1944); Hawksley (1951); Richardson & Zaki (1954a); Oliver (1961); Barnea & Mizrahi (1973).

we need to calculate $f(\phi)$ through a more accurate mathematical analysis in the sedimentation problem for various particles. Unfortunately, due to the complexity of the physical problem as well as from a mathematical point of view, the analysis has been carried out for systems with low concentrations of particles and therefore its applicability in engineering sciences is limited.

When the particle concentration is very high, the analysis is complicated, because in most cases, the integrals obtained from the calculations diverge. To solve this kind of mathematical problem, various techniques have been used. Batchelor (1972) first introduced normalization techniques for

analysis of sedimentation in a statistically homogeneous and diluted suspension. Subsequently other authors have worked on mathematical techniques for the study of sedimentation (Jeffrey, 1974; O'Brien, 1979; Batchelor, 1974). Additionally, Hinch (1977) who proposed a set of differential equations describing the behaviour for the two-phase macroscopic homogeneous materials and showed that parameters such as the sedimentation rate could be calculated iteratively. In the 80s, Feuillebois (1984) investigated the sedimentation for monodisperse spheres in a dilute suspension, which is homogeneous in the horizontal axis but having a different concentration profile in the vertical axis. In dilute systems, the origin of the function $f(\phi)$ depends on the configuration of the particles. Saffman (1973) discussed this topic and he considered three possibilities: (a) regular periodicity matrix particle, (b) fixed periodicity matrices (c) random matrix periodicity. In a regular array, strength and speed are the same for each particle (Sangani & Acrivos, 1982), $f(\phi) \sim 1 - \beta\phi^{1/3} + O(\phi)$, where β is a constant depending on the chosen configuration, $\beta = 1.76$. Regarding (b), Hinch (1977) proposed an expression described by

$$f(\phi) \sim 1 - \frac{3}{\sqrt{2}}\phi^{1/2} - \frac{135}{64}\phi \ln \phi - 12\phi + ... \tag{1.2.7}$$

The vast majority of the work, both experimental and theoretical, sedimentation has focused on monodisperse suspensions. The problem is that most practical cases are related to engineering processes of polydisperse particle sedimentation, whereas, due to the distribution of sizes and shapes, the particles move at different speeds. In general, the discussion is restricted for suspensions with rigid spherical particles and small Reynolds numbers. One feature that differs from monodisperse suspensions is the relative movement between particles of different sizes. If this movement between two particles is close enough, then a permanent doublet attraction due to Van der Waals force acting between them will form, for some values of Peclet number.

Davis (1984) and Melik & Fogler (1984) studied the stability of a polydisperse suspension and conditions for the coagulation of particles in an unstable suspension. Investigations of stable flows, i.e. suspensions that did not show particle coagulation indicate that the particle concentration is not constant. Instead, when the sedimentation develops the particles fall faster and moving away from each other and in turn creating different regions within the suspension. The lower region before the sediment layer, contains all particle species, whilst the region that is above is devoid of the faster moving particles. Each region contains fewer particles than the region below whereas the region above has the slower moving particles, Figure 1.2.2.

In many cases the regions are separated by a discontinuity within the distribution of particle concentration. In general, it has been assumed that the spatial distribution of the particles in the horizontal plane is uniform, being completely true in dilute suspensions, i.e. suspensions with low concentrations, however, not in the case of bi-dispersed suspensions. The first researcher to show this was Whitmore (1955), who described this phenomenon after performing experiments in suspensions with two types of particles: heavy and neutrally buoyant particles. Their results showed that after leaving the well-mixed suspension, therein started a lateral segregation of the particles which caused the appearance of vertical fingers. The appearance of vertical fingers is an interesting phenomenon from the point of view of fluid physics, but not from the practical point of view, of which it poses no improvement in the sedimentation rate, etc. Figure 1.2.3 shows a typical scheme of the formation of vertical fingers during a sedimentation process.

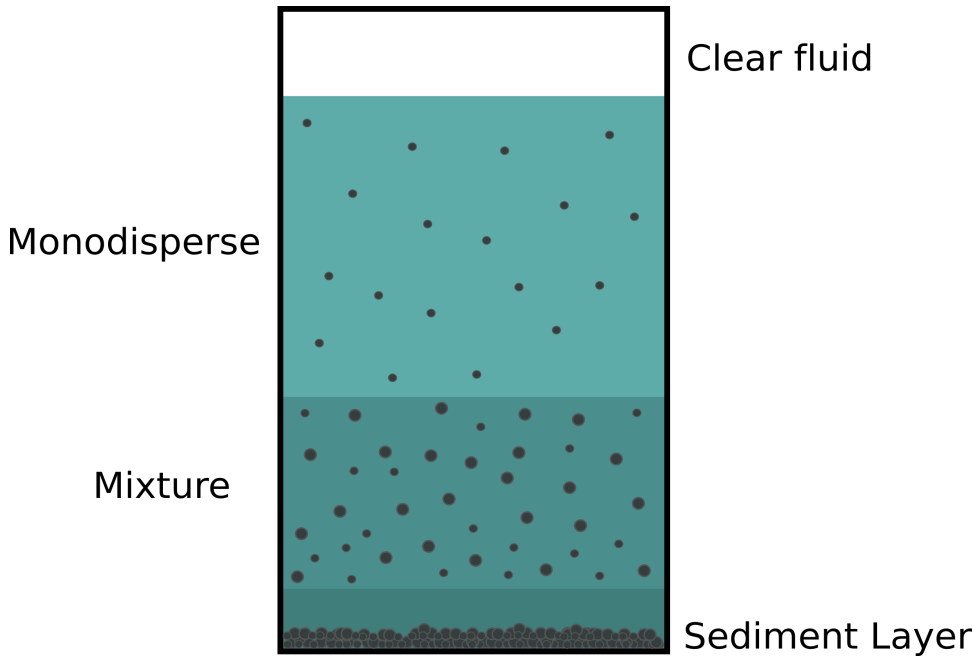

Figure 1.2.2: Regional sedimentation processes for the different types of particles.

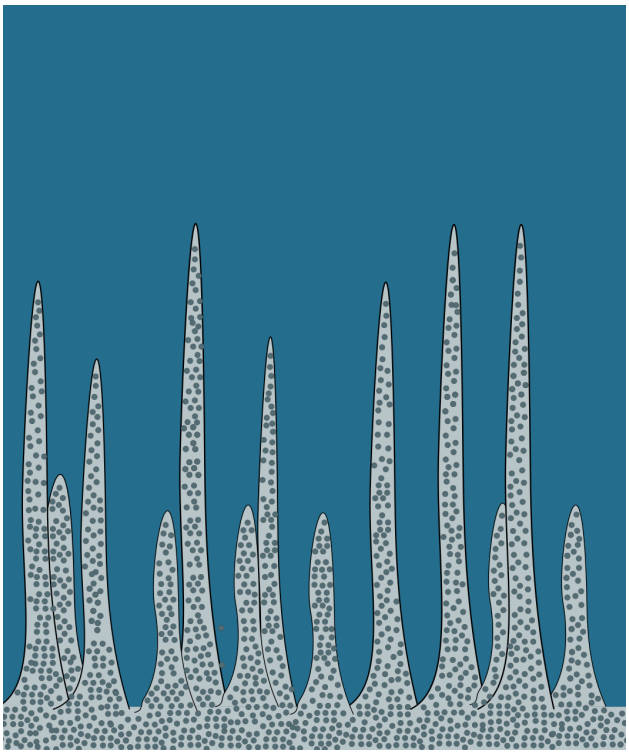

Figure 1.2.3: Diagram of vertical fingers over a sedimentation process for various types of particles. The experimental picture can be seen in the publication of Weiland *et al.* (1984) and Davis & Acrivos (1985).

Herein, we will focus on the process of polydisperse sedimentation maintaining constant particle distribution in the horizontal axis. When we have a diluted dispersion of particles, each particle falls with the Stokes velocity, equation (1.2.1). The Stokes' model provides an adequate quantitative

description for particle sedimentation at low concentrations. However, when the concentration of total particles of the particles exceeds the value of 0.01, the behaviour is totally different from that predicted by the above law, due to the physical interaction of particles for different sizes. Generally speaking, when a polydisperse suspension is insufficiently diluted, the concentration of particles in the different regions will be different. Smith (1966) and then Stamatakis & Tien (1988) derived a sedimentation model for a discrete distribution of N particles. They proposed the following model for calculating the variation of the suspension interface,

$$\frac{\mathrm{d}h_{\mathrm{i}+1}}{\mathrm{d}t} = -\frac{\sum_{\mathrm{i}=1}^{k} u_{st\,\mathrm{i},j}\phi_{\mathrm{i},j}}{\varepsilon_{\mathrm{i}} - \varepsilon_s} \quad k = 1, 2, 3, ..., N. \tag{1.2.8}$$

Here, h is the distance of the interface between the particle suspension and the sediment layer, j is type particle and i is the zone. The type particle j has a radius a_j, density ρ_j, particle concentration ϕ_j and Stokes settling velocity $u_{st,j}$, where the average sedimentation rate depends on the concentration of local particles with all particles present. This can be expressed mathematically as

$$v_j = u_{st} f_{\mathrm{i}}(\vec{\phi}). \tag{1.2.9}$$

Where $\vec{\phi}$ is the vector associated with the particulate concentration. In general, the function $f(\vec{\phi})$ will be different for each type of particle and depending on the physical effects between them, Brownian forces, etc. As noted, average speeds are related to the concentration of particles for all types of particles in suspension, equation (1.2.8) involves a system of algebraic equations nonlinear coupled with $\phi_{\mathrm{i}}^{(k+1)}$ unknowns. Once known the value of $\phi_{\mathrm{i}}^{(k+1)}$, and equation (1.2.9) can describe the complete phenomenology of the sedimentation process. As shown above, algebraic equations are transformed into differential equations; they can easily be solved by finite differences. To solve the systems of equations described above (algebraic and differential), it is vital to know the function $f(\phi)$ for many types of particle suspensions, i.e., polydisperse. In the mid-60s, Smith (1965) published a theoretical work, which showed a model for the sedimentation of particles for various sizes; extending the work of Happel (1958) that was presented some years before. The Smith's theoretical model allows prediction of the trends in particle velocities that are descending as a function of particle concentration, however, often this model underestimates the velocities.

Two decades later, Lockett & Al-Habbooby (1973, 1974) conducted sedimentation experiments for the binary mixture particles. In these studies, researchers suggested that the function f given by Richardson & Zaki (1954b) could be used in each of the particles in the suspension, simply by using the total particle local concentration $\phi = \Sigma\phi_{\mathrm{i}}$. In a later work, Mirza & Richardson (1979) found that velocities theoretically predicted by the models of Lockett & Al-Habbooby (1973, 1974) were greater than those found in experiments. To solve this inconsistency and to obtain a better representation of the experimental results, an empirical correlation factor $(1-\phi)^{0.4}$ to the predicted rates was applied. In the described mathematical models, the results of the sedimentation monodisperse processes were used to describe the effects of interactions between particles in the processes of sedimentation for various particles. Moreover, in the processes where low concentration of particles is dominant for interacting pairs, the process of interference that is due to the presence of particles can be determined analytically (Batchelor, 1982). Subsequently, Batchelor (1982) published a paper that extended this results for a distribution of N particles. The expression can be written as

$$v_{\mathrm{i}} = u_{\mathrm{i}} \left[1 + \sum_{j=1}^{N} Z_{\mathrm{i}j} \phi_j \right], \quad \mathrm{i} = 1, 2, 3, ..., N, \tag{1.2.10}$$

where $Z_{\mathrm{i}j}$ is a dimensionless parameter which depends on the reduced density $\lambda = (\rho_j - \rho)/(\rho_{\mathrm{i}} - \rho)$ and the size ratio $\lambda = a_j/a_{\mathrm{i}}$ and the Peclet number. The calculation of the sedimentation term $Z_{\mathrm{i}j}$ for a pair of particles of different sizes is much more complicated than for identical particles.

1.3 Sedimentation in inclined containers

In general, the sedimentation process is slow when the particles are small. Therefore, there is a necessity in engineering to improve the efficiency and speed of these processes. One of the most used systems in recent decades, consists of a container where the inclined settling times may be decreased by an order of magnitude. Sedimentation processes in inclined ducts have been among the subject of study in recent decades. The first person to see an improvement in settling time was a doctor called Boycott almost a century ago. Boycott (1920) observed that blood cells settle much faster at the bottom of the test tubes, when they were inclined with respect to the vertical, unlike in tubes that were completely vertical. Following this discovery, published in the journal Nature (Boycott, 1920), many scientists have worked on this phenomenon, for monodisperse, including polydisperse and, slightly polydisperse suspensions.

An interesting summary of all the investigations carried out in the first decades of the last century is the Hill *et al.* (1977). The improvement in the rate of the sedimentation process is that the particles must travel a much shorter distance until they reach a wall, consequently, as soon as the particles reach the bottom wall they begin to slide, as shown in Figure 1.3.1. Once the particles reach the bottom wall, a layer of sediment rapidly moves downward reaching the bottom of the container, this is formed due to the action of gravity. As a result of being a closed system, the downflow of particles occurs immediately in an upward flow towards the particle free zone, accelerating the process of sedimentation.

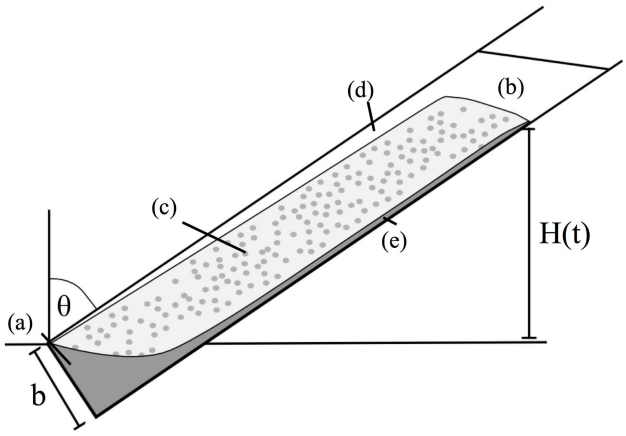

Figure 1.3.1: Different regions of a tilted sedimentation process in a container.

The so-called Boycott effect has been analysed in recent decades analytically by various author. Hill *et al.* (1977) were the first to analyse the phenomenon theoretically using equations of continuous media, particularly fluid mechanics to understand and get through to numerical flow profiles as well as sedimentation rates simulations. Some years later, Probstein & Hicks (1978), Rubinstein (1980) and Leung (1983); Leung & Probstein (1983) made analyses from first principles of the process of inclined sedimentation in two dimensions where the assumed fluid was viscous. They classified the flow into three zones, a layer of clear fluid, a layer in suspension and finally a layer of sediment. Herbolzheimer & Acrivos (1981) developed a theory to determine the velocity profiles in the aforementioned three layers. After the work of Boycott (1920), Ponder (1926), Nakamura & Kuroda (1937) developed a kinematic model (now known as model PNK) to describe the production rate of clear fluid in the container by

$$S(t) = u_{\mathrm{st}} f(\phi) b \left(\cos\theta + \frac{L}{b} \sin\theta \right), \tag{1.3.1}$$

where S is the rate in production volume of clear fluid, u_{st} is the speed of Stokes, $f(\phi)$ is the function of concealment, b is the width of the container, L is the length of the container and θ is the angle to the vertical. We know that the speed improvement in the settling process described by equation (1.3.1) is valid when the flow is in a laminar regime. Under certain conditions to be described later, waves appear on the interface of the sediment layer and the layer of clear fluid. Several studies have been developed in this area in recent years from a theoretical and experimental view (Probstein & Hicks, 1978; Leung, 1983; Davis *et al.* , 1983). In particular, the theory of linear stability has been used to understand under what physical conditions occur instabilities (waves) within the process of sedimentation (Herbolzheimer, 1983; Leung, 1983; Davis *et al.* , 1983), as seen in Figure 1.3.2.

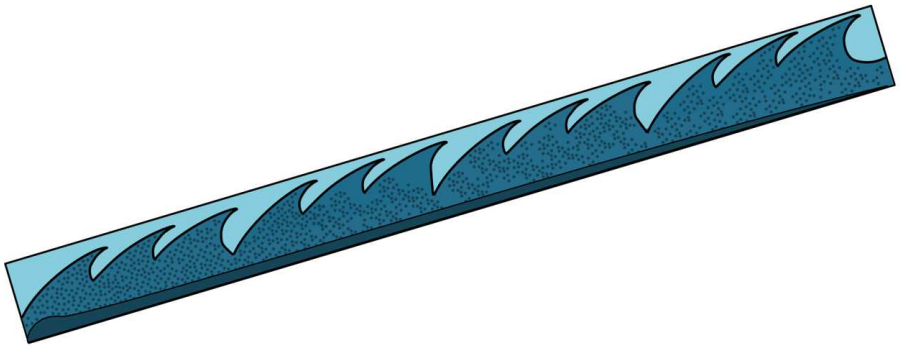

Figure 1.3.2: Instabilities (waves) in a settling particle process in a tilted container.

Acrivos & Herbolzheimer (1979) developed a theory to quantitatively describe the sedimentation of small particles in inclined ducts. In this work, they assumed that the flow was laminar and the Reynolds number was small, also the concentration of particles and the geometry were variable. They found that the rate of sedimentation S depends on two dimensionless groups, besides the geometry of the container: a Reynolds sedimentation number of the system Re, typically in the range $(1-10)$ and

Λ, the ratio between a sedimentation number Grashof and Reynolds number of the system, which is typically very large. The definition of these dimensionless numbers are presented below,

$$Re \equiv \frac{L\rho_f u_0}{\mu_f} = \frac{2}{9}\frac{La^2\rho_f(\rho_s - \rho_f)g}{\mu_f^2}, \tag{1.3.2}$$

$$\Lambda \equiv \frac{L^2 g(\rho_s - \rho_f)\phi_0}{u_0\mu_f} = \frac{9}{2}\left(\frac{L}{a}\right)^2 \phi_0, \tag{1.3.3}$$

where L is a characteristic length of the macroscopic system, ϕ_0 is the initial concentration of particles, u_0 is Stokes velocity, ρ_s is the density of suspended particles, a is the particle radius, ρ_f is the fluid density and μ_f is the fluid viscosity. Using asymptotic analysis they concluded that when $\Lambda \longrightarrow \infty$ for a duct, S can be predicted very well by the Ponder-Nakamura-Kuroda theory, which was obtained using only kinematic arguments. The theory proposed by Acrivos & Herbolzheimer (1979) gives an expression for the layer thickness for the clear fluid that is formed below the upper face of the container, also the velocity profiles in the clear fluid layer as well as in the suspension region. The sedimentation rate and the layer thickness for the clear fluid were measured in an inclined container under the following experimental conditions: $\phi_0 \leq 0.1$, $Re \sim O(1)$, Λ values ranging from $(10^5 - 10^7)$ and θ values between $(0° - 50°)$, where θ is the tilt angle. This research suggests that deviations from theory PNK reported in other studies are likely due to flow instabilities causing re-suspension of particles generating a reduction in the efficiency of the sedimentation process.

It has been said that in certain cases the interface between the fluid layer and the clear suspension layer become wavy. It is very clear that the appearance of this type of wave limits the efficiency of the sedimentation inclined containers, particularly when the waves break on the bottom of the container. Davis *et al.* (1983) performed a linear stability analysis to investigate in detail the conditions of formation and growth of waves during a long monodisperse sedimentation particle process, narrow ducts are inclined with respect to the vertical. They found that the highest rates of amplification waves were predicted by solving differential equations governing the instabilities both asymptotically for disturbances of long wavelength perturbations as well as moderate wave lengths. The theory showed good agreement with the experimental results. In particular, they found that for long and narrow ducts were efficient settlers. In later works, Herbolzheimer (1983) found using asymptotic solutions for long waves, that the critical Reynolds number is proportional to the tangent of the angle of the conduit, multiplied by the ratio between the thickness of the clear fluid layer and b/H For long waves in the sedimentation process, the flow is stable only if

$$R_c < \frac{140}{57}\frac{\Lambda^{-1/3}\delta}{b/H}\frac{\tan\theta}{\rho}, \tag{1.3.4}$$

where b is the width of the duct, H is the height of the suspension, δ is the clear fluid layer, ρ the density of the suspension and θ is the angle of inclination relative to the vertical. Figure 1.3.3 shows the theoretical and experimental curves of the stability analysis of the dimensionless variables proposed by Herbolzheimer (1983) as a function of the angle. A clear correspondence between experiments and theory can be seen.

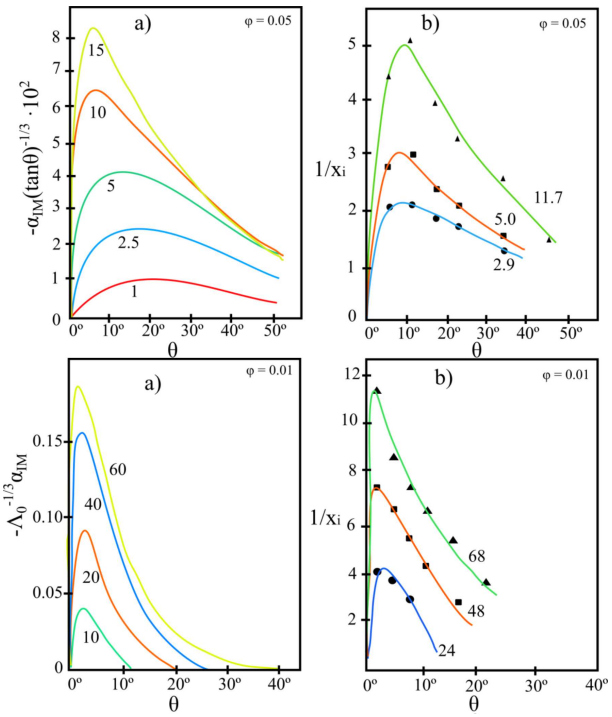

Figure 1.3.3: Comparison between experiment and theory of the dimensionless functions associated with the stability of the suspension, depending on the angle of the system (Herbolzheimer, 1983).

1.4 Dense granular flows

The dynamics of granular materials has been extensively studied over the past 40 years due to the great importance in engineering and basic sciences (Nedderman, 2005; Duran, 2012; Andreotti *et al.* , 2013). Granular materials are unique to behave as gases and solids. In gaseous state, kinetic theory has been widely used to simulate this kind of behaviour (Brilliantov & Poschel, 2010). On the other hand, the quasi static regime is often described using the plasticity theory. During the last 15 years, many experimental studies were conducted to characterize dense granular flows. Here, we present the most relevant results (Jop *et al.* , 2006; Pouliquen *et al.* , 2006; Forterre & Pouliquen, 2008).

Let us assume a granular material composed of spherical particles of diameter d and density ρ, under a confining pressure P. Da Cruz *et al.* (2005) suggested that the shear stress τ is proportional to the confining pressure P through

$$\tau = P\mu(I), \tag{1.4.1}$$

where the friction coefficient μ depends on the inertial number I, defined by

$$I = \frac{\dot{\gamma}\mathrm{d}}{\sqrt{\frac{P}{\rho_s}}}. \tag{1.4.2}$$

As discussed by MiDi (2004) and Forterre & Pouliquen (2008), the number I can be interpreted as two times that control the granular movement: (a) a microscopic time scale $\mathrm{d}/\sqrt{P/\rho_\mathrm{d}}$, which represents the time it takes for a single particle to fall in a hole of size d under the pressure P and which gives the typical time of rearrangements, and (b) a macroscopic time scale $1/\dot{\gamma}$ related to the mean deformation. The shape of $\mu(I)$ was obtained from numerical simulations and experiments for simple geometries. Figure 1.4.1(a) and (b) show the evolution of the ratio of shear stress to normal stress τ/P as function of I, for a plane shear and inclined geometry, respectively. Additionally, Figure 1.4.1(c) shows the friction coefficient μ as a function of I. The numerical and experimental results for these two geometries show that $\mu(I)$ is

$$\mu(I) = \mu_s + \frac{\mu_2 - \mu_s}{I_0/I + 1}, \tag{1.4.3}$$

where I_0 is a physical constant. The adjustable parameters from experiments are: $\mu_s = \tan 21°$, $\mu_2 = \tan 33°$ and, $I_0 = 0.3$. This empirical model goes from a minimum value μ_s for very low I up to a value μ_2 when I increases. Jop *et al.* (2006) found that the average volume fraction ϕ can be express as

$$\phi = \phi_{max} - (\phi_{max} - \phi_{min})I, \tag{1.4.4}$$

where $\phi_{max} = 0.6$ and $\phi_{min} = 0.5$. These two equations can be applied to predict and describe different flow configurations.

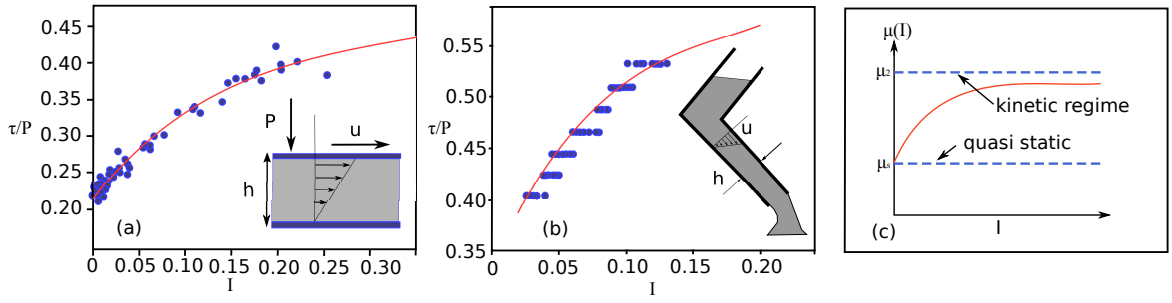

Figure 1.4.1: Rheology of dense granular flows. (a) Ratio of shear stress to normal stress τ/P as a function of I for a plane shear geometry. (b) Ratio of shear stress to normal stress τ/P as a function of I for an inclined geometry and (c) Friction coefficient μ as a function of I. (Jop *et al.* , 2006; Pouliquen *et al.* , 2006; Forterre & Pouliquen, 2008)

Following the success of the dense granular media rheology applied to some simple configurations, it has encouraged some researchers to extend the model to a tensorial formulation. Jop *et al.* (2006) assumed that the volume fraction is constant in the limit of dense granular systems. In their work, Jop *et al.* (2006) proposed that the constitutive law of the granular fluid takes the following form

$$\sigma_{ij} = -P\delta_{ij} + \tau_{ij}, \tag{1.4.5}$$

where P is the isotropic pressure and

$$\tau_{ij} = \eta \dot{\gamma}_{ij}, \quad \text{with } \eta = \frac{\mu(I)P}{|\dot{\gamma}|}. \tag{1.4.6}$$

Here, $|\dot{\gamma}|$ is second invariant of the shear rate tensor, $|\dot{\gamma}| = \sqrt{(1/2)\dot{\gamma}_{ij}\dot{\gamma}_{ij}}$. This tensorial formulation is obtained by assuming that the stress and strain rate tensors are parallel. However, Cortet *et al.* (2009) showed that this assumption is not true in all cases. Although this rheological model has been experimentally validated for simple configurations, it is still an open problem that requires further investigation.

In the following chapters, two original research papers developed during the PhD work are presented. The focus of this thesis is the sedimentation of slightly polydisperse particles and the characterization of the sediment layer in open and closed geometries, using an experimental and numerical approach. The first is entitled "Particle organization after viscous sedimentation in tilted containers", published in Physics of Fluids, 2016; and the second one is entitled "Characterization of a sediment layer of concentrated fluid-solid mixtures in tilted ducts at low Reynolds numbers" under revision in the International Journal of Multiphase Flow, 2016.

Chapter 2

Particle organization after viscous sedimentation in tilted containers

This chapter has been submitted as research paper, authored by Sergio Palma, Christian Ihle, Aldo Tamburrino and Stuart Dalziel, in Physics of Fluids (2016) (published).

Abstract

A series of sedimentation experiments and numerical simulations have been conducted to understand the factors that control the final angle of a static sediment layer formed by quasi-monodisperse particles settling in an inclined container. The set of experiments includes several combinations of fluid viscosity, container angle and solids concentration. A comparison between the experiments and a set of two-dimensional numerical simulations shows that the physical mechanism responsible for the energy dissipation in the system is the collisions between the particles. The results provide new insights into the mechanism that sets the morphology of the sediment layer formed by the settling of quasi-monodisperse particles onto the bottom of an inclined container. Tracking the interface between the suspension solids and the clear fluid zone reveals that the final angle adopted by the sediment layer shows strong dependencies on the initial particle concentration and the container inclination, but not the fluid viscosity. It is concluded that (1) the hindrance function plays an important role on the sediment bed angle, (2) the relation between the friction effect and the slope may be explained as quasi linear function of the projected velocity along the container bottom, and (3) prior to the end of settling there is a significant interparticle interaction through the fluid affecting to the final bed organization. We can express the sediment bed slope as a function of two dimensionless numbers, a version of the inertial number and the particle concentration. The present experiments confirm some previous results on the role of the interstitial fluid on low Stokes number flows of particulate matter.

2.1 Introduction

Sedimentation is a process by which solid particles are separated from a fluid under the action of the gravitational force (Davis & Acrivos, 1985). Such a process is one of the oldest known techniques used in petroleum, pharmaceutical, mining and chemical industry to clean fluids or, alternatively, to recover solid particles (Guazzelli & Hinch, 2011). The sedimentation of particles at high concentrations has been studied from a kinematic perspective in the context of vertical gravitational settlers (Kynch, 1952; Burger *et al.* , 2011).

Differently from the case of settling in upright containers, where fluid-particle and interparticle interactions can be expressed as a function of the local concentration only (Davis & Acrivos, 1985), settling on inclined planes also depends on local shear (Herbolzheimer & Acrivos, 1981; Phillips *et al.* , 1992). The impact of shear on particle dynamics in confined or inclined geometries can be further amplified by shear-induced diffusion occurring at sufficiently high particle sizes and concentrations (Phillips *et al.* , 1992; Leighton & Acrivos, 1987). The settling process at high concentrations has been studied in the context of sheared Couette cells as effectively Newtonian fluids (Leighton & Acrivos, 1987; Phillips *et al.* , 1992), and also to explain the flow and particle organization process in flows over inclined planes with a constant particle supply (Nir & Acrivos, 1990; Kapoor & Acrivos, 1995). In particular, the flow of a sediment layer that forms on an inclined surface as a consequence of the steady sedimentation of monodisperse spherical particles was investigated experimentally and theoretically by Kapoor & Acrivos (1995). They modified the model proposed by Nir & Acrivos (1990) to include shear-induced diffusion due to gradients in the shear stress as well as a slip velocity along the wall due to the finite size of the particles. When sedimentation occurs in an upright container with vertical walls and a horizontal bottom, particles tend to be distributed in horizontal layers according to their size and relative volume fractions (e.g. Davis & Acrivos (1985)). In contrast with upright containers, iso-concentration lines are not necessarily aligned with an inclined lower boundary for the container and have been found to follow a power law of the bottom coordinate (Nir & Acrivos, 1990; Kapoor & Acrivos, 1995).

A related boundary-induced flow is driven by the Boycott effect, which results in the enhancement of the sedimentation process due to the presence of an inclined upper boundary in the system that creates a clear fluid layer on top that accelerates the settling compared to the upright situation, where particles must settle over the entire depth into the bottom in a container with vertical walls. Around 30 years ago there were several investigations (e.g. Acrivos & Herbolzheimer (1979); Herbolzheimer & Acrivos (1981); Leung & Probstein (1983); Shaqfeh & Acrivos (1986)) that examined theoretically the flow fields within the various zones of inclined geometries. Such researchers derived analytic expressions for the velocity profiles within the clear fluid layer underneath the downward facing wall and within the suspension for a wide range of parameters. The formation and flow of the sediment layer on the upward facing surface was neglected in most of these studies. Leung & Probstein (1983) studied the sediment layer as an effective Newtonian fluid, but since no theory was available for determining the volume fraction of particles within the flowing concentrated sediment, such a model assumed a stepwise particle concentration distribution. Particle settling in viscous fluids upon inclined planes has been extensively investigated for small Stokes and particle Reynolds numbers (Herbolzheimer & Acrivos, 1981; Kapoor & Acrivos, 1995; Peacock *et al.* , 2005). Motivated by the study of submarine granular flows, Cassar *et al.* (2005) have focused on the dense flow regime occurring when the whole sediment layer is flowing down the slope and when no deposition occurs (Cassar *et al.* , 2005). They studied

the variation of the mean velocity and the pore pressure below the avalanche as a function of the two control parameters, the surface inclination and the layer thickness. Such results were analysed using a theoretical model obtained from dry granular flows substituting the inertial time scale by a viscous time scale. Their model was expressed in terms of a so-called inertial number (Forterre & Pouliquen, 2008), a dimensionless ratio of time scales that we shall employ in our interpretation of results.

Courrech du Pont *et al.* (2003) have suggested that granular avalanches can flow according to three different regimes depending on the time scale associated to the particle motion in the fluid. In particular, prior to the collision of a single particle with a neighbour, the particle may have not reached its terminal velocity, thus defining the free-fall regime. If the terminal velocity has been reached, it can be within a viscous or an inertial regime, depending on the balance of forces. The parameters controlling these dynamics are the Stokes number, the particle to fluid density ratio, and the particle Reynolds number. In particular, for small values of the Stokes number, they confirm the previous observation that the presence of a viscous fluid has the ability to exhaust the available kinetic energy after collisions, rendering them inelastic (Gondret *et al.* , 2002; Joseph *et al.* , 2001). This is a key element to understanding the particle and fluid dynamics of dense mixtures flowing in liquids confined in rotating cylinders and on inclined planes. On one hand, the settling in an initially homogeneous suspension in an inclined container may be effectively the same as that in an upright container away from the bottom, where particle hindrance is a dominant effect during the settling. This behaviour has been observed in thickeners and clarifiers, whose bottom is often conical (Concha, 2014). On the other hand, those particles moving near the inclined boundary may experience close interactions via the interstitial fluid or direct contacts, which may cause particle velocity gradients. The result of these three stages with different dynamics form a particle bed that is not parallel to the bottom.

In the present paper, we study the final shape of the particle bed within a large inclined container by means of numerical simulations and experiments. The particle motion is in the viscosity-dominated regime, and thus the particle Reynolds number, and the Stokes number, are small. We seek a relation between the angle of inclination of the container and the angle of the surface of the particle bed. The aforementioned flow characteristics —both away from and close to the sediment layer— are captured using scaling arguments to explain the prevailing mechanisms that control the final bed organization. In Section 2.2, we detail the experimental procedure used to track the interface between the suspension and the clear region and measure the final angle of inclination of the sediment layer. Also, we present the mathematical model and the numerical procedure used for the numerical simulations. In Section 2.3, we discuss the results of our experiments and numerical simulations, and conclude in Section 2.4.

2.2 Materials and Methods

2.2.1 Experiments

The experimental set-up is shown schematically in Figure 2.2.1(a) and consists of an inclined transparent acrylic settling container of $25 \times 21 \times 3\ \mathrm{cm}^3$ (width $\times$ height $\times$ thickness) filled with an initially homogeneous suspension of negatively buoyant spheres in a viscous liquid. We considered different combinations of initial particle concentration (ϕ_0), container inclination angle measured from

the horizontal plane (θ_s), and liquid viscosity (η_f).

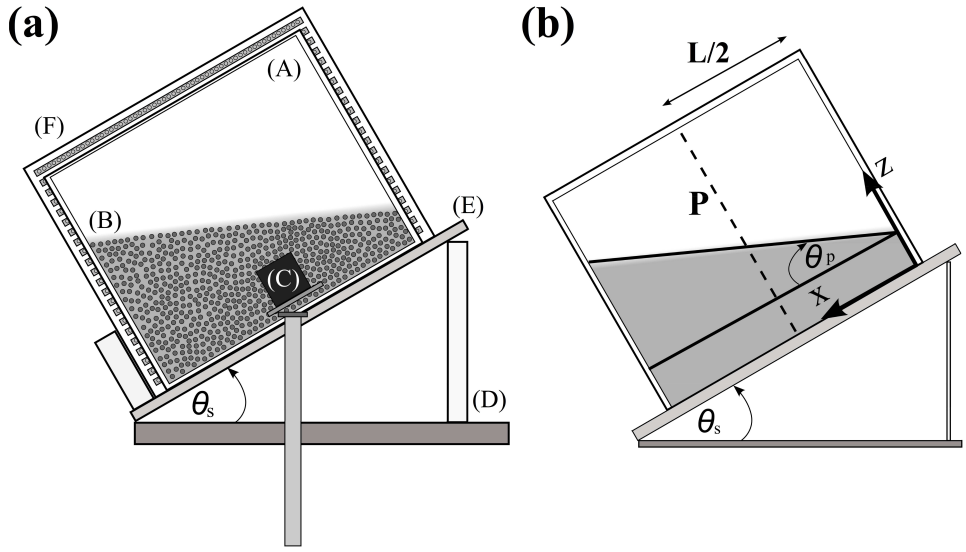

Figure 2.2.1: (a) Schematic of the experimental setup. (A): acrylic container, (B): resin beads, shown in grey, (C): video camera, (D): adjustable lab jack, (E): inclined support, (F): LED back lighting. (b) General configuration of the problem. In all the experiments, the camera is aligned with the bottom of the tank. The angle of the sediment layer measured respect to the base of the container is θ_p.

A solution of glycerine ($C_3H_8O_3$) and water was used in all experiments. The glycerine concentrations ranged from 45% to 55% by volume, resulting in dynamic viscosities between 6.30 ± 0.08 mPa·s and 11.48 ± 0.15 mPa·s, and densities between $1.13 \pm 0.02\,\mathrm{g/cm^3}$ and $1.16 \pm 0.02\,\mathrm{g/cm^3}$, (Cheng, 2008). For all the experiments we kept the fluid at 20°C, and thus controlled both the density and viscosity with the glycerine concentration.

The particles used were spherical, partially translucent resin beads (Purolite® PCR833 Gel SAC - Special Grading, Na+ Form) with radius $a = 125 \pm 13\,\mu$m and density $\rho_s = 1.31 \pm 0.07\,\mathrm{g/cm^3}$. We measured a loose packing volume fraction of 0.61 ± 0.02, close to that expected for monodisperse spheres. We estimated this value by measuring the volume of water displaced when a known volume of packed particles was immersed in water. We measured the angle of repose of the dry particles with respect to the horizontal plane, $\theta_\mathrm{d} = 19.9° \pm 0.3°$. This has been measured as the cone angle obtained after releasing the particles from a height of 15 cm on a rough surface made of the same particles, stuck to the bottom, horizontal plane. This experiment has been repeated 20 times to obtain statistical convergence. The parameter θ_d has been used as a reference to define the reservoir inclination angles from 0 to $1.51\theta_\mathrm{d}$, the former case corresponding to a horizontal sediment layer.

We illuminated the flow trough an acrylic diffuser using a 24 W cool white LED panel consisting of 200 emitters giving a diffusive backlighting without significant heating. In the present measurements we used an 8-bit, 12 frames/sec UniqVision UP900DS-CL RGB camera with a spatial resolution of 640×480 pixels^2, to record a region of 25×14 cm^2. This region excludes a 7 cm length band at the top of the tank. Although the camera's resolution precluded the use of pattern matching algorithms to obtain the downslope component of the particle velocity field, it allowed the measurement of the location of the solids interface with considerable accuracy, as was later verified with the output of the numerical simulations. The length of influence of the walls have been found to be of about 5 cm, whereas the edges of the interrogation windows are at a minimum distance of 10 cm from the walls.

Table 2.1: Set of experimental conditions.

	Values
System angle θ_s (°), $\pm$ 0.5°	$[0, 10, 20, 30]$
Fluid viscosity η_f (mPa·s), $\pm$ 1.3%	$[6.30, 7.25, 8.40, 9.78, 11.48]$
Initial volume fraction ϕ_0 (%), $\pm$0.1%	$[5.0, 7.5, 10.0, 12.5, 15.0, 17.5, 20.0]$

In addition, we have attached black tape to the bottom of the tank, where the transparent acrylic walls are joined, in order to minimize the light penetration from the walls into the particles. The image post-processing was undertaken with DigiFlow ver 3.4 (Dalziel, 2012). We conducted a total of 140 experiments, exploring all different combinations of 4 inclination angles, 5 fluid viscosities and 7 particle volume fractions, as listed in Table 2.1.

The procedure for each experiment is summarized as follows. The empty container was positioned on top of the inclined surface after this had been carefully set an angle of θ_s, with the same angle set for the camera. The suspension, previously stored in a beaker, is then poured into the inclined container. Immediately after, it was gently agitated for 2 min to keep the particles in suspension while allowing bubbles to rise to the surface. To minimize air entrainment, this step was undertaken avoiding sloshing or splashing of the mixture. We have tested the initial homogeneity of the suspension comparing different concentration profiles along the x axis for the case $\theta_s = 0$. We started the video recording during the mixing process to ensure the whole settling experiment was captured. The particle settling process in the system with an inclined container took between 60 s and 240 s, depending on the glycerin/particle concentration combination.

The settling process finally evolved into the formation of a sediment layer, whose upper surface was found to be approximately linear in most of the experiments (see Figure 2.2.8, Section 2.3). Previous work (Kapoor & Acrivos, 1995) has suggested that the sediment layer can be modelled by, $h(x) \sim x^a$, $a \leq 1$, with the coordinate x aligned with the tank bottom. The present set of experiments showed that $a \approx 1$ gives a reasonable approximation of the finally settled condition in the central region of the container. This allows a simple description of the settled bed using a uniform slope as a relevant single parameter. Once the settling process was completed, the sediment layer formed an angle $\theta = \theta_s - \theta_p$ with respect to the horizontal, where, θ_p is the angle measured from the base of the container, as depicted in Figure 2.2.1(b). This angle was determined using linear regression on measurements of the height of the interface between the fluid and the sediment layer. The angle θ was, in general, less and equal to the angle of repose θ_d. The back lighting of the translucent particles in these quasi-two-dimensional experiments allowed the transmitted light intensity to be related to the particle concentration.

Figure 2.2.2 shows the experimental calibration curve obtained from the volume fraction of particles as a function of the mean normalized transmitted light intensity over the container, $\overline{\mathrm{i}_n} = (1/NM)\sum_j \sum_k \mathrm{i}_n(j,k)$, where i_n is the light intensity at the nodes i and j, with $1 \leq \mathrm{i} \leq N$ and $1 \leq j \leq M$. Here, N and M correspond to the vertical and horizontal number of nodes in the measurement window, respectively. The calibration experiment consisted of relating the mean normalized intensity of light at $t = 0$ in a centred 60×60 mm^2 window, with the mean concentration of particles, measured by a mass balance. We repeated these steps for different concentrations of particles and fluids. Each experiment was repeated three times. A relation between concentration and the normalized mean intensity over the container, $\overline{\mathrm{i}_n}$, is given by the empirical fit

$$\phi = \alpha_1 \overline{\mathrm{i}_n}^{\,\alpha_2} + \alpha_3 \overline{\mathrm{i}_n} + \alpha_4 \tag{2.2.1}$$

We determined the coefficients α_1 to α_4 using a Levenberg-Marquardt algorithm (More, 1978), the results of which are given in Table 2.2. In the same figure, the inset shows the mean normalized transmitted light intensity as a function of the vertical axis in a calibration experiment using a vertical container, for a viscosity of $\eta_{f1} = 6.30 \pm 0.08$ mPa·s and an initial volume fraction of $\phi_0 = 5.0 \pm 0.1$ %. The profile corresponds to the final state of the particle sedimentation. For each initial volume fraction, vertical profiles of the light intensity (taken as the Euclidean norm of the RGB vector of the pixel values) were determined at 25 evenly spaced locations along the horizontal axis of the acrylic container. These profiles were then averaged and normalized to yield the transmitted light. The grey line represents the mean normalized intensity profile $\mathrm{i}_n(z)$ and the black lines correspond to the fluctuations in the concentration profiles. It shows that the scatter is small compared to the mean profile obtained.

The mean normalized transmitted light intensity over the container $\overline{\mathrm{i}_n}$ has an error of 1% for $\overline{\mathrm{i}_n} > 0.20$ and 0.3% for $\overline{\mathrm{i}_n} \leq 0.20$. The corresponding uncertainties have been calculated as the standard deviation of intensity curves corresponding to the 25 light intensity profiles. This calibration allowed us to determine the concentration of quasi-monodisperse particles at any instant along the vertical axis, $\phi = \phi(z,t)$. The error in the volume fraction has been calculated in terms of the error in the intensity measurement using the uncertainty theory. The model proposed for the volume fraction of particles has an error less than 1% for $\overline{\mathrm{i}_n} \leq 0.05$, 0.2% for $0.05 < \overline{\mathrm{i}_n} < 0.40$ and 5% for $0.40 < \overline{\mathrm{i}_n} < 0.80$. Figure 2.2.3 shows the volume fraction of particles and the mean normalized transmitted light intensity as a function of the vertical axis for different times. This profile, $\phi = \phi(x = L/2, z)$, corresponds to the vertical centerline of the tank for an upright container ($\theta_s = 0.0 \pm 0.5°$), an initial volume fraction $\phi_0 = 5.0 \pm 0.1\%$ and a liquid phase dynamic viscosity of $\eta_{f1} = 6.30 \pm 0.08$ mPa·s. The concentration profiles were calculated from the normalized light intensity using equation (2.2.1).

Given the relation between the light intensity and the local concentration, the upper surface of the sediment layer is found by simply identifying the normalized intensity contour where $\overline{\mathrm{i}_n} = 0.0435$, corresponding to $\phi \approx 40\%$. The orientation θ_p of the deposit was then determined from the least squares fit of a straight line to the central 10 cm of the tank.

2.2.2 Numerical simulations

We have complemented the experiments with a set of two-dimensional numerical simulations using a mixture model. Although numerical models such as dynamic contact, molecular dynamics and discrete elements are capable of capturing more aspects of the interactions between the particles, such techniques are very expensive computationally for dry granular flows, and even more so if considering the interaction with a fluid (Poschel & Schwager, 2005). Due to the favourable relation between

Table 2.2: Fit coefficients for light intensity function (2.2.1). The values Δ_{α_j} represent the corresponding fit errors. The obtained correlation coefficient for the fit parameters is $R^2 = 0.9998$.

Values	1	2	3	4
α_j	0.0080	−2.21	−33.50	33.50
Δ_{α_j}	0.0001	0.01	0.01	0.01

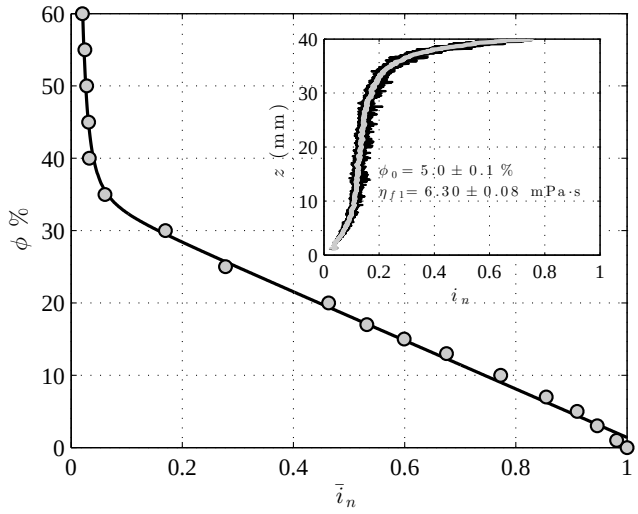

Figure 2.2.2: Experimental calibration curve, showing the volume fraction of particles as a function of the mean normalized transmitted light intensity over the container at $t = 0$, $\overline{\mathrm{i}_n} = (1/NM)\sum_j \sum_k \mathrm{i}_n(j,k)$. Inset: Mean normalized transmitted light intensity as a function of the vertical axis in a calibration experiment using a vertical container, for a viscosity of $\eta_{f1} = 6.30 \pm 0.08$ mPa·s and an initial volume fraction of $\phi_0 = 5.0 \pm 0.1$ %. The profile corresponds to the final state of the particle sedimentation.

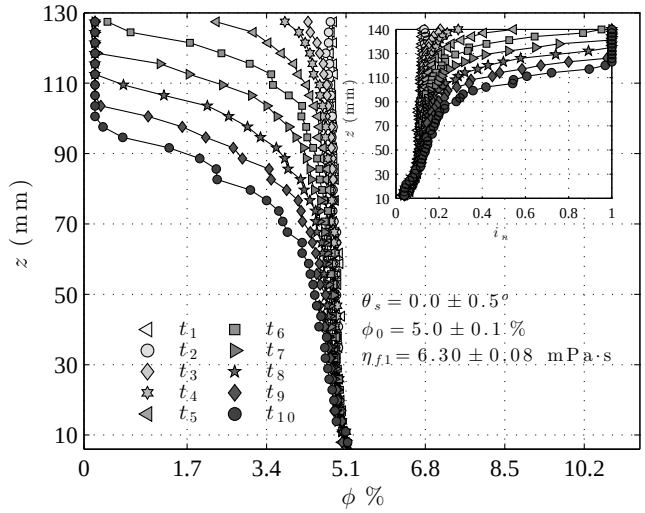

Figure 2.2.3: Volume fraction of particles as a function of the vertical axis for various times. Inset: Mean normalized transmitted light intensity as a function of the vertical coordinate normal to the bottom. Experimental conditions: $\theta_s = 0.0 \pm 0.5^\circ$, an initial volume fraction $\phi_0 = 5.0 \pm 0.1\%$ and a liquid phase dynamical viscosity of $\eta_{f1} = 6.30 \pm 0.08$ mPa·s. The curves correspond, from top to bottom elapsed times between 1 s and 10 s after the start of the experiment, with 1 s increments. The measurements between $z = 0$ and $z = 10$ mm have been discarded due to the reflection of light at the junctions of the acrylic container.

computational accuracy and economy (Poschel & Schwager, 2005; Zienkiewicz *et al.* , 2013), we have chosen this continuum approach. The objective of these simulations is two-fold. First, the numerical simulations allowed tracking of the settling process through the concentration and flow velocity output before the final settling condition. Second, the present mixture model does not have a built-in repose angle (or internal friction) condition. Consequently, this model allows us to assess whether or not the internal friction is an important mechanism for setting the final slope of the sediment layer.

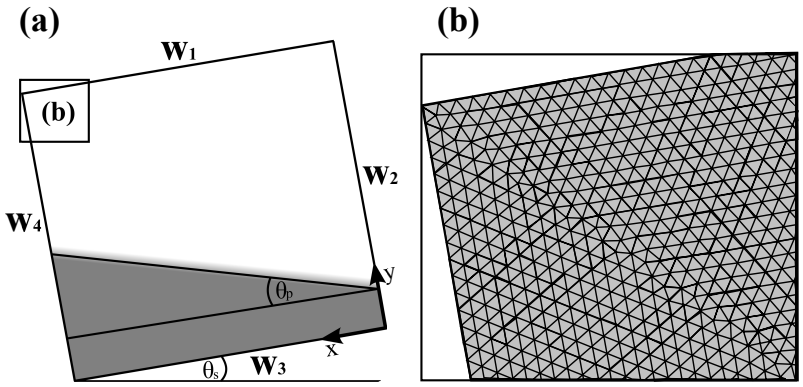

Figure 2.2.4: (a) Computational domain and Boundary conditions. (b) Detail of free triangular mesh used in all numerical simulations (upper left corner).

The dynamics of the suspension can be modeled by two momentum equations, one for the particles and the other for the fluid, plus a continuity equation for each of the two phases present (Enwald *et al.* , 1996). Assuming that there is no mass transfer between the two phases, the continuity equations for the continuous and dispersed phase are, respectively, $\partial_t (\rho_f \phi_f) + \boldsymbol{\nabla} \cdot (\rho_f \phi_f \mathbf{u}_f) = 0$ and $\partial_t (\rho_s \phi_s) + \boldsymbol{\nabla} \cdot (\rho_s \phi_s \mathbf{u}_s) = 0$. The subscripts f and s refer to quantities associated with the continuous phase (fluid) and the dispersed phase (solids). In this model, both the continuous and the dispersed phases are considered incompressible and, in the case of the dispersed phase, inelastic. In the present case, particle Reynolds numbers are within the Stokes regime, which justifies the incompressibility assumption for both phases.

An elasticity hypothesis of the dispersed phase would affect the particle motion after inter-particle collisions and their potential to squeeze fluid out of the sediment layer differently than in the rigid case. Here, as Stokes numbers are very small, all liquid-mediated collisions are indeed inelastic, as discussed below. On the other hand, particle elasticity would alter the loose packing fraction well below the sediment surface, due to the effect of lithostatic pressure. As our experiments and simulations include only relatively shallow particle layers, overburden pressures are not enough to deform the disperse phase at the bottom, thus allowing to plausibly assume that particles are effectively rigid. On the other hand, the intent of the present work is to study particle organization of natural sediments, which are rigid indeed. As the continuous and the dispersed phase are coupled by the total mass conservation requirement, $\phi_f + \phi_s = 1$, the following continuity equation for the mixture is obtained:

$$\boldsymbol{\nabla} \cdot (\phi_s \mathbf{u}_s + \mathbf{u}_f (1 - \phi_s)) = 0. \tag{2.2.2}$$

The momentum equations for the continuous and disperse phase, using a non-conservative form (Ergun, 1952), are, respectively,

$$\rho_f \frac{\partial \mathbf{u}_f}{\partial t} + \rho_f (\mathbf{u}_f \cdot \boldsymbol{\nabla}) \mathbf{u}_f = -\boldsymbol{\nabla} p + \boldsymbol{\nabla} \cdot \boldsymbol{\tau}_f + \frac{\boldsymbol{\nabla} \phi_f \cdot \boldsymbol{\tau}_f}{\phi_f} + \rho_f \mathbf{g} + \frac{\mathbf{F}_{m,f}}{\phi_f}, \tag{2.2.3}$$

$$\rho_s \frac{\partial \mathbf{u}_s}{\partial t} + \rho_s \left(\mathbf{u}_s \cdot \boldsymbol{\nabla}\right) \mathbf{u}_s = -\boldsymbol{\nabla} p + \boldsymbol{\nabla} \cdot \left(\frac{\boldsymbol{\tau}_s}{\phi_s}\right) + \boldsymbol{\nabla}\phi_s \cdot \left(\frac{\boldsymbol{\tau}_s}{\phi_s^2}\right) - \frac{\boldsymbol{\nabla} p_s}{\phi_s} + \rho_s \mathbf{g} + \frac{\mathbf{F}_{m,s}}{\phi_s}. \tag{2.2.4}$$

Here, p is the pressure of the mixture, which is assumed equal for both phases, and p_s is a pressure term related to the contribution of the disperse phase to the total pressure, in this case attributed to a purely collisional mechanism, a function ultimately related to the local gradient of the solid fraction and an empirical function mimicking an effective modulus of elasticity, as used in fluidised systems (see, for a review, Massoudi *et al.* , 1992).

The viscous stress tensor of each phase is indicated by $\boldsymbol{\tau}$ in the momentum equations and $\mathbf{g}$ is the acceleration due to gravity. The momentum transfer between the phases, $\mathbf{F}_m$, is a volume force exerted upon one of the phases on the other phase. In the momentum equations described above, the continuous phase is considered Newtonian. Hence, the viscous stress tensor is defined as,$\boldsymbol{\tau}_f = \eta_f[\boldsymbol{\nabla}\mathbf{u}_f + (\boldsymbol{\nabla}\mathbf{u}_f)^T - 2(\boldsymbol{\nabla}\cdot\mathbf{u}_f)\mathbb{I}/3]$ and $\boldsymbol{\tau}_s = \eta_s[\boldsymbol{\nabla}\mathbf{u}_s + (\boldsymbol{\nabla}\mathbf{u}_s)^T - 2(\boldsymbol{\nabla}\cdot\mathbf{u}_s)\mathbb{I}/3]$ (Enwald *et al.* , 1996), where η_f and η_s are the dynamic viscosities of the respective phases and $\mathbb{I}$ is the identity tensor. The dispersed phase requires a viscosity term to model the behaviour of the particles at low and high concentrations. Here, $\eta_s = \eta_f (1 - \phi_s/\phi_{s,\max})^{-5/2\phi_{s,\max}}$ is calculated using the model proposed by Krieger & Dougherty (1959). If $\phi_\mathrm{d} \to 0$, then $\eta_s = \eta_f$, and if $\phi_s \to \phi_{s,\max}$, then $\eta_s = \infty$. The interphase momentum transfer is governed by the drag force modelled as $\mathbf{F}_{m,f} = -\mathbf{F}_{m,s} = \beta(\mathbf{u}_s - \mathbf{u}_f)$, where β is the drag coefficient. In the present set of simulations, the method proposed by Gidaspow (1994) for the particle pressure term, and that of Wen & Yu (1966) for the drag coefficient for fluids with a high concentration of particles in volume, are considered and detailed in the Appendix 2.5.1.

The continuity equation of the mixture (2.2.2) and momentum transport equations of both phases, (2.2.3) and (2.2.4), are discretized by the Galerkin finite element method (Zienkiewicz *et al.* , 2013). We have used COMSOL Multiphysics with the CFD package to solve the system of differential equations described above for the experimental conditions of the Table 2.1. The boundary conditions associated with the computational domain are depicted in Figure 2.2.4(a). First, we consider no-slip conditions and no penetration for both phases in all the domain borders, so that $\mathbf{u}_f = \mathbf{u}_s = \mathbf{0}$ at w_j, with $j \in \{1, ..., 4\}$ (Figure 2.2.4(a)). Regarding the dispersed phase, we imposed a zero-outflow condition in the container, i.e., $\phi_s \mathbf{u}_s \cdot \mathbf{n} = 0$ at w_j. Figure 2.2.4(b) shows the free triangular mesh used in this work for the discretization of the differential equations. In order to choose the appropriate mesh size for the calculations, a set of simulations for different mesh sizes has been performed under three different numerical conditions, $\theta_s = 10°$, $\eta_f = 6.30$ mPa·s and $\phi_0 = 0.05$, 0.10 and 0.20.

Figure 2.2.5 shows an example of the sediment layer angle dependence with the number of mesh elements for the case with $\theta_s = 10°$, $\phi_0 = 0.20$ and $\eta_f = 6.30$ mPa·s. We see that the angle of the sediment layer reaches $\theta_p \approx 8°$ with about 10,000 mesh elements, increasing slightly to $\theta_p = 8.07°$ when 20,000 mesh elements are used and reaching a constant value $\theta_p = 8.09°$ when over 25,000 mesh elements are used in the calculations. A compromise between convergence and computational time has been used with 40,000 triangular elements and a 0.10 s time step for the subsequent calculations. The latter corresponds to 1/4 of the time it takes one sphere to displace its own size at the Stokes settling velocity. Notably, the time step depends on the fluid viscosity, in our case requiring Δt between 0.1 s and 0.2 s. All runs were set to simulate 500 s of real time, thus exceeding the overall bed formation times in the experiments, with output saved every 2 s.

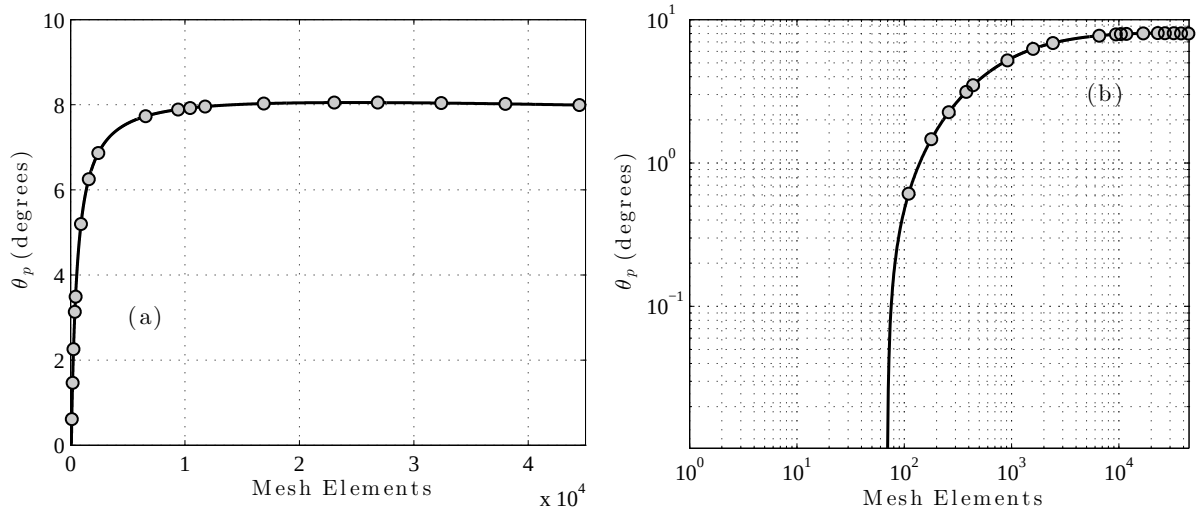

Figure 2.2.5: (a) Convergence of free triangular mesh. θ_p as a function of number of mesh elements. The solid line represents the trend points. Numerical conditions, $\theta_s = 10°$, $\phi_0 = 20\%$, $2\eta_f = 6.30$ mPa·s. (b) Same graph on a logarithmic scale.

Convergence was assessed when the sediment layer angle, defined as the locus of a solids volume fraction equal 0.40, remained static. This concentration cut-off criterion is justified by the abrupt transition predicted by the mixture model at about this value of the particle concentration as the sedimentation progresses for sufficiently long times, as depicted in Figure 2.2.6. The inset in Figure 2.2.6 shows the component of the velocity of particles $\mathbf{u}_s$ parallel to the bottom of the container, for different times. An example showing the computed concentration field and the boundary of the sediment layer below is shown in Figure 2.2.7. The upper, dashed white line in the bottom-right panel represents the sediment layer definition according to the threshold limit for $\phi = 0.40$, defined herein. The grayscale bar represents the concentration of particles.

The set of differential equations and the corresponding initial and boundary conditions used in this work represent a continuum mixture model, and therefore it provides a continuous description of the velocity and particle concentration field. In contrast, when the actual settling process is finished, a discontinuity on the particle concentration field appears at a finite time. This sharp change in the particle concentration may not be captured by the present continuum mixture model in detail. The result of equations (2.2.3) and (3.2.4) for steady state and the zero-velocity condition represent a hydrostatic particle concentration field, which contradicts the various final angles of the sediment layer found herein. The adjustment of the continuum model from the sloping sediment layer to a hydrostatic state occurs over a much longer time scale than the formation of the bed. The present continuum mixture model is thus only useful during the transient process where the sediment layer is in progress. However, the identification of an abrupt change in the numerical output in the concentration as described above gives a robust and reasonable indication of such a settled condition. This is exposed by comparison with the experimental results in the next section.

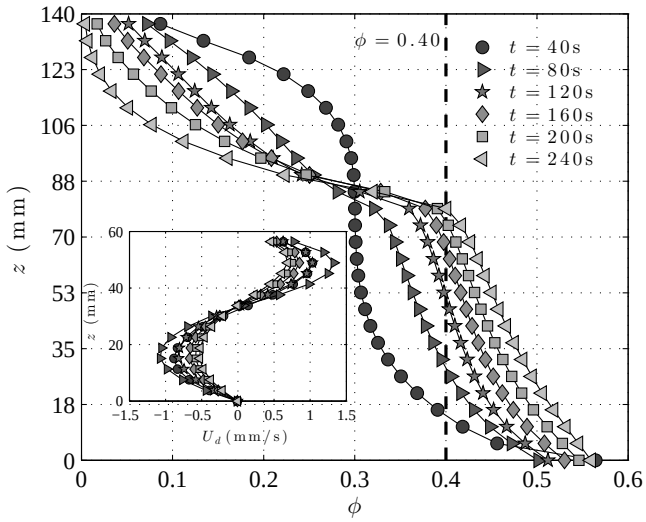

Figure 2.2.6: Particle concentration profile for $\phi_0 = 15.0 \pm 0.1\%$, $\eta_{f1} = 6.30 \pm 0.08$ mPa·s and $\theta_s = 10.0 \pm 0.5°$, measured at $(x = L/2, z)$ for various times. Inset: component of velocity $\mathbf{u}_s$ parallel to the bottom of the container. The vertical, dashed line represents $\phi = 0.4$.

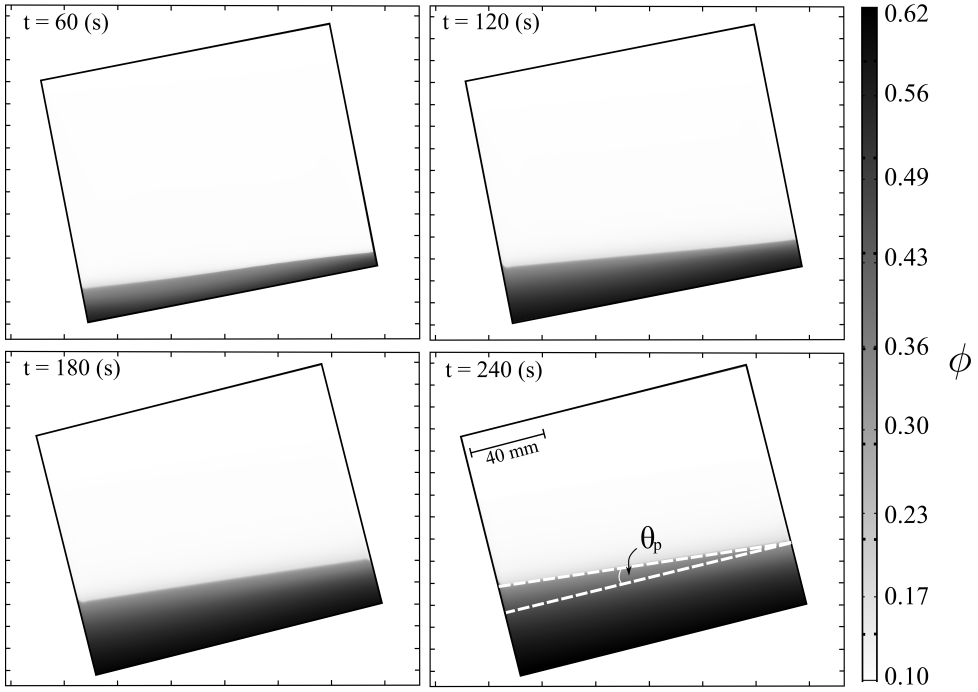

Figure 2.2.7: Particle concentration field obtained from numerical simulations for 60 s, 120 s, 180 s and 240 s. The upper, dashed white line in the bottom-right panel represents the sediment layer definition according to the threshold limit for ϕ, equal 0.40, defined herein. The experimental conditions are the same as shown in Figure 2.2.6. The grayscale bar represents the concentration of particles.

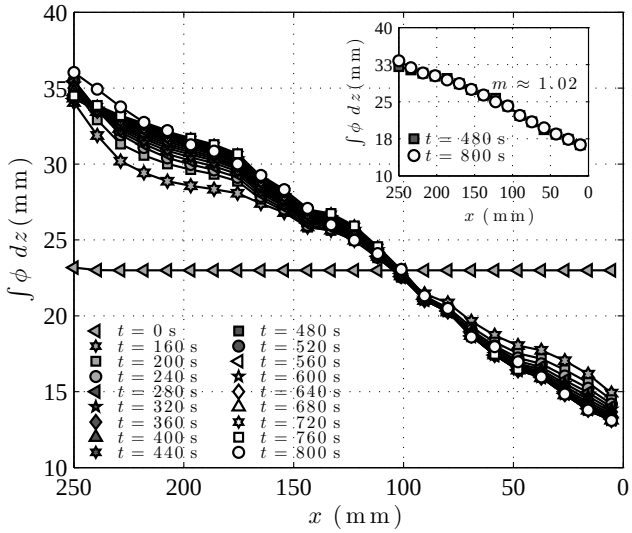

Figure 2.2.8: Accumulated particle mass, $\int \phi(x,z)\mathrm{d}z$, as a function of the longitudinal coordinate for different times. Inset: Particle accumulation for long times, with a slope close to $m \approx 1.02$. The corresponding integral has been calculated within the measurement window. Experimental conditions: $\phi_0 = 15.0 \pm 0.1\%$, $\eta_{f1} = 6.30 \pm 0.08$ mPa ·s and $\theta_s = 10.0 \pm 0.5^\circ$.

2.3 Results and discussion

A comparison between the experimental and simulated bed formation processes, summarized in Figure 2.3.1, shows an excellent agreement between the experiments and the numerical output. The striking similarity between simulations and experiments suggests that the dominant mechanism of sediment formation is not given by interparticle friction, but by fluid-mediated collisions. The rationale for this conclusion is that while the numerical model determines the pressure in both the continuous (fluid) and discrete (solid) phases, and so determines pressure forces for collision, and determines viscous shear stresses, it does not provide the contact friction associated with settling the angle of repose for dry material. This is consistent with the experimental observation of inelastic collisions for Stokes numbers below about 10, the latter defined by Courrech du Pont *et al.* (2003) as $St = (1/9)[\rho_s(\rho_s - \rho_f)ga^3 \sin(\theta_s - \theta_p)]^{1/2}/\eta_f$, whereas in the present set of experiments the Stokes and particle Reynolds number ranges are $0.00721 - 0.001474$ and $0.00370 - 0.03380$, respectively. A consequence of such a particle interaction mode is that there is no available kinetic energy left for bouncing (Gondret *et al.* , 2002; Joseph *et al.* , 2001).

Figure 2.3.2 shows the numerical particle velocity field superimposed on the experimental particle concentration obtained using the light extinction method described above, for an initial volume fraction of $\phi_0 = 0.15$, a viscosity of $\eta_f = 6.30$ mPa·s and two angle system (a) $\theta_s = 0^\circ$ and (b) $\theta_s = 20^\circ$. The numerical simulation predicts velocities below 0.5 mm/s above the sediment layer, whereas within the high concentration zone (extending about 15 mm above the bottom), the velocity is almost zero, indicating the final settled configuration of particles is reached.

The particle settling process that forms the sediment layer and controls its final angle is the consequence of three different processes that the particles experience in sequence, as anticipated in

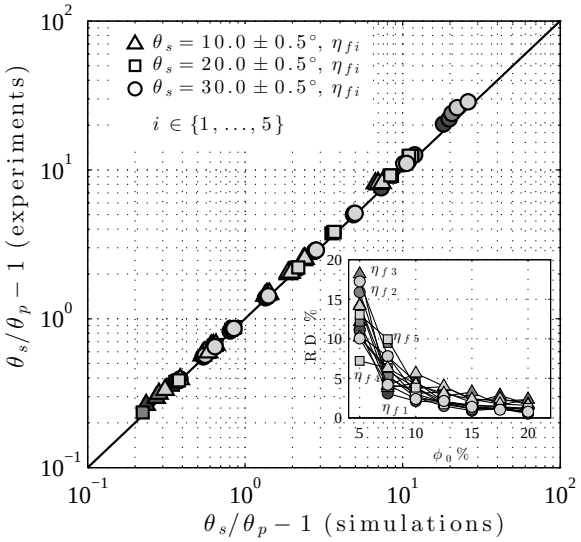

Figure 2.3.1: Comparison between experimental and numerical results. The solid line indicates the identity. Inset: Relative difference (RD %) between experiments and numerical simulations as a function of the initial volume fraction for different viscosities.

Section 3.1. Figure 2.2.8 shows that the settling process finally evolves into the formation of a sediment layer, whose upper surface was found to be approximately linear in most of the experiments and simulations. The first process is the quasi-vertical sedimentation of particles (Figure 2.3.3) that drives the linear increase with time seen in the height of the deposit. As particles approach, the sediment layer they contribute to the second process, the formation of a particle flow at a concentration near the packing value. This down-slope flow redistributes the particles towards the lower parts of the container, leading to the observed $\theta < \theta_s$. Additionally, this layer introduces the possibility of some degree of reorganisation due to collisions and local mixture viscosity values (Leighton & Acrivos, 1987). The final settled condition is obtained, with θ less than the angle of repose, after concentration increases and finally the direct contacts among each other render the particles immobile. Despite the existence of velocity fluctuations as predicted by Ham & Homsy (1988) (and references therein), for a many-particle interaction process and seen in the velocity fields of Figure 2.3.2, a Kynch-like sedimentation process, where local shearing is not predominant (except by the fluid-particle shearing) (Kynch, 1952), gives a good description of the settling.

The lower panel shows the sedimentation of quasi-monodisperse particles in a tilted container for different times. As the time passes, the particles begin to settle to the bottom of the container and progressively increase their angle θ_p, measured from the bottom of the container. Unlike the case when the container is upright, once the particles reach the bottom of the container, they start to move down due to the angle of inclination and gravity, until finally the motion ceases because of the increasing concentration of particles and the rapid dissipation of energy from the particle interactions (Gondret *et al.* , 2002; Joseph *et al.* , 2001) and, the final layer of sediment is formed. The dominance of the hindered settling mechanism is shown to fit the experimental concentration profile correction to the settling velocity with the hindrance function proposed by Richardson & Zaki (1954a), $F = (1 - \phi_0)^n$ (Figure 2.3.4). In addition to the excellent fit between experimental data and this model, the fit parameter ($n = 4.98$) closely resembles the typical value $n \approx 5$ referred in the literature (e.g. Davis & Acrivos, 1985; Guazzelli & Hinch, 2011). As the resulting dynamics of the sedimentation away from the container bottom (including the velocity fluctuations and particle

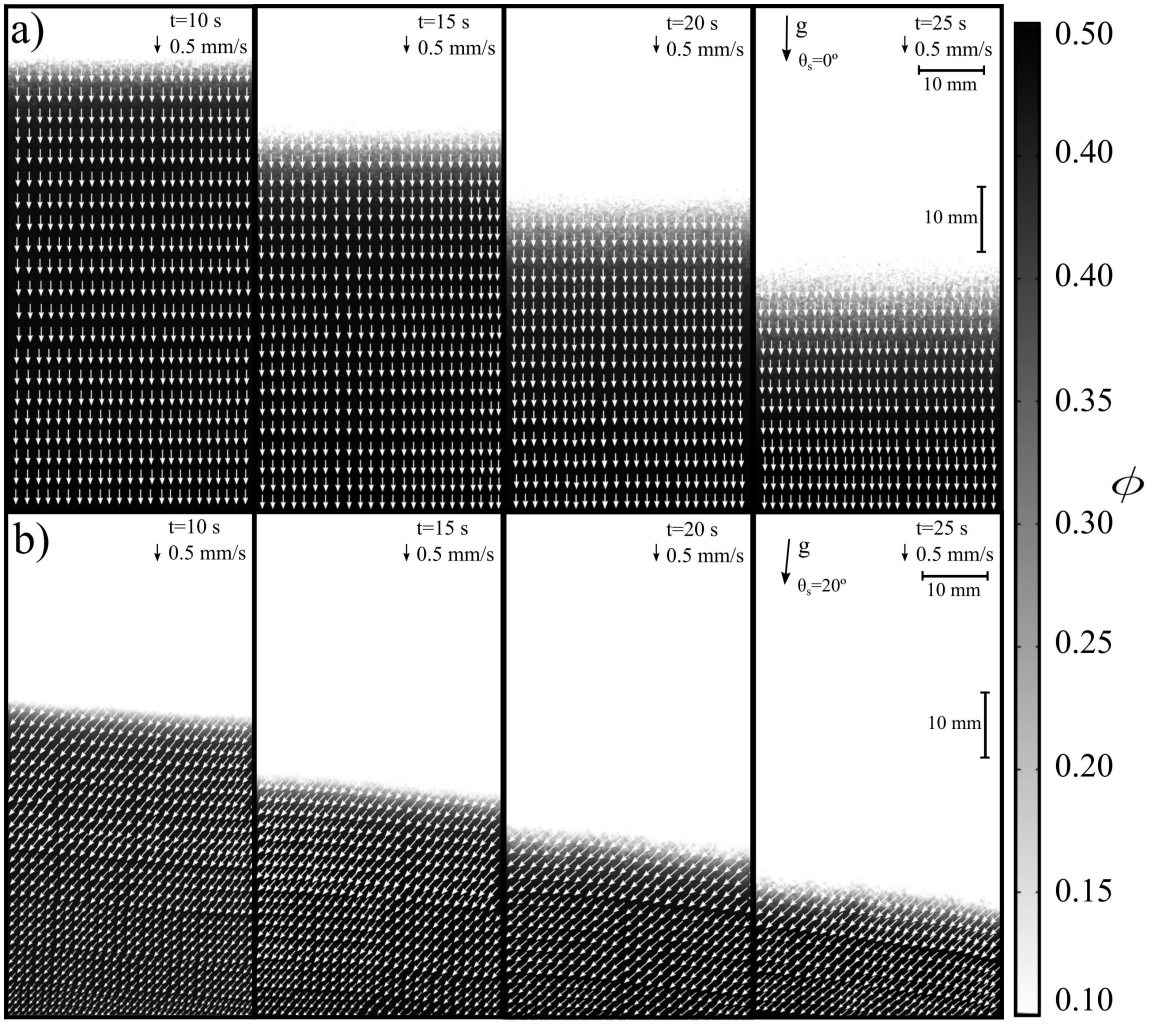

Figure 2.3.2: Evolution of the interface of the suspension, from 10 s to 25 s after the start of the experiment considering a frame of reference aligned with the bottom of the tank. θ_s corresponds to the angle of the bottom of the tank measured from the horizontal plane. The experimental conditions are $\phi_0 = 0.15$, $\eta_f = 6.3 \pm 0.08$ mPa·s for (a) $\theta_s = 0.0 \pm 0.5°$ and (b) $\theta_s = 20.0 \pm 0.5°$. The white arrows represent the computed particle velocity of the disperse phase, $\mathbf{u}_s$ from the numerical simulation for the same experimental conditions.

self-diffusion) has been found to be independent of the container size (Guazzelli & Hinch, 2011), the details of the flow near the boundaries of the container remain irrelevant for the purposes of the particle dynamics in the interior.

The mean height of the sediment layer increases with the bottom plane slope. (Figure 2.3.5). This result is consistent with the trend predicted by Kapoor & Acrivos (1995) using boundary layer arguments. As in their work, the present observations show a quasi-linear thickness profile in the range $\phi \in [0.05, 0.20]$. Figure 2.3.6 shows the final angle of the settled layer measured with respect to the horizontal, $\theta = \theta_s - \theta_p$, as a function of the initial volume fraction of particles, ϕ_0, for different viscosities, η_f, and container angles of inclination θ_s.

While for the smaller values of θ_s the final angle of the sediment layer tends to change linearly with the initial concentration, at the highest bottom angle, θ tends to decrease more abruptly with concentration. This is explained by both the nonlinearity of the individual particle velocity projection

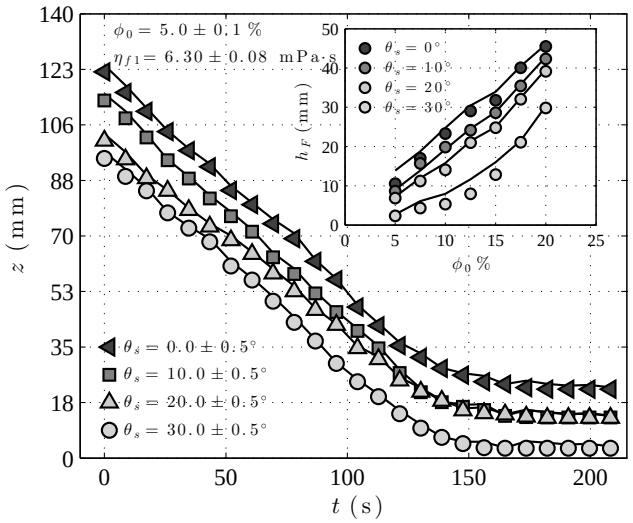

Figure 2.3.3: Time evolution of the height of the interface of the suspension, at $x = L/2$, for various container angles, $\phi_0 = 5\%$ and $\eta_f = 6.30 \pm 0.08$ mPa·s. The black solid lines represent the numerical simulations. Inset: Measured final height of the sediment layer as a function of the initial volume fraction of particles.

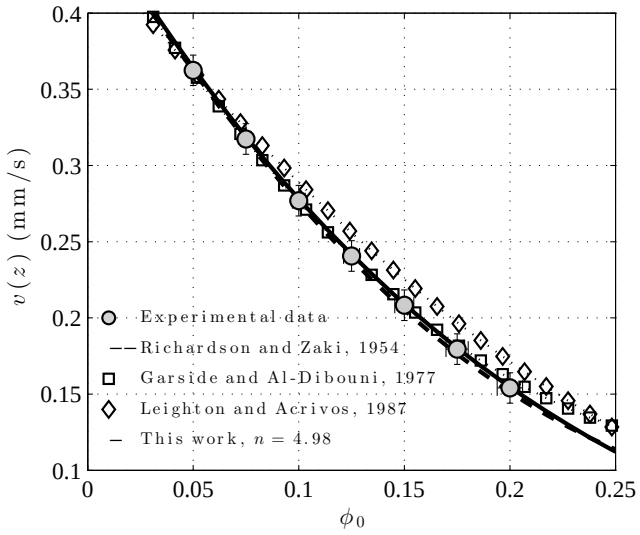

Figure 2.3.4: Velocity of the interface of the suspension, $w_s = w_0(1-\phi_0)^n$, in terms of the particle concentration. The best fit of the experimental data, using the Richardson-Zaki model corresponds to $n = 4.98$(Garside & Al-Dibouni, 1977; Leighton & Acrivos, 1987).

on the bottom slope and the increasingly important effect of the particle concentration on the settling bottom. Figure 2.3.6(a) shows that increasing the initial concentration towards the packing limit causes the difference between the angle of the sediment layer and the container to decrease to zero, implying that the sediment layer evolves to a position parallel to the bottom. An interpretation of this trend is that for initial concentrations approaching the packing limit, the mean free path between particles is on the order of one particle diameter. A time scale for the encounter of two of them, before an inelastic contact occurs, is $4\rho_f a^2/\eta_f$. Assuming that the prevailing energy dissipation precludes the occurrence of interparticle friction, then at volume fractions near the maximum packing fraction, particles tend to end their motion near their starting point, and thus $\theta \to 0$ in this limit. However, for volume

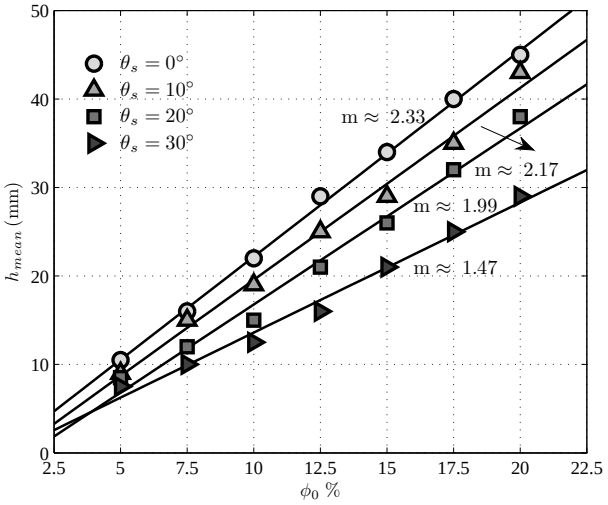

Figure 2.3.5: Mean height of the sediment layer, h_{mean}, as a function of the initial volume fraction and container inclination. The solid lines are for visual aid purposes.

fractions much smaller than the packing limit, it is possible to see, in light of the present numerical simulations and experimental results, that the vertical settling stage accounts for a significant part of the overall effect of the particle concentration in the formation of the final angle of the sediment layer. Figure 2.3.6(b) shows that θ is independent of viscosity in the viscous flow experiments range investigated. Courrech du Pont *et al.* (2003) have explained this as the result of the flow of particles for small Stokes numbers.

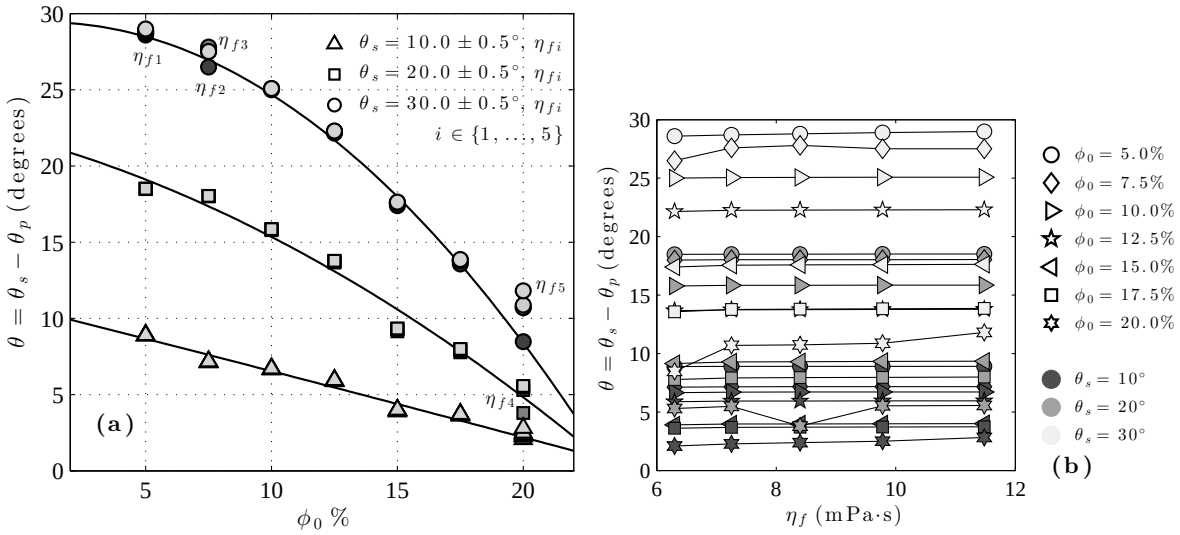

Figure 2.3.6: Final angle of the sediment layer, $\theta = \theta_s - \theta_p$, as a function of: (a) the initial volume fraction and (b) of different viscosities, η_{fi}. The solid lines are for visual aid purposes.

During the final stages of the particle motion, the individual particle momentum decays due to the collisions with their neighbours and due to the interaction with the ambient fluid. This process may be explained following a rheological constitutive model relating particle microscopic rearrangements with the time scale resulting from the (macroscopic) shear rate, modelled by Forterre & Pouliquen (2008)

(and references therein) as

$$\tau = P\mu(I). \tag{2.3.1}$$

Here, τ is the shear stress, P is the pressure and μ is a friction coefficient, expressed in terms of $I = 2a\dot{\gamma}/\sqrt{P/\rho_s}$. The dimensionless variable I can be interpreted as the ratio between two time scales: (a) a microscopic time scale $2a/\sqrt{P/\rho_d}$, which represents the time it takes for a single particle to fall in a hole of size $2a$ under the pressure P and which gives the typical time of rearrangements, and (b) a macroscopic time scale $1/\dot{\gamma}$ related to the mean deformation. Here, $\dot{\gamma}$ is the shear rate and a is the particle radius. It has been recently shown that both (2.3.1) and the dimensionless number I are useful not only for characterising dry granular flows, but also for granular flows when the ambient fluid is viscous (Courrech du Pont *et al.* , 2003; Cassar *et al.* , 2005). An example is given by Courrech du Pont *et al.* (2003), where they used a rotating drum geometry to predict the final angle of both dry and liquid-immersed spheres: the corresponding equilibrium angles have been effectively expressed in terms of I using the Stokes number as a means to distinguish whether the particle motion is dominated by gravity, inertia or viscous dissipation. While in the first case the particles keep accelerating, in the last they effectively reach their terminal velocities.

In the present experiments, the spheres fall and feed a dense layer until all the particles are within the sediment layer. A downward motion occurs until the overall system energy is exhausted and a static layer of angle $\theta_s - \theta_p$ is formed. It is observed that a relevant velocity scale in the problem is the sedimentation velocity, $w_s = w_0 F(\phi_0)$ (w_0 is the settling velocity of an individual particle in an infinite medium), with F a hindrance function as described above. In the present flow, the sheared region near the bottom is a few spheres thick, and so the particle radius will be considered as a characteristic length scale. Although during the particle vertical descent phase (before the influence of the inclined bottom) there is no significant shear, the bottom of the container induces some vorticity in its vicinity and a thin, particle-rich layer develops to carry the particles down slope as they sediment onto the sediment layer. In this layer, the shear rate scales with $\dot{\gamma} \sim w_s \sin\theta_s/a$, the settling velocity projection parallel the container bottom. This flowing layer provides a scale for the granular pressure from the immersed weight and projected area of the particles giving $P \sim (4/3)g(\rho_s - \rho_f)a$. The dimensionless parameter I may be then expressed in this viscosity dominated system as $I = Re_p\,(I_0 r)^{1/2}\sin\theta_s$, where $Re_p = 2a\rho_f w_s/\eta_f$ is the usual definition for the particle Reynolds number, $r = \rho_s/\rho_f$ and $I_0 = (3/4)\eta_f^2/\rho_f g(\rho_s - \rho_f)a^3$. In the present set of experiments the particle Reynolds numbers are in the Stokes regime. The weak dependence of the final angle of the sediment layer on the ambient fluid viscosity, along with the fundamental idea in the constitutive model of Cassar *et al.* (2005) that the friction coefficient is a simple function of the dimensionless parameter I, suggests a relation $\mu \sim I = (Re_p \sin\theta_s)^{c_1}\,(I_0 r)^{\frac{c_2}{2}}$, where for $c_1 = c_2 = 1$ the expression becomes independent of the fluid viscosity within Stokes flow.

Near the bottom, the inertia of the layer flowing down slope is likely to scale with buoyancy. If v_b is the velocity of this layer, then $g(\rho_s - \rho_f) \sim \rho_f v_b^2/\ell$, where the corresponding length scale is taken as the interparticle distance near the bottom, $\ell = 2a(\phi_m/\phi)^{1/3}$ (Bagnold, 1954; Coussot & Ancey, 1999). Thus, $\frac{2ag(\rho_s-\rho_f)/\rho_f}{v_b^2} \sim (\phi/\phi_m)^{1/3}$. Again, adding a monomial function to μ yields $\mu \sim (Re_p \sin\theta_s)^{c_1}\,(I_0 r)^{\frac{c_2}{2}}(\phi/\phi_m)^{\frac{c_3}{3}}$, where this time $c_3 = 1$ reflects the proposed scaling. Figure 2.3.7 shows the best fit for this model in terms of the slope of the final angle of the sediment layer, $\mu = \tan\theta$, and the dimensionless combination $(Re_p \sin\theta_s)^{c_1}\,(I_0 r)^{\frac{c_2}{2}}(\phi/\phi_m)^{\frac{c_3}{3}}$. The results indicate an excellent

fit, with $c_1 = 1.09 \pm 0.01$, $c_2 = 1.03 \pm 0.02$ and $c_3 = 1.11 \pm 0.02$ with a prefactor close to 2.4. The fact that the parameters c_1, c_2 and c_3 are close to the unity confirms that the viscosity does not play a significant role, provided it is high enough to ensure that the particle Reynolds number is well below the unity.

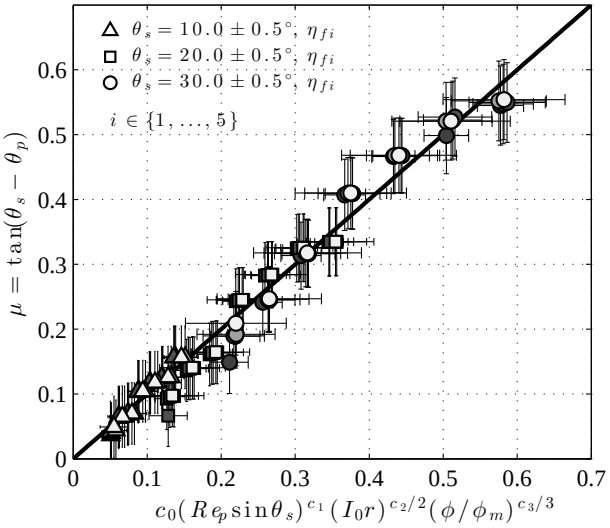

Figure 2.3.7: Data fit for μ as a function of the dimensionless group $(Re_p \sin\theta_s)^{c_1} (I_0 r)^{\frac{c_2}{2}} (\phi/\phi_m)^{\frac{c_3}{3}}$. The solid line indicates the identity.

2.4 Conclusions

The work presented here provides new insight into the mechanism that sets the morphology of the sediment layer formed by the settling of quasi-monodisperse particles onto the bottom of an inclined container. A key finding is that the final angle adopted by the sediment layer shows strong dependencies on the initial particle concentration and the container inclination, but not the fluid viscosity. The idea of hindered settling is central to understanding these results as it allows the formation of a particle-rich layer that advects particles down-slope just above the sediment layer as it forms. Indeed, our results suggest that the result of this mechanism scales directly with the projection of the hindered settling velocity onto the sloping deposit.

While hindered settling depends on viscous forces as well as continuity requirements, the fluid viscosity does not play a direct role in setting the final morphology for low particle Reynolds numbers as it enters the settling velocity $w_s = w_0 F(\phi)$, and consequently the settling flux ϕw_s, only through w_0. Viscosity does, however, control the time scale over which the morphology is established. In contrast, the final state depends strongly on the initial concentration as this enters the settling flux in a nonlinear manner. That fluid-mediated particle interactions (via the hindrance function) dominate over solid friction is demonstrated through our numerical simulations. These simulations that reproduce the experimental results despite using a mixture model that is devoid of any solid friction term and considers the granular material as incompressible. This, in turn, confirms that the dissipation is dominated by viscous forces as the particles approach rather than solid friction after they collide.

Although the present study has been performed in a container with a fixed aspect ratio, it is reasonable to speculate how this may affect the morphology of the sediment layer. For a given initial concentration and container width, increasing the container height will increase the period of time during which the particle-rich layer flows down slope above the developing sediment deposit, and so we would expect the surface of the final deposit to be more horizontal in a manner similar to the decrease in θ seen here by increasing the initial concentration. Conversely, increasing the width of the container (while keeping the height constant) will not significantly alter the down-slope flux while increasing the volume of particles needing to be transported to achieve a given θ. Thus, we would expect θ to increase towards θ_s and the deposit to be of a more uniform thickness (for extreme high or low aspect ratios, the Boycott effect may become important and contribute to the final slope in a manner not described here). Additionally, simply changing the size of the container while maintaining the same aspect ratio will change the time scale over which the sediment layer is created, but not its morphology.

Finally, from a practical point of view, these results are important for future application in engineering sciences, specifically in chemical and pharmaceutical industry (e.g., the application of blood cell sedimentation for monitoring of the bioequivalence of drugs based on acetylsalicylic acid), petroleum and mining industry (e.g., transporting of copper concentrates and mining waste), as well as in many kinds of industrial separation processes of granular material from a fluid (e.g., water treatment). In mineral processing, the concentration stage uses water as a carrier fluid for comminution products, where an important part of the fluid is recovered in thickeners. Although the settling mechanism in the mid section of thickeners is vertical, the bottom of these equipment is conical, inducing a particle flow component parallel to the bottom. On the other hand, in the wastewater treatment industry it is common to find lamella settlers, whose working principle is the Boycott effect. Knowing that the final angle adopted by the sediment layer shows strong dependencies on the initial particle concentration and the container inclination, but not the fluid viscosity in this Stokes number range, might improve the design and operation in these examples.

Acknowledgements

The authors acknowledge the support of the National Commission for Scientific and Technological Research of Chile, CONICYT, Grant N° 21110766, Fondecyt Projects N° 11110201 and N° 1130910, the Department of Civil Engineering, the Department of Mining Engineering and the Advanced Mining Technology Center of the University of Chile, as well the staff of the G.K. Batchelor Laboratory, Department of Applied Mathematics and Theoretical Physics, University of Cambridge.

2.5 Appendix

2.5.1 Drag coefficient

To characterize the drag coefficient β for the drag force $\mathbf{F}_{m,f} = -\mathbf{F}_{m,s} = \beta(\mathbf{u}_s - \mathbf{u}_f)$ in the numerical model, the method proposed by Gidaspow (1994) along with the model by Wen & Yu (1966) has been used. Specifically,

$$\beta = \begin{cases} \frac{150\eta_f\phi_s^2}{\phi_f \mathrm{d}_s^2} + \frac{1.75\phi_s\rho_f|\mathbf{u}_{\mathrm{slip}}|}{\mathrm{d}_s} & \phi_{\mathrm{d}} < 0.20 \\ \frac{3\phi_f\phi_s\rho_f c_D|\mathbf{u}_{\mathrm{slip}}|\phi_f^{-2.65}}{4\mathrm{d}_s} & \phi_s > 0.20, \end{cases} \tag{2.5.1}$$

where $\mathbf{u}_{\mathrm{slip}} = \mathbf{u}_s - \mathbf{u}_f$, the diameter of the particles is d_s and c_D is the drag coefficient for a single particle. The drag coefficient is a function of the particle Reynolds number, and is determined from,

$$c_D = \begin{cases} \frac{24}{Re_p}\left[1 + 0.15Re_p^{0.687}\right] & Re_p < 1000 \\ 0.44 & Re_p > 1000. \end{cases} \tag{2.5.2}$$

The particle Reynolds number in the model is defined as $Re_p = \phi_f \mathrm{d}_s \rho_f |\mathbf{u}_{\mathrm{slip}}| / \eta_f$. Finally, for mixtures of particles and fluid, it is necessary to have a model for the solid pressure, p_s in (3.2.4). The solid pressure models the particle interaction due to collisions and friction between the solid particles. The implemented approach uses a gradient-based diffusion model expressed as $\boldsymbol{\nabla} p_s = -\chi(\phi_f)\boldsymbol{\nabla}\phi_f$, where the empirical function $\chi(\phi_f)$ has the form $\chi(\phi_f) = 10^{a_1\phi_f + a_2}$. The function $\chi(\phi_f)$ represents the modulus of elasticity for the dispersed phase and has dimensions of pressure in the international system of units (Ettehadieh *et al.* , 1984). Here, $a_1 = -10.50$ and $a_2 = 9.00$ (Gidaspow *et al.* , 1989).

2.5.2 Error analysis of ϕ

If ϕ is a function that depends on five variables $\phi = \phi(\alpha_1, \alpha_2, \alpha_3, \alpha_4, \overline{\mathrm{i}_n})$, equation (3.2.1), where $\Delta\alpha_1$, $\Delta\alpha_2$, $\Delta\alpha_3$, $\Delta\alpha_4$ and $\Delta\overline{\mathrm{i}_n}$ are the uncertainties of the variables, respectively. The error of ϕ can be calculated by $\Delta\phi = \sqrt{\sum_{\mathrm{i}=1}^{N}\left(\left(\partial\phi/\partial x_{\mathrm{i}}\right)\Delta x_{\mathrm{i}}\right)^2}$, (Taylor, 1982). Then, the final expression for the error of ϕ can be expressed as follow,

$$\Delta\phi = \sqrt{\Delta\nu^2\left(\alpha_1\alpha_2\nu^{\alpha_2-1} + \alpha_3\right)^2 + \nu^{2\alpha_2}\Delta\alpha_1^2 + \nu^{2\alpha_2}\log(\nu)^2\alpha_1^2\Delta\alpha_2^2 + \nu^2\Delta\alpha_3^2 + \Delta\alpha_4^2} \tag{2.5.3}$$

where we have defined, $\nu \equiv \overline{\mathrm{i}_n}$. Figure 2.5.1 shows the results of the error calculations.

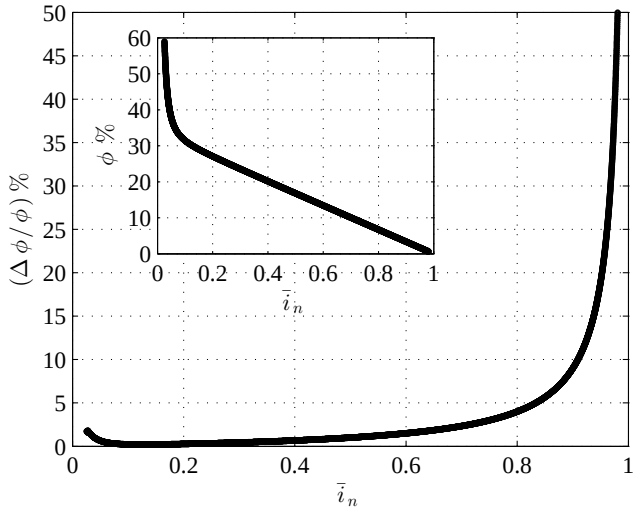

Figure 2.5.1: Percentage error of the volume fraction of particles $(\Delta\phi/\phi)$ % as a function of the mean normalized transmitted light intensity over the container, equation (2.5.3). Inset: Volume fraction of particles as a function of the mean normalized transmitted light intensity over the container, equation (3.2.1).

Chapter 3

Characterization of a sediment layer in tilted ducts

This chapter has been submitted as research paper, authored by Sergio Palma, Christian Ihle and Aldo Tamburrino, in the International Journal of Multiphase Flow (2016) (under revision).

Abstract

In this paper we use a continuum mixture model to solve numerically the momentum and continuity equations associated with the sedimentation dynamics of highly concentrated fluid-solid mixtures in tilted duct at low Reynolds numbers. The set of numerical simulations include several combinations of fluid viscosity, duct angle and solid concentration of particles. This research aims to show the phenomenology and dynamics associated with the sedimentation of monodisperse particles under different physical conditions and the characterization of the final stage of the sediment layer in two kinds of inclined geometries, with and without a horizontal section. Using scaling arguments, a mathematical expression formed by three dimensionless groups including the inertial number, particle concentration and the ratio between the sedimentation Grashof number to the Reynolds number is proposed to explain the height of the sediment layer in the slope change zone of a duct. Additionally, we have found that the initial particle concentration is a very relevant variable for knowing under what conditions the duct could get obstructed. In combination with some system angles, they might represent a risk of duct plug. Imposing a condition of obstruction, we have found dimensionless parameters that result in the blockage of the duct in the slope change zone. The results can be applied in the transport of fluid-solid mixtures and, in the engineering design of ducts with abrupt slope changes.

3.1 Introduction

Sedimentation is the process by which solid particles immersed in a fluid are deposited at the bottom by the action of gravity. Sedimentation is one of the oldest known techniques used in industry to clean fluids or, alternatively, to recover particles from suspensions (Guazzelli & Hinch, 2011). In 1920, Boycott noted that certain blood corpuscles settled faster at the bottom in inclined test tubes than in test tubes that were in an upright position. This improvement in the sedimentation velocity is due to that in an inclined duct, the suspension has a short distance to reach the lower side of the duct, before they start to slide down to the bottom of the duct, whereas in a upright duct all the sediment is slow and there is no vertically rapid sliding (Leung & Probstein, 1983; Leung, 1983).

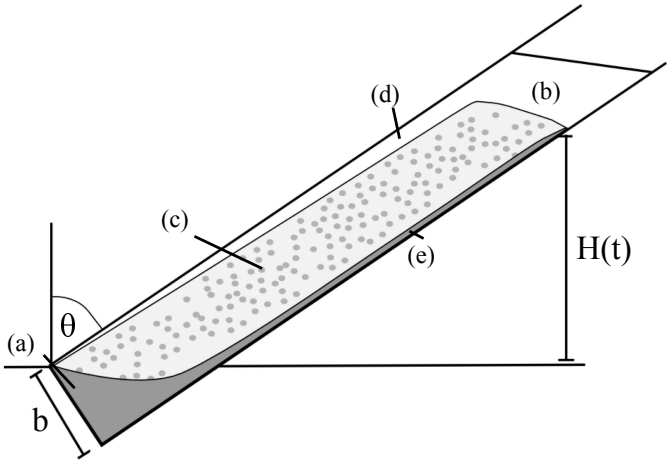

Figure 3.1.1: Schematic of the conceptual model: (a) Sediment bed, (b) Clear fluid region, (c) Suspension region, (d) Clear fluid region and (e) Sediment layer.

For almost five decades the behaviour of inclined settlers was described using a kinematic model called PNK in recognition of Ponder (1926) and Nakamura & Kuroda (1937) who developed it. A typical phenomenon observed in inclined settlers for laminar flow is displayed in Figure 3.1.1. The PNK model states that the production rate of clear fluid per unit depth of a rectangular settler is given by $S = w_0 F\,[\cos\theta + H\tan\theta/b]$, where w_0 is the sedimentation velocity of a particle, F is a hindered function which accounts for the interaction of many particles immersed in a fluid, θ is the angle of inclination of the system, H is the instantaneous height of the suspension and b is the space between the walls of the duct. PNK theory often overestimates the efficiency of an inclined settler, however it does not consider the dynamics of fluid movement as it is based solely on a mass balance (Acrivos & Herbolzheimer, 1979). When a settler is inclined, a thin layer of clear fluid is formed along the upper wall. Due to the density of the fluid being less than the density of the suspension in the vicinity, a force is experienced which causes the fluid to accelerate upwards (Guazzelli & Morris, 2012).

Resistance to this upward movement is given by the viscous and inertial forces acting within the clear fluid layer as well as the upper wall of the settler and regions of particle suspension. If the velocities within the layer of clear fluid are very large, it might be possible that waves appear along

the interface between the suspension region and the clear fluid layer. These waves can grow and break as they ascend to the settler, thus dragging the suspension to the clear fluid layer and decreasing the efficiency of the settler (Herbolzheimer, 1983). In order to predict the performance of an inclined settler, it is necessary to describe the formation and growth of these instabilities.

Works related to the dynamics of suspensions in tilted settlers in the decade preceding ninety, can be found in Davis & Acrivos (1985). Current analytical theories to describe the dynamics of suspensions in tilted ducts are generally based on the analysis presented by Acrivos & Herbolzheimer (1979), who studied the process using a simplified model. The equations used consist of a continuity equation for each phase, i.e., one for the solid phase and one for the fluid phase, an equation of momentum mixture describing the suspension of particles as a whole and a relationship between the velocities of each phase. Neglecting inertial effects and assuming that the suspension region has a uniform concentration of solids, these authors used boundary layer analysis to find expressions for the geometry and flow within the clear fluid layer. In addition, they determined that the kinematics of the sedimentation process is described by two dimensionless groups, a sedimentation Reynolds number and quotient of a settler Grashof and Reynolds number, which are given by $R\mathrm{e} = Hw_0F\rho_f/\eta_f$ and $\Lambda = H^2g(\rho_s - \rho_f)\phi/\eta_f w_0 F$, respectively. In this expression, ϕ is the volume fraction of particles in the suspension zone. The hypothesis of negligible inertial forces established in the work of these authors implies that the analysis is limited to the settlers where $\Lambda \gg 1$ and $R\mathrm{e}\Lambda^{-1/3} \ll 1$.

Finally, they found that the rate of production of clear fluid would be predicted by the theory PNK whenever the interface between the suspension region and the clear fluid layer remains stable and $\Lambda \to \infty$. Herbolzheimer (1983) developed this analysis to settlers under viscous conditions ($R\mathrm{e}\Lambda^{-1/3}$) and he compared his theoretical results with experimental results of instability waves on the interface. Later, Shaqfeh & Acrivos (1986) included inertial effects and extended the theory for all values of $R\mathrm{e}\Lambda^{-1/3}$. Comparisons between experimental and analytical results for the clear fluid layer predicted by this theory have been very satisfactory, particularly for the more viscous cases where $R\mathrm{e}\Lambda^{-1/3}$ is small. In this paper we have used a continuum mixture model to solve numerically the momentum and continuity equations associated with the sedimentation dynamics of high concentrated fluid-solid mixtures in tilted ducts. While previous works were able to describe the operation of settlers when the interface of clear fluid layer is stable, they do not define under what kind of conditions this occurs. Acrivos and other researchers have applied linear stability theory to the region surrounding the clear fluid layer to find conditions under which small perturbations in the interface will grow over time. Subsequently, Nir & Acrivos (1990) did experiments on inclined surfaces and found that for given values of the concentration of particles in the suspension, the sediment flow remained constant only if the angle of the system exceeded a minimum value. Additionally, a discontinuity in the concentration of particles in the suspension was found.

Afterwards, Kapoor & Acrivos (1995) implemented the model proposed by Nir & Acrivos (1990) but including the effects of shear-induced diffusion due to gradients in the shear stress likewise the slip velocity along the walls of the duct. The focus of this research is on the nonlinear dynamics associated with the migration of particles at low slopes, and in particular the consequences for axial transport of solid material under these conditions, with emphasis on the conditions for the generation of obstructions at high particle fractions. In Section3.2, we provide the mathematical model used for our numerical simulations, and the numerical procedure used in our calculations. In Section 3.3, the results of our numerical simulations are presented and discussed. Finally, the conclusions are showed in Section 3.4.

3.2 Governing equations

A set of numerical simulations has been made using COMSOL Multiphysics with the CFD package, featuring the multiphase model proposed by (Enwald *et al.* , 1996), which is described as follows. The dynamics of a suspension can be modelled by two equations of momentum transfer, one for particles and the other for the fluid, plus a continuity equation for both phases. Assuming that the mass transfer between the two phases is zero, the continuity equations for the continuous and dispersed phase are, respectively, $\partial_t(\rho_f\phi_f) + \boldsymbol{\nabla}\cdot(\rho_f\phi_f\mathbf{u}_f) = 0$ and $\partial_t(\rho_s\phi_s) + \boldsymbol{\nabla}\cdot(\rho_s\phi_s\mathbf{u}_s) = 0$, where ϕ is the volume concentration, ρ is the density and $\mathbf{u}$ is the velocity. The subscripts f and s refer to quantities associated with the continuous phase (fluid) and the dispersed phase (particles). In this model, both the continuous and the dispersed phase are considered incompressible. Therefore, the above equations can be simplified as,

$$\frac{\partial\phi_f}{\partial t} + \boldsymbol{\nabla}\cdot(\phi_f\mathbf{u}_f) = 0, \tag{3.2.1}$$

$$\frac{\partial\phi_s}{\partial t} + \boldsymbol{\nabla}\cdot(\phi_s\mathbf{u}_s) = 0. \tag{3.2.2}$$

If equations (3.2.1) and (3.2.2) are coupled by the volume conservation condition $\phi_f + \phi_s = 1$, an equation of continuity for the mixture is obtained,

$$\boldsymbol{\nabla}\cdot(\phi_s\mathbf{u}_s + \mathbf{u}_f(1-\phi_s)) = 0. \tag{3.2.3}$$

The momentum equations for the continuous and dispersed phase, respectively, using the non-conservative form introduced by Ergun (1952) are,

$$\rho_f\phi_f\left[\frac{\partial\mathbf{u}_f}{\partial t} + (\mathbf{u}_f\cdot\boldsymbol{\nabla})\mathbf{u}_f\right] = -\phi_f\boldsymbol{\nabla}p + \boldsymbol{\nabla}\cdot(\phi_f\boldsymbol{\tau}_f) + \phi_f\rho_f\mathbf{g} + \mathbf{F}_{m,f}, \tag{3.2.4}$$

$$\rho_s\phi_s\left[\frac{\partial\mathbf{u}_s}{\partial t} + (\mathbf{u}_s\cdot\boldsymbol{\nabla})\mathbf{u}_s\right] = -\phi_s\boldsymbol{\nabla}p + \boldsymbol{\nabla}\cdot(\phi_s\boldsymbol{\tau}_s) + \phi_s\rho_s\mathbf{g} + \mathbf{F}_{m,s}. \tag{3.2.5}$$

Here, p is the pressure of the mixture, which is assumed equal for both phases. The viscous stress tensor of each phase is indicated by $\boldsymbol{\tau}$ in the momentum equations, $\mathbf{g}$ is the acceleration due to gravity and $\mathbf{F}_m$ corresponds to the exchange of momentum between the phases, thus corresponding to a volume force exerted by one of the phases on the other phase. In the equations presented above, the influence of the polydispersity of the particles in the dispersed phase has been neglected. Equation (3.2.5) can be written as (Enwald *et al.* , 1996),

$$\rho_s\phi_s\left[\frac{\partial\mathbf{u}_s}{\partial t} + (\mathbf{u}_s\cdot\boldsymbol{\nabla})\mathbf{u}_s\right] = -\phi_s\boldsymbol{\nabla}p + \boldsymbol{\nabla}\cdot\boldsymbol{\tau}_s - \boldsymbol{\nabla}p_s + \phi_s\rho_s\mathbf{g} + \mathbf{F}_{m,s}, \tag{3.2.6}$$

where p_s is the solid pressure. In the momentum equations described above, the continuous phase is considered Newtonian. Hence, viscous stress tensor is defined as

$$\boldsymbol{\tau}_f = \eta_f \left[\boldsymbol{\nabla}\mathbf{u}_f + (\boldsymbol{\nabla}\mathbf{u}_f)^T - \frac{2}{3}(\boldsymbol{\nabla}\cdot\mathbf{u}_f)\mathbb{I} \right], \tag{3.2.7}$$

$$\boldsymbol{\tau}_s = \eta_s \left[\boldsymbol{\nabla}\mathbf{u}_s + (\boldsymbol{\nabla}\mathbf{u}_s)^T - \frac{2}{3}(\boldsymbol{\nabla}\cdot\mathbf{u}_s)\mathbb{I} \right], \tag{3.2.8}$$

where η is the dynamic viscosity of the respective phase and $\mathbb{I}$ is the identity tensor (Enwald *et al.* , 1996). In order to model the Newtonian viscosity associated to a set of particles in a mixture there is a variety of formulations. In this paper, we have worked with the model proposed by Krieger (1972) because is one of the most validated experimentally at high concentrations of particles over the years (Krieger & Dougherty, 1959; Frankel & Acrivos, 1967; Stickel & Powell, 2005). Specifically, we take

$$\eta_s = \eta_f \left(1 - \frac{\phi_s}{\phi_{s,\max}} \right)^{-2.5\phi_{s,\max}}. \tag{3.2.9}$$

In order to avoid singularities in the numerical solutions when volume concentrations tend to zero, the momentum equations are divided by their corresponding volume concentrations. Therefore, equation (3.2.4), corresponding to the continuous phase, becomes

$$\rho_f \frac{\partial \mathbf{u}_f}{\partial t} + \rho_f(\mathbf{u}_f\cdot\boldsymbol{\nabla})\mathbf{u}_f = -\boldsymbol{\nabla}p + \boldsymbol{\nabla}\cdot\boldsymbol{\tau}_f + \frac{\boldsymbol{\nabla}\phi_f\cdot\boldsymbol{\tau}_f}{\phi_f} + \rho_f\mathbf{g} + \frac{\mathbf{F}_{m,f}}{\phi_f}, \tag{3.2.10}$$

and equation (3.2.6), corresponding to the dispersed phase, becomes

$$\rho_s \frac{\partial \mathbf{u}_s}{\partial t} + \rho_s(\mathbf{u}_s\cdot\boldsymbol{\nabla})\mathbf{u}_s = -\boldsymbol{\nabla}p + \boldsymbol{\nabla}\cdot\left(\frac{\boldsymbol{\tau}_s}{\phi_s}\right) + \boldsymbol{\nabla}\phi_s\cdot\left(\frac{\boldsymbol{\tau}_s}{\phi_s^2}\right) - \frac{\boldsymbol{\nabla}p_s}{\phi_s} + \rho_s\mathbf{g} + \frac{\mathbf{F}_{m,s}}{\phi_s}. \tag{3.2.11}$$

The equations to be solved numerically simultaneously are (3.2.3), (3.2.10) and (3.2.11). On the other hand, the term associated to the interphase momentum transfer, especially in fluids having a high concentration of particles, is given by the drag force, defined as $\mathbf{F}_{m,f} = -\mathbf{F}_{m,s} = \beta(\mathbf{u}_s - \mathbf{u}_f)$, where β is the drag coefficient. For fluids with a high concentration of particles by volume, it can be calculated by the method proposed by Gidaspow (1994) in conjunction with the model proposed by Wen & Yu (1966) for the drag coefficient

$$\beta = \begin{cases} \dfrac{150\eta_f\phi_s^2}{\phi_f \mathrm{d}_s^2} + \dfrac{1.75\phi_s\rho_f|\mathbf{u}_{slip}|}{\mathrm{d}_s} & \phi_s < 0.20, \\ \dfrac{3\phi_f\phi_s\rho_f c_D|\mathbf{u}_{slip}|\phi_f^{-2.65}}{4\mathrm{d}_s} & \phi_s > 0.20. \end{cases} \tag{3.2.12}$$

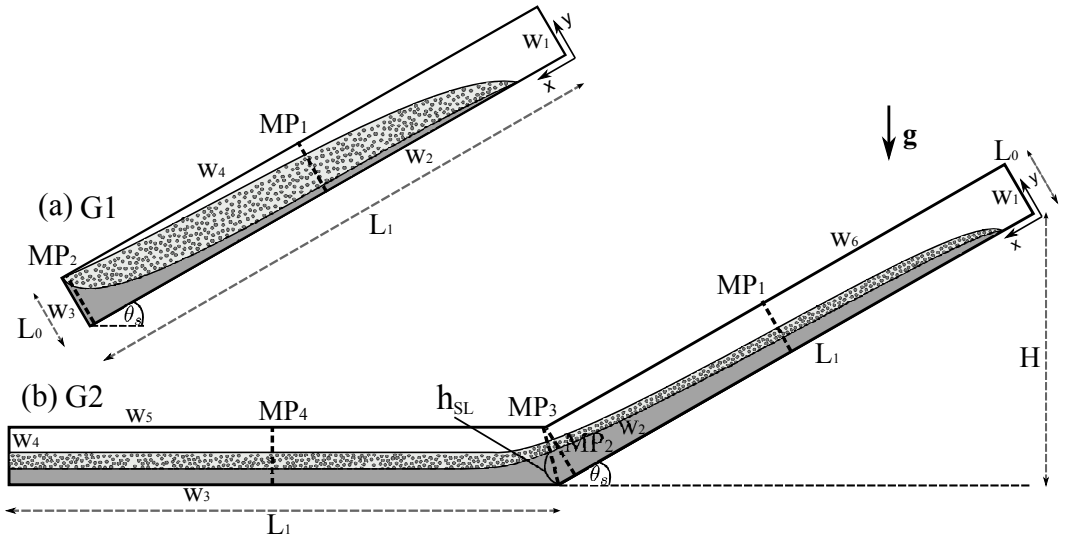

Figure 3.2.1: Schematic of the conceptual model: (a) G1: Inclined duct geometry. (b) G2: Inclined duct geometry plus a horizontal section. The walls of the ducts and measurement profiles are represented by w_j, with $j \in \{1, ..., 6\}$ and MP_j, with $j \in \{1, ..., 4\}$, respectively. The variable h_{SL} is used to test the convergence, as detailed in Figure 3.2.2.

Here, $\mathbf{u}_{slip} = \mathbf{u}_s - \mathbf{u}_f$ is the relative velocity between the solid and liquid phases, d_s is the diameter of the particles and c_D is the drag coefficient for a single particle in an infinite medium. The drag coefficient is a function of the particle Reynolds number, which is determined from

$$c_D = \begin{cases} \frac{24}{Re_p}\left[1 + 0.15 Re_p^{0.687}\right] & Re_p < 1000, \\ 0.44 & Re_p > 1000. \end{cases} \tag{3.2.13}$$

Furthermore, the local particle Reynolds number is defined as, $Re_p = \phi_f d_s \rho_f |\mathbf{u}_{slip}| / \eta_f$. For mixtures of particles and fluid, it is necessary to have a term associated with the interaction of particles. This term is commonly called solid pressure (p_s) (Gidaspow, 1994). The solid pressure models the particle interaction due to collisions and friction, between the solid particles. The solid pressure model implemented herein uses a gradient diffusion based assumption in the manner of $\boldsymbol{\nabla} p_s = -\chi(\phi_f)\boldsymbol{\nabla}\phi_f$, whereas the empirical function $\chi(\phi_f)$ has the form $\chi(\phi_f) = 10^{a_1\phi_f + a_2}$. The function $\chi(\phi_f)$ represents the modulus of elasticity for the dispersed phase (Ettehadieh *et al.* , 1984). Empirical values for the constants of this function have been obtained by different researchers (Gidaspow & Ettehadieh, 1983; Ettehadieh *et al.* , 1984). Although there are several coefficients a_1 and a_2 in the literature, the numerical results of the sedimentation process do not change significantly depending on the choice. Here, $a_1 = -10.50$ and $a_2 = 9.00$, with χ in Pa (Gidaspow *et al.* , 1989). This model is valid in the international system of measures.

The continuity equation of the mixture (3.2.3) and the momentum transport equations of both phases, (3.2.10) and (3.2.11), are discretized by the Galerkin finite element method (FEM) (Zienkiewicz *et al.* , 2013). The various simulation conditions have been given in Table 3.1. The boundary conditions associated with the computational domain can be seen in detail in Figure 3.2.1. Firstly, we consider no-slip conditions and no penetration for both phases in all domain borders, so that $\mathbf{u}_f = \mathbf{u}_s = \mathbf{0}$ at w_j, with $j \in \{1, ..., 6\}$, where w_j stands for the surface defining the wall j. Regarding the dispersed phase, we imposed a condition of no-flow to outside the settler, i.e., $\phi_s \mathbf{u}_s \cdot \mathbf{n} = 0$ at w_j and

$(1-\phi_s)\mathbf{u}_f \cdot \mathbf{n} = 0$ for the continuous phase. The system of equations has been integrated from 0 to 800 s, with a time step of 0.1 s which is about 1/4 of the time it takes a particle of the above features, to travel a distance equal to its own size at a velocity equal to the Stokes. However, due to the high storage space required for each of the simulations, only the information every 2 s has been stored.

Equations (3.2.3), (3.2.10) and (3.2.11) are nonlinear convection-diffusion equations. These may

Table 3.1: Set of parameters of numerical simulations.

Fluid-Solid properties	Value
Particle density, ρ_s (Kg/m^3)	1200
Fluid density, ρ_f (Kg/m^3)	1000
Particle diameter, d_s (μm)	600
Max. vol. fraction, $\phi_{s,max}$	0.62
Angle system, θ_s (°)	$[5, 10, 15, 20, 25, 30]$
Initial vol. fraction, ϕ_{d0} (%)	$[10, 15, 20, 25, 30, 35, 40]$
Fluid viscosity, η_f (mPa·s)	$[100, 200, 300]$
Numerical parameters	**Value**
Length scale 1, L_0 (mm)	40
Length scale 2, L_1 (mm)	500
Time step, Δt (s)	0.1
Simulation Time, T (s)	800

become numerically unstable when the Galerkin method is used for discretization. Therefore, it is necessary to apply stabilization techniques to the finite element method in order to obtain physically meaningful solutions. There are three types of methods in COMSOL Multiphysics to numerically stabilize the equations of the form $\partial_t u + (\beta \cdot \nabla)u = \nabla \cdot (c\nabla u) + F$, namely isotropic diffusion, diffusion of streamlines and crosswind diffusion. In the above equation, β is the convective velocity vector, c is the diffusion coefficient and u is the scalar property transported. When the convection-diffusion equation is discretized using the Galerkin finite element method, numerical problems occur for Peclet numbers greater than 1 that necessarily should be controlled in each time step, (Johnson, 1988).

The isotropic diffusion is equivalent to add a term, $c_{art} = \delta_{\text{id}} h\,|\beta|$, where h is the mesh size. Here, δ_{id} is an adjustable parameter. Thus, the equation which is solved in simple terms is $\partial_t u + (\beta \cdot \nabla)u = \nabla \cdot ((c + c_{art})\,\nabla u) + F$. It has used a value of $\delta_{\text{id}} = 0.25$ in all simulations because it is the best parameter value that allows to obtain properly the convergence of all calculations after a series of 30 preliminary tests. In order to choose an appropriate mesh size for the calculations, a set of simulations for different mesh sizes has been performed under four physical and numerical conditions as can be seen in Table 3.2. Figure 3.2.2 shows the height of the sediment layer at location MP_3 for the inclined geometry G2 (Figure 3.2.1) as function of the number of mesh elements. The solid line in Figure 3.2.2 represents the trend points for different physical conditions and the gray region represents the area of convergence of the numerical solutions.

Considering the input conditions of Table 3.2, it is observed that the height of the sediment layer reaches to $h_{SL} \approx 35$ mm, $h_{SL} \approx 33$ mm, $h_{SL} \approx 30$ mm and $h_{SL} \approx 10$ mm for Case 1, Case 2, Case 3 and Case 4, respectively, with about $10,000$ mesh elements, whereas it rapidly approaches to $h_{SL} \approx 35.21$ mm, $h_{SL} \approx 33.08$ mm, $h_{SL} \approx 30.14$ mm and $h_{SL} \approx 10.04$ mm for Case 1, Case 2, Case 3 and Case 4, respectively. Here, the convergence plateau starts using about $20,000$ mesh elements. Inside this region it was not possible to observe a significant difference in the variable h_{SL}

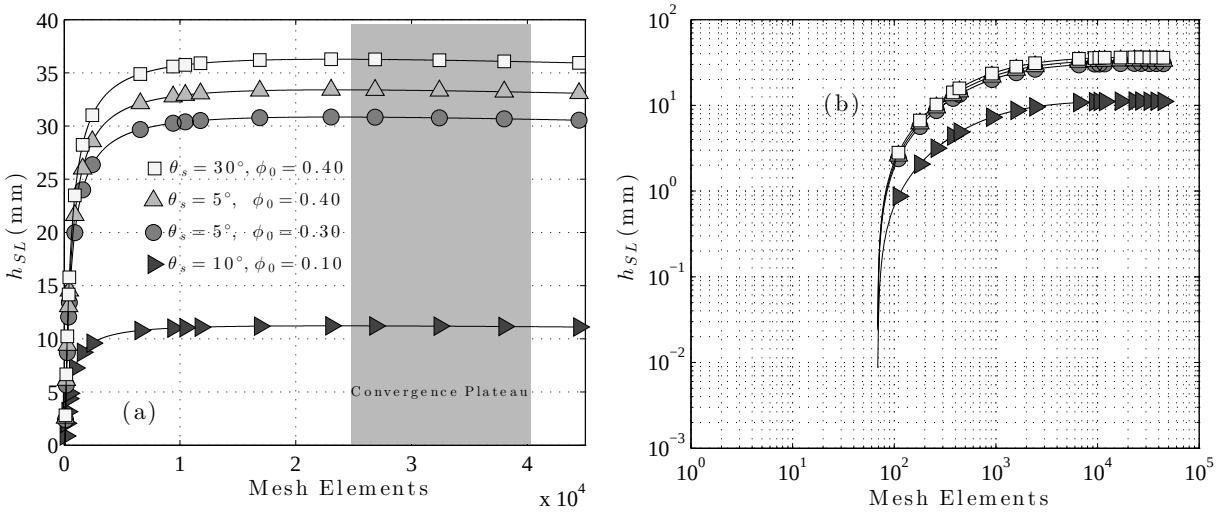

Figure 3.2.2: (a) Convergence of free triangular mesh. h_{SL} (mm) as function of number of mesh elements. The solid line represent the trend points for different physical conditions and gray region represents the area of convergence of the numerical solutions. (b) Same graph on a logarithmic scale.

with increasing the value of mesh elements. Given that, the finest mesh implies an 8 hours calculation in excess of the intermediate mesh within the plateau, and 12 hours relative to the coarsest using a 4th generation Intel Core i7 Processor.

In this work we have used a compromise number of free triangular mesh composed by $30,000$ elements in order to optimize the calculation time of all numerical simulations. The same procedure was performed to analyse the convergence of the solutions for geometry G1, thus obtaining the similar results. We have done the convergence analysis in MP_3 of the geometry G2 because of its relevance in the flux of particles in the sedimentation process. A physical validation of the results is given in the next section.

Table 3.2: Set of conditions for convergence analysis.

	Angle	Initial volume fraction
Case 1:	$\theta_s = 30°$	$\phi_0 = 0.40$
Case 2:	$\theta_s = 5°$	$\phi_0 = 0.40$
Case 3:	$\theta_s = 5°$	$\phi_0 = 0.30$
Case 4:	$\theta_s = 10°$	$\phi_0 = 0.10$

3.3 Results and discussion

A set of sedimentation numerical experiments was carried out under different physical conditions, including duct angles and particle concentrations. In order to measure and characterize the sediment layer in this type of geometry, a decision must be made to define the boundary between the sediment layer and the fluid clear layer. The height of the sediment layer, h_{SL}, has been defined when the

particle concentration along MP_3 is greater than or equal to 0.40. This value of the volume fraction corresponds to the abrupt transition in the particle concentration from 0.40 to very small values near to zero, (see Figure 2.2.6).

Figure 3.3.1 shows the sedimentation process of an initial homogeneous mixture of $\phi_0 = 0.30$ for geometry G1 (Left panel) and G2 (Right panel). Both panels correspond to the particle concentration field for $t = 200$ s, $t = 400$ s, $t = 600$ s and $t = 800$ s, whereas $t = 800$ s is the final time of the sedimentation process. In each figure, the insets show the detail of the particle concentration at the bottom of the duct as well as at the slope change zone, respectively, where the colour bar represents the concentration of particles. Here, the minimum and maximum concentration are 0 and 0.60, respectively. The numerical conditions are $\theta_s = 30°$, $\phi_0 = 0.30$ and $\eta_f = 100$ mPa·s. Such conditions have been chosen because they represent an experimental condition for a large angle, additionally a high concentration of particles, without necessarily being the largest concentration calculated. From this figure, we can infer that there is a difference of 25% in the height of the sediment layer at the extreme left of geometry G1 and G2 for $t = 800$ s. This difference in the build-up of granular material is due to the shape in the geometries; while a duct with a horizontal section shows a 73% of the accumulation of particles, the tilted geometry shows an accumulation near to the 100% of its total capacity, 98%.

On the other hand, Figure 3.3.2 shows the magnitude and direction of the velocity field of the dispersed phase (particles) for $t = 50$ s, $t = 100$ s, $t = 150$ s and $t = 200$ s for geometry G1 (Left panel) and G2 (Right panel), where the black arrows represent the particle flow direction and the colour bar represents the magnitude of the velocity of particles. Here, the minimum and maximum speed are 0 and 3.5 mm/s, respectively. We have shown the sedimentation process only for short times because at this time it is possible to observe more clearly the different stages of particle flow, both upward and downward the duct. The different stages of particle flow, both upward and downward the duct, have been described for other researchers considering only a tilted duct without a horizontal section (geometry G1) (Acrivos & Herbolzheimer, 1979; Herbolzheimer, 1983; Guazzelli & Morris, 2012). A comparison of the particle flow between G1 and G2 shows that although in the latter there is a horizontal section where the boundary condition is further away, the most important zone where the flow of particles is developed is in the inclined section. In particular, the inset of Figure 3.3.2 shows that there is a fraction of particles that move towards the horizontal section. Such amount of particles is quantified below.

Figure 3.3.3(a), shows the maximum magnitude of the velocity of the dispersed phase for: $\theta_s = 5°$, $\theta_s = 10°$, $\theta_s = 20°$ and $\theta_s = 30°$ for geometry G1 and G2 as a function of time. Such maxima occurs at $t = 100$ s, $t = 130$ s, $t = 160$ s and $t = 200$ s for $\theta_s = 30°$, $\theta_s = 20°$, $\theta_s = 10°$ and $\theta_s = 5°$, respectively. The measurements correspond to the line MP_1 (see Figure 3.2.1) and the numerical conditions are $\phi_0 = 0.30$ and $\eta_f = 100$ mPa·s. In addition, from Figure 3.3.3(a) it is observed that the upward flow is always faster than the downward flow independently of the angle of the system. In general, the magnitude difference between the upstream and downstream is 31%, 24%, 17% and 13% for $\theta_s = 5°$, $\theta_s = 10°$, $\theta_s = 20°$ and $\theta_s = 30°$, respectively, for both geometry G1 and G2. Once the process of settling on an inclined duct begins, a thin layer of free fluid particle appears in the upper wall of the duct. In this small layer free of particles, the fluid velocity is greater because it has a smaller section area than the suspension region, as can be seen in Figure 3.1.1, (see also (Herbolzheimer & Acrivos, 1981; Davis & Acrivos, 1985; Peacock *et al.* , 2005)). Figure 3.3.3(a) shows that the larger the angle of the duct, the velocities of the particles are larger both upward and downward. On the other hand, Figure 3.3.3(b) shows the measurements along MP_2. Here, the behaviour is totally different as mentioned

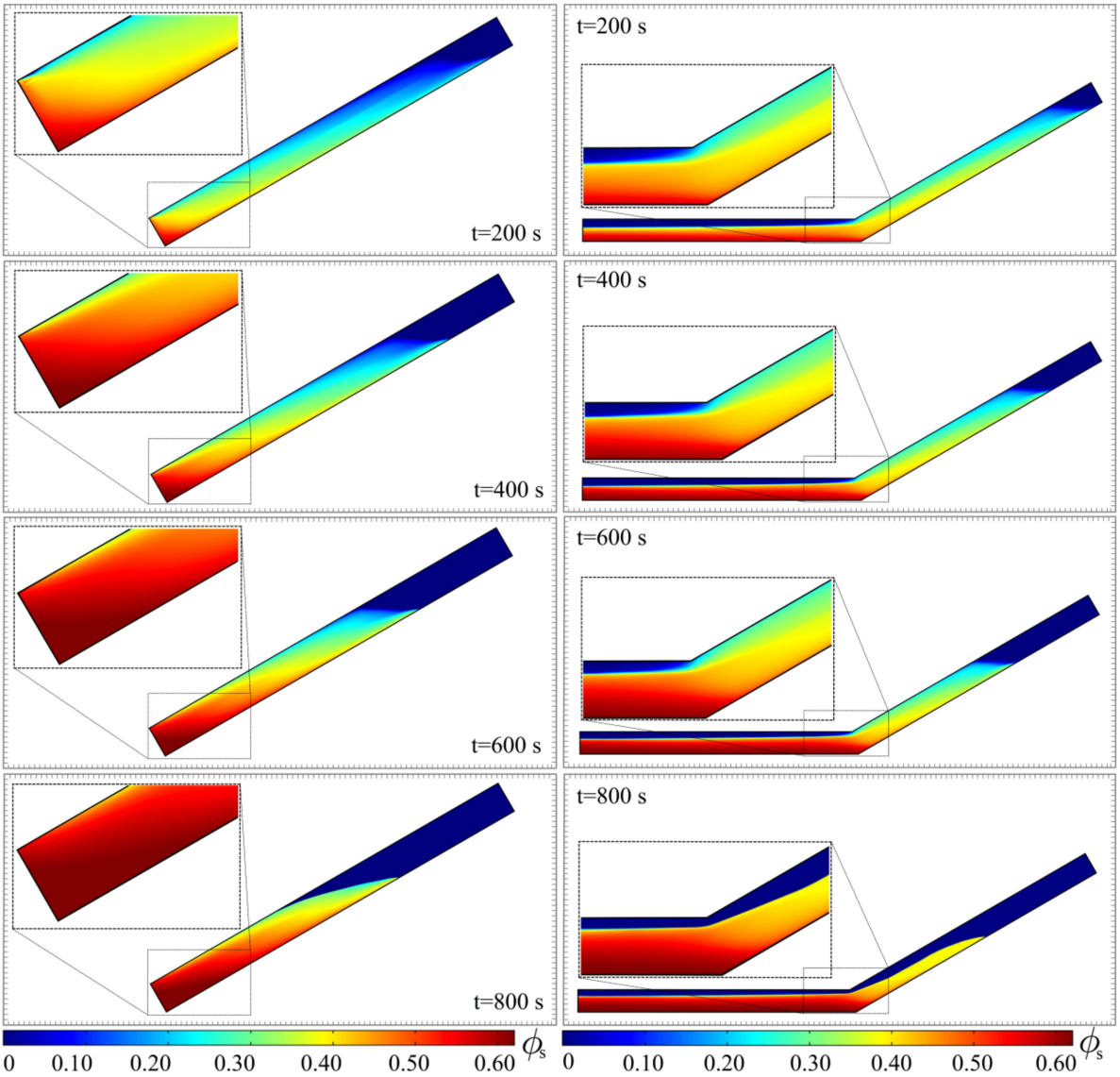

Figure 3.3.1: Sedimentation process and particle concentration field for $t = 200$ s, $t = 400$ s, $t = 600$ s and $t = 800$ s. Left panel: geometry G1 and right panel: geometry G2. Inset: detail of ϕ_s, at the bottom of the duct and at the slope change zone, respectively. The numerical conditions are $\theta_s = 30°$, $\phi_0 = 0.30$ and $\eta_f = 100$ mPa·s. The colour bar represents the concentration of particles.

above. It cannot clearly see when the peak in the velocity of the dispersed phase occurs, as in the previous case. However, the downward flow is faster than the upward flow. It can be seen from this figure that the maximum velocities of the particles decrease with the angle of the system. In this case, the maximum speeds only reach 2 mm/s. This value is approximately 1.5 times smaller than the value obtained in MP_1 for an angle of 30°. Here, the particle flow during the early stages of motion is greater going downwards than upwards. This can be attributed to the proximity to the change in slope area where conditions of symmetry in geometry are lost, unlike what happens in the previous case.

On the other hand, Figure 3.3.4 shows the maximum magnitude of the velocity of the dispersed phase for: $\theta_s = 5°$, $\theta_s = 10°$, $\theta_s = 20°$ and $\theta_s = 30°$ for G2 as a function of time. The measurements correspond to MP_3 and MP_4. Here, the measurements obtained from MP_4 show that the speeds are

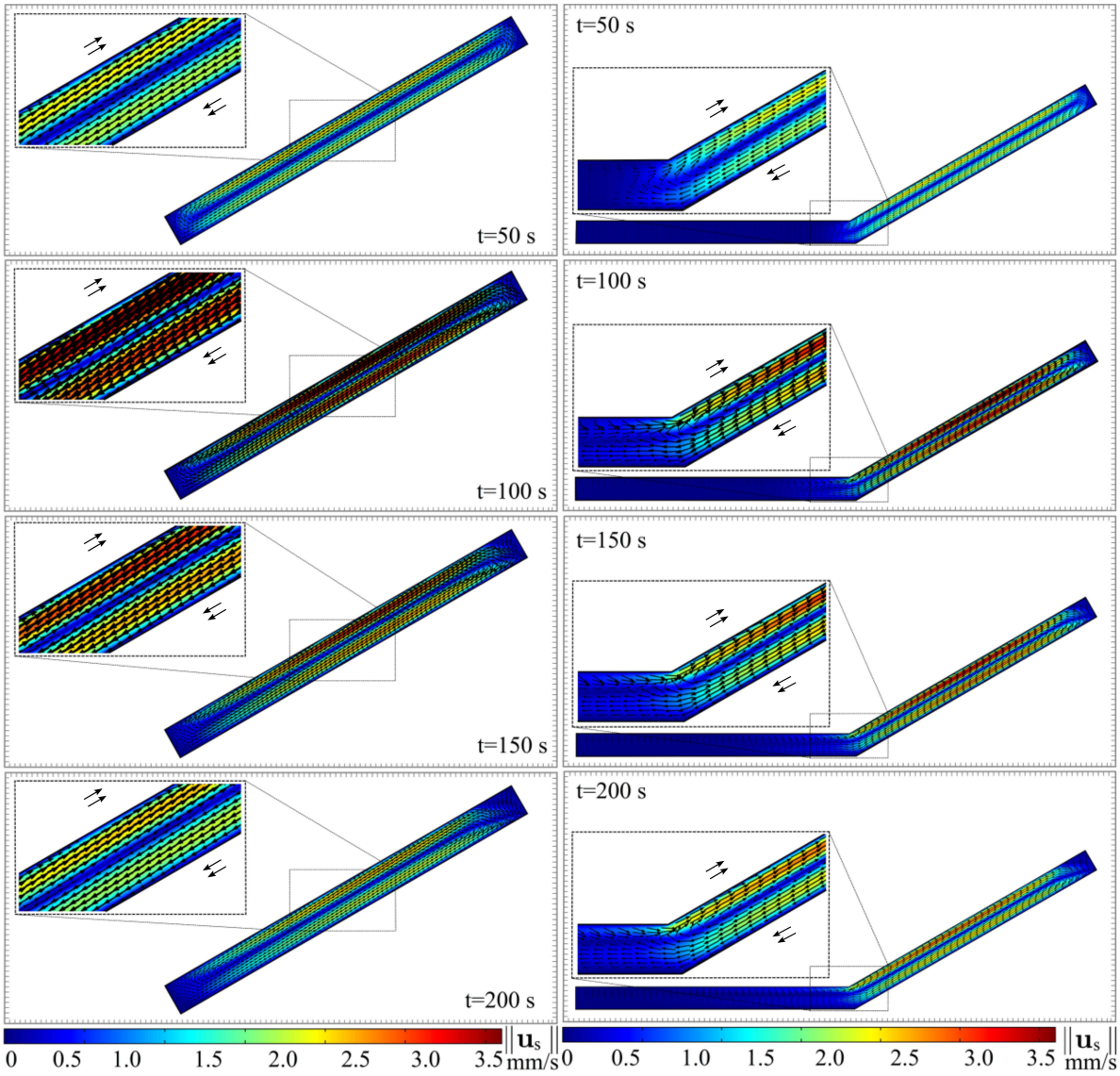

Figure 3.3.2: Magnitude of the velocity field of the dispersed phase for $t = 50$ s, $t = 100$ s, $t = 150$ s and $t = 200$ s. Left panel: geometry G1 and right panel: geometry G2. Inset: detail of $\mathbf{u}_s$, at the middle of the duct and at the slope change zone, respectively. The black arrows represent the particle flow direction. The numerical conditions are $\theta_s = 30°$, $\phi_0 = 0.30$ and $\eta_f = 100$ mPa·s. The colour bar represents the magnitude of velocity of particles.

very small compared with those obtained from MP_3. This behaviour of the particles is expected due to the largest flows related to the Boycott effect and are in fact in the inclined section. Here, the particle flow during the early stages of motion is 1.2 times higher for particles that are going upward than for particles going down. Regarding the accumulation of particles in the slope change, the top panel of Figure 3.3.5 shows the accumulated particle mass $\int \phi \mathrm{d}z$ for (a) $\theta_s = 10°$ and (b) $\theta_s = 30°$ as a function of the horizontal distance of geometry G2. In all cases, we have made the calculations using an initial concentration of $\phi_0 = 0.30$. Additionally, we have shown only the time curves corresponding to $t = 0$ s , $t = 200$ s, $t = 400$ s, $t = 600$ s and $t = 800$ s for clarity. These figures show that the larger the angle of the system, the greater the build-up of granular material near to the slope change zone ($x = 0$). Furthermore, the amount of material transported along the horizontal section can be seen in the lower panel of Figure 3.3.5. Here, we can infer that the area in the horizontal section affected

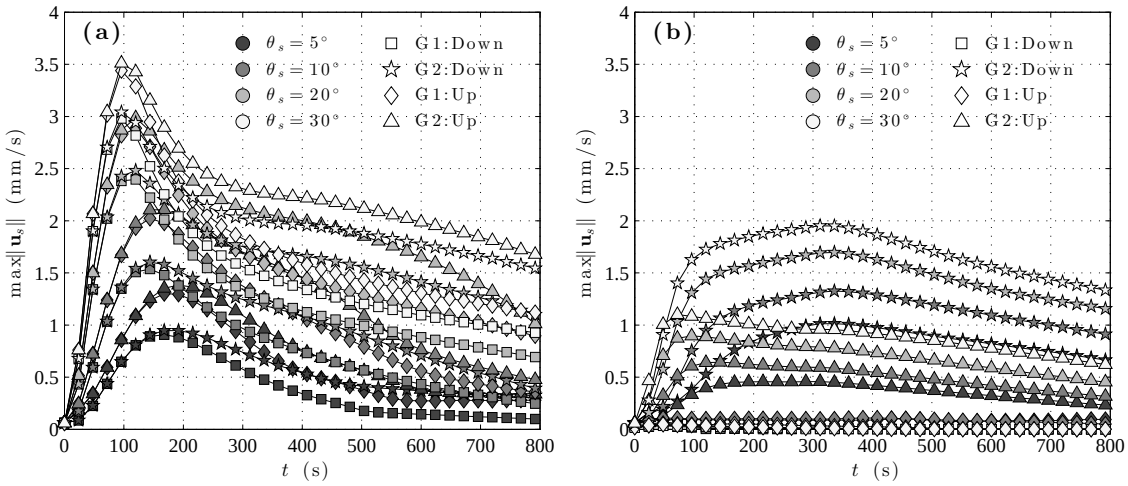

Figure 3.3.3: Maximum magnitude of the velocity of the dispersed phase for: $\theta_s = 5°$, $\theta_s = 10°$, $\theta_s = 20°$ and $\theta_s = 30°$ for G1 and G2 as a function of time. The measurements correspond at (a): MP_1 and (b): MP_2. The numerical conditions are $\phi_0 = 0.30$ and $\eta_f = 100$ mPa·s.

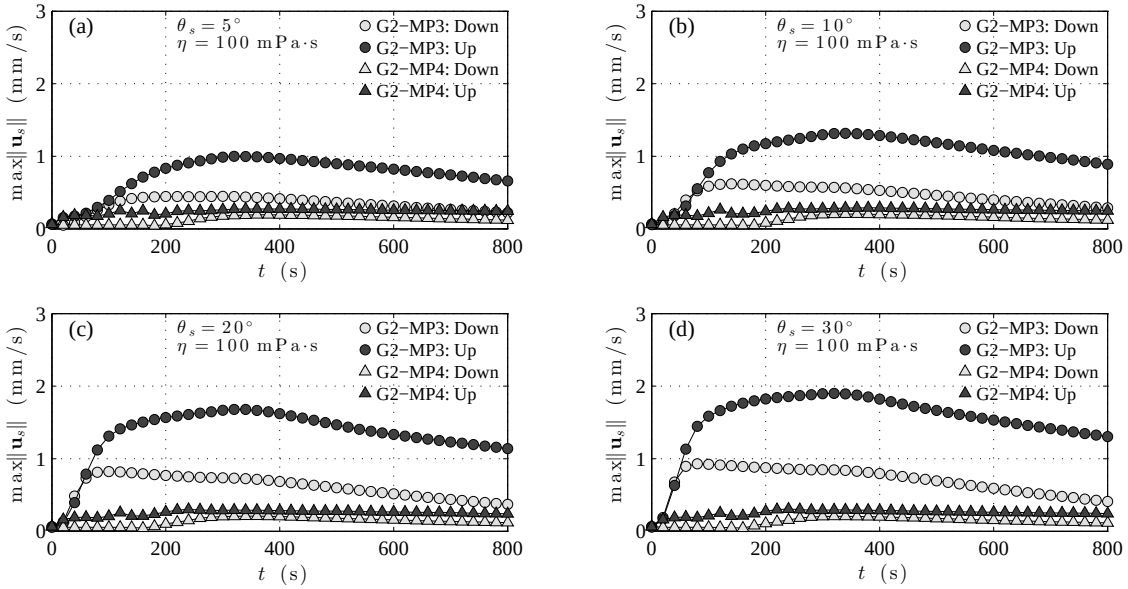

Figure 3.3.4: Maximum magnitude of the velocity of the dispersed phase for (a): $\theta_s = 5°$, (b): $\theta_s = 10°$, (c): $\theta_s = 20°$ and $\theta_s = 30°$ for G2 as a function of time. The measurements correspond at MP_3 and MP_4. The numerical conditions are $\phi_0 = 0.30$ and $\eta_f = 100$ mPa·s.

by the flow of particles has a range of about 150 mm from the slope change ($x = 0$) having a greater influence due to an angle (b) $\theta_s = 30°$ than to (a) $\theta_s = 10°$. The accumulation of granular material in the slope change zone is better identified in Figure 3.3.6 at final settling times.

Figure 3.3.6 shows the height of the sediment layer along MP_3 normalized by the width of the duct, h_{SL}/L_0, as a function of: (a) the angle duct for different initial concentrations of particles and fluid viscosities, and (b) the initial concentrations of particles for distinct inclination angles of the system and fluid viscosities. In other words, the data represents the build-up of granular material in the slope change between the inclined section and the horizontal section of the duct, under different physical

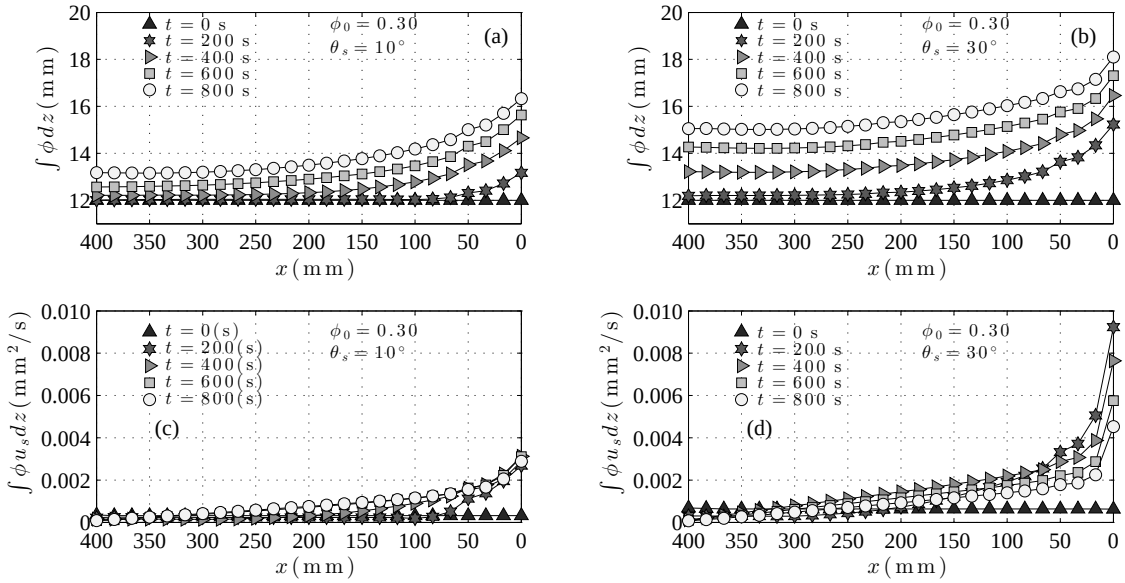

Figure 3.3.5: Top panels: Accumulated particle mass $\int \phi \mathrm{d}z$ for (a): $\theta_s = 10°$ and (b): $\theta_s = 30°$. Bottom panels: Mass flux $\int \phi u_s \mathrm{d}z$ along the horizontal section for (c): $\theta_s = 10°$ and (d): $\theta_s = 30°$.

situations. Moreover, from Figure 3.3.6 it is observed that the dependence between the normalized height and the initial concentration of particles is much more relevant than the dependence on the inclination of the system but that, in light of the resulting numbers, it is the combination of duct slopes and concentrations which control the risk of plug formation. In particular, we can see that for initial particle concentrations greater than 30% (0.30), an accumulation of solid material of 70% (0.70) is obtained at MP_3. On the other hand, when the concentration is around 40%, the accumulation of solid material reaches a value of 80% and 94% of the duct width for $\theta_s = 5°$ and for $\theta_s = 30°$, respectively, for a viscosity of $\eta_{f1} = 100$ mPa·s and, 74% and 88% of the duct width for $\theta_s = 5°$ and for $\theta_s = 30°$, respectively, for a viscosity of $\eta_{f3} = 300$ mPa·s.

The present analysis thus suggests the existence of better and worse combinations of angles and concentrations, for the duct obstruction in the slope change zone. In light of the above results, we can find the obstruction condition of the duct, making a simple linear extrapolation (i.e., $h_{SL}/L_0 = 1$), from the data of Figure 3.3.6b. Hence, the particle concentration values for which the duct is obstructed are $\phi_0 = 47.9\%$ and $\phi_0 = 45.0\%$ for $\theta_s = 5°$ and $\theta_s = 30°$, respectively, for a viscosity of $\eta_{f1} = 100$ mPa·s. In Table 3.3, the results of duct obstruction for the rest of the variables are summarized. The results show that the conditions of obstruction (initial concentration of particles) increased 2.2% to increase the viscosity of 100 mPa·s to 200 mPa·s and 1.6% by increasing the viscosity of 200 mPa·s to 300 mPa·s, in all cases, regardless of the angle of inclination; being a total increase of 3.8%.

Finally, we will make an analysis of scale that allows to define an expression for the height of the sediment layer on the slope change based on certain dimensionless numbers. Thus, it has been shown with experiments and numerical simulations that the shear stress in mixtures and granular flows can be written as $\tau = P\mu(I)$, where the friction coefficient depends o, a single dimensionless parameter, I, (Forterre & Pouliquen, 2008; Cassar *et al.* , 2005). Although there is no friction term in our numerical model, we mentioned the work of Forterre & Pouliquen (2008); Cassar *et al.* (2005) to put in context the inertial number. The latter dimensionless parameter is called the inertial number and is defined

Table 3.3: Duct obstruction conditions.

	$\eta_{f1} = 100$ mPa·s	$\eta_{f2} = 200$ mPa·s	$\eta_{f3} = 300$ mPa·s
	ϕ_0	ϕ_0	ϕ_0
$\theta_s = 5°$	47.9%	49.0%	49.8%
$\theta_s = 10°$	47.5%	48.6%	49.4%
$\theta_s = 15°$	46.9%	47.9%	48.8%
$\theta_s = 20°$	46.3%	47.5%	48.4%
$\theta_s = 25°$	45.2%	46.4%	47.1%
$\theta_s = 30°$	45.0%	45.6%	46.3%

as,

$$I = \frac{2a\dot{\gamma}}{\sqrt{P/\rho_s}}, \tag{3.3.1}$$

where this dimensionless number can be interpreted as the ratio between two time scales: (a) a microscopic time scale $t_{micro} = 2a/\sqrt{P/\rho_s}$ which represents the time it takes for a single particle to fall to a hole of size $2a$ under the pressure P and which gives the typical time of rearrangements, and (b) a macroscopic time scale $t_{macro} = 1/\dot{\gamma}$ related to the mean deformation. Here, $\dot{\gamma}$ is the shear stress rate and a is the particle radius. It is observed that a relevant velocity scale in the problem is the sedimentation velocity, $w_s = w_0 F$, where $w_0 = (2/9)a^2(\rho_s - \rho_f)g/\eta_f$, it is the velocity for an individual particle in an infinite medium and F is a hindrance function. In this work we have used the model proposed by Richardson & Zaki (1954a), $F = (1-\phi)^n$, with a typical value of $n = 5$, (Guazzelli & Hinch, 2011).

In a recent work to describe sediment bed formation in inclined containers, Palma *et al.* (2016b,a)

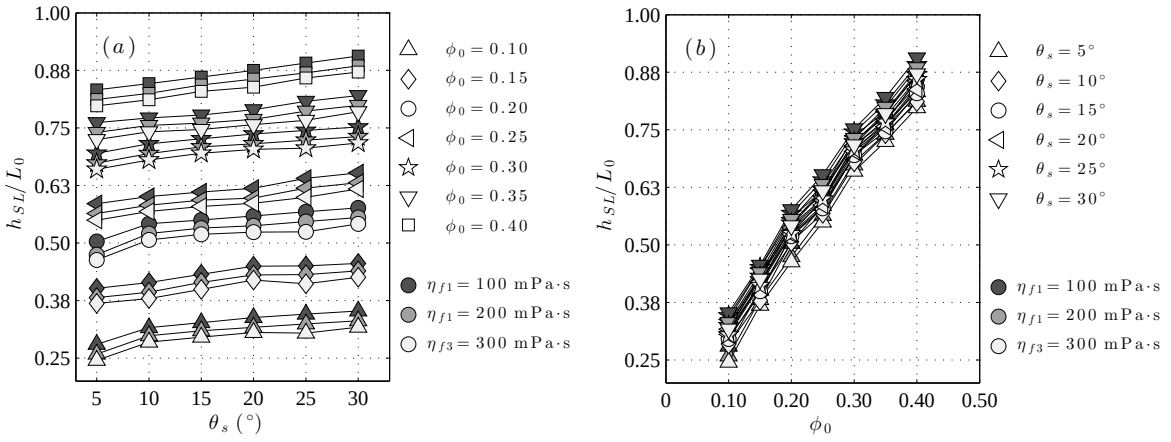

Figure 3.3.6: Normalized height of the sediment layer as a function of (a): the angle of the system for different initial volume fraction of particles and fluid viscosities, and (b): the initial volume fraction of particles for different angles and fluid viscosities. The measurements correspond at MP_3.

have expressed the inertial number as $I \equiv Re_p(I_0 r)^{1/2}\sin\theta_s$, where $Re_p = 2a\rho_f w_s/\eta_f$ is the definition for the particle Reynolds number, $r = \rho_s/\rho_f$ and $I_0 = (3/4)\eta_f^2/\rho_f g(\rho_s - \rho_f)a^3$ and, the concentration particle number as $\Phi \equiv (\phi/\phi_m)^{1/3}$. In this context, it has been found that such time scale balance is appropriate to describe a dimensionless version of the sediment layer. On the other hand, it has

been shown that the kinematics of a sedimentation process of monodisperse particles in an inclined duct (without a horizontal section) is described very well by two dimensionless numbers, R and Λ, (Hill *et al.* , 1977; Acrivos & Herbolzheimer, 1979; Herbolzheimer & Acrivos, 1981; Herbolzheimer, 1983; Davis & Acrivos, 1985). Thus, the ratio of a sedimentation Grashof number to the Reynolds number can be written as $\Lambda = 18\left(\frac{H}{2a}\right)^2 \frac{\phi}{F}$, Herbolzheimer & Acrivos (1981). Here, it is possible define $H = L_1 \sin\theta_s$, (see Figure 3.2.1) and $\Gamma = \frac{9\phi}{2F}$.

Finally, the latter dimensionless number can be written as $\Lambda \equiv \Gamma\left(\frac{L_1 \sin\theta_s}{a}\right)^2$. In the present set of numerical experiments the latter dimensionless numbers R and Λ, are in the range $10^{-3} - 10^{-1}$ and $10^4 - 10^6$, respectively. In this manner, when the condition $\Lambda \gg 1$ and $\mathrm{R}\Lambda^{-1/3} \ll 1$ are satisfied, the flow is laminar and viscous, and the sedimentation process in the inclined duct can be explained by the PNK theory. For our numerical experiments $\Lambda \sim 10^6$ and $\mathrm{R}\Lambda^{-1/3} \sim 10^{-4}$. Due to the evidence presented above, it is natural to propose Λ as a relevant dimensionless number for the inclined duct with a horizontal section. Although numerically we are in the same ranges where it has developed several quantitative approaches using asymptotic analysis (Acrivos & Herbolzheimer, 1979; Herbolzheimer & Acrivos, 1981; Herbolzheimer, 1983), the complicated geometry presented here precludes the development of a rigorous theoretical formulation to calculate the concentration of particles in the slope change zone and speed of the particles. In summary, the relevant dimensionless parameters are

$$I = Re_p (I_0 r)^{1/2} \sin\theta_s, \tag{3.3.2}$$

$$\Phi = \left(\frac{\phi}{\phi_m}\right)^{1/3}, \tag{3.3.3}$$

$$\Lambda = \Gamma\left(\frac{L_1 \sin\theta_s}{a}\right)^2. \tag{3.3.4}$$

The present results suggest that the numerical measurements of the height of the sediment layer at MP_3, h_{SL}, can be represented by I, Φ and Λ dimensionless groups. In this work, we have left fixed the ratio $L_0/L1$ constant. Figure 3.3.7 shows the best fit in terms of the dimensionless height of the sediment layer, h_{SL}/L_0, and the dimensionless group $c_0\left[Re_p(I_0 r)^{1/2}\sin\theta_s\right]^{c_1}\left[(\phi/\phi_m)^{1/3}\right]^{c_2}\left[\Gamma(L_1\sin\theta_s/a)^2\right]^{c_3}$. The corresponding fit was obtained using a multi-dimensional Levenberg-Marquardt nonlinear regression algorithm, (Bard, 1974; More, 1978). The results indicate an excellent fit, with $c_0 = 1.79 \pm 0.04$, $c_1 = 1.02 \pm 0.03$, $c_2 = 1.07 \pm 0.01$ and $c_3 = 0.51 \pm 0.02$, with an error of 0.1% compared to the theoretical slope of value 1. We can express the height of the sediment layer at MP_3 approximately as

$$h_{SL} = 1.8 L_0 I \Phi \sqrt{\Lambda}. \tag{3.3.5}$$

Finally, applying the obstruction condition of the duct (i.e., $h_{SL}/L_0 = 1$) to the equation (3.3.5), we obtain

$$\Phi = \frac{\alpha}{I\sqrt{\Lambda}}, \tag{3.3.6}$$

being $\alpha \equiv 1/1.8$. In this manner, using the equation (3.3.6) is feasible to generalize the results of Table 3.3.

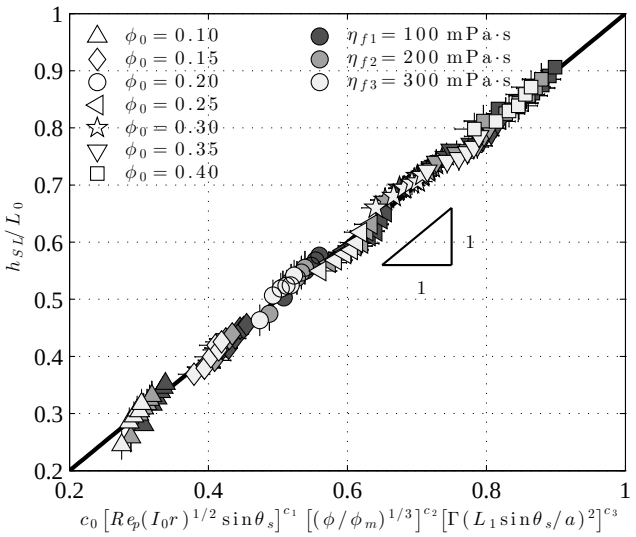

Figure 3.3.7: Data fit for h_{SL}/L_0 as a function of the dimensionless group $\Pi = c_0 \left[Re_p(I_0 r)^{1/2} \sin\theta_s\right]^{c_1} \left[(\phi/\phi_m)^{1/3}\right]^{c_2} \left[\Gamma(L_1 \sin\theta_s/a)^2\right]^{c_3}$. The solid line indicates the identity. The fitted coefficients are $c_0 = 1.79 \pm 0.04$, $c_1 = 1.02 \pm 0.03$, $c_2 = 1.07 \pm 0.01$ and $c_3 = 0.51 \pm 0.02$.

3.4 Conclusions

In this paper we have solved numerically the continuity and momentum equations associated with the problem of sedimentation of fluid-solid mixtures at high concentrations in tilted ducts, under different physical conditions using COMSOL Multiphysics with the CFD package. The variables studied were the initial particle concentration, the fluid viscosity and the angle of the duct. A rich phenomenology associated with the dynamics of mixtures at high particle concentrations and at different angles was observed. The present results shown that the initial particle concentration is a very relevant variable for knowing under what conditions the duct could get obstructed and, in combination with some system angles, such conditions might represent a risk of duct plug. In particular, we have found that viscosity is not as important as the initial concentration of particles and the angle of the system.

Additionally, we found a mathematical expression using scaling arguments, formed by three dimensionless groups including the inertial number, particle concentration and the ratio between the sedimentation Grashof number to the Reynolds number to explain the height of the sediment layer in the slope change zone of a duct. Imposing a condition of obstruction, we have found a combination of initials concentrations of particles and fluid viscosities that shall block the duct in the slope change zone. Finally, we have related and extended these results with a dimensionless expression describing the phenomenon of obstruction. Although the present results are expressive of the effect of solids concentration and duct angles, a more in depth analysis is required to unveil the physics of the particle organization near the zone where the slope change occurs. This is currently being done experimentally by the present group of researchers.

Acknowledgements

The authors acknowledge the support of the National Commission for Scientific and Technological Research of Chile, CONICYT, Grant N° 21110766, Fondecyt Projects N° 11110201 and N° 1130910, the Department of Civil Engineering, the Department of Mining Engineering and the Advanced Mining Technology Center of the University of Chile, as well the staff of the G.K. Batchelor Laboratory, Department of Applied Mathematics and Theoretical Physics, University of Cambridge.

Chapter 4

Conclusions

The present thesis has successfully presented the results of a set of different numerical and laboratory experiments in order to study distinct relevant features of sedimentation of mono and polydisperse particles in inclined geometries. During this PhD work, an experimental set-up was designed, built and operated to investigate the process of sedimentation of particles in open and closed inclined geometries. Additionally, the optical light transmission technique has implemented for tracking the interface between the particle suspension and the clear fluid zone, during a sedimentation process. Finally, the dimensional analysis theory has been used to characterize the slope of a sediment layer in tilted containers and, the height of the sediment layer of inclined ducts. The realization of these specific objectives has helped to achieve in very good terms the main goal of this doctoral thesis.

To carry out this experimental work, it has been necessary to test and implement various experimental techniques for studying the movement of particles at high concentrations within a viscous fluid. Two experimental techniques were implemented: PTV (particle tracking velocity) and PIV (particle image velocity). Unfortunately, these techniques do not work well in the presence of a high concentration of particles. After many attempts to obtain consistent results, it was decided to use another but easier technique. This technique described in chapter one, it is called TLI (transmitted light intensity). Even though the principle of this technique is simply based on illuminating a container from behind with a light in order to quantify and relate the transmitted intensity to the concentration of particles, it worked extremely well. This technique has allowed to track the interface between the suspension zone and the clear fluid zone of particles. Also, it was used to measure the height of the sediment layer at the end of the sedimentation process.

On the other hand, although there are different methods and numerical techniques to simulate the flow of dry and wet granular materials (discrete and continuous models), which have advantages and disadvantages in terms of calculations' time and accuracy of their results, the continuum mixture used has proven to give consistent and accurate results for the sedimentation processes studied in this thesis. However, adding a term related to friction and particle's angle of repose would mean that this model can be applied in many more circumstances, especially in engineering problems, where the friction is more relevant.

Particle organization after viscous sedimentation in tilted containers

Regarding the experimental and numerical work carried out. Here, it has been presented a new point of view of the mechanism that sets the morphology of the sediment layer formed by the settling of mono and slightly polydisperse particles onto the bottom of an inclined container. One of the most significant results of the experiments was that the final angle adopted by the sediment layer showed firm dependencies on the container inclination and the initial particle concentration, but not in the fluid viscosity within the small particle Reynolds number range tested. Additionally, the experimental and numerical results showed that the concept of hindered settling is crucial to understand the formation of a particle layer that move particles down-slope just above the sediment layer as it forms. The results suggested that this mechanism scales directly with the projection of the hindered settling velocity onto the sloping deposit.

On the other hand, the fluid viscosity does not play a direct role in setting the final morphology of particles for low particle Reynolds numbers. Thus, it plays a weak role in the settling velocity. Furthermore, for long times the process depends strongly on the initial concentration as this enters the settling flux in a nonlinear manner. The numerical simulations have demonstrated that the fluid-particle interactions dominate over solid friction. These simulations have reproduced the experimen tal results despite using a mixture model that considers the granular material as incompressible.

This result confirms that the dissipation is dominated by viscous forces as the particles approach rather than solid friction after they collide. In the case of the dispersed phase, as well inelastic. Here, particle Reynolds numbers are within the Stokes regime, which justifies the incompressibility assumption for both phases. As our experiments and simulations include only relatively shallow particle layers, overburden pressures are not enough to deform the disperse phase at the bottom, thus allowing to plausibly assume that particles are effectively rigid.

Even though the present experiment has been performed in a container with a fixed aspect ratio, it is reasonable to speculate how this may affect the morphology of the sediment layer. Increasing the container height will increase the period of time during which the particle-rich layer flows down slope above the developing sediment deposit, for a given initial concentration particle and container width and so we would expect the surface of the final deposit to be more horizontal in a manner similar to the decrease in θ seen here by increasing the initial concentration.

Contrarily, increasing the width of the container will not significantly alter the down-slope flux while increasing the volume of particles needing to be transported to achieve a given θ. Thus, we would expect θ to increase towards θ_s and the deposit to be of a more uniform thickness (for extreme high or low aspect ratios, the Boycott effect may become important and contribute to the final slope in a manner not described here). Additionally, simply changing the size of the container while maintaining the same aspect ratio will change the time scale over which the sediment layer is created, but not its morphology.

Finally, from a practical point of view, these results are important for future application in engineering sciences, specifically in chemical and pharmaceutical industry (e.g., the application of blood cell sedimentation for monitoring of the bioequivalence of drugs based on acetylsalicylic acid), petroleum and mining industry (e.g., transporting of copper concentrates and mining waste), as well as in many kinds of industrial separation processes of granular material from a fluid (e.g., water treatment). In mineral processing, the concentration stage uses water as a carrier fluid for comminution products, where an important part of the fluid is recovered in thickeners. Although the settling mechanism in the mid section of thickeners is vertical, the bottom of these equipment is conical, inducing a particle flow component parallel to the bottom.

On the other hand, in the wastewater treatment industry it is common to find lamella settlers, whose working principle is the Boycott effect. Knowing that the final angle adopted by the sediment layer shows strong dependencies on the initial particle concentration and the container inclination, but not the fluid viscosity in this Stokes number range, might improve the design and operation in these examples.

Characterization of a sediment layer in tilted ducts

Regarding the numerical work carried out, we have solved the continuity and momentum equations associated with the problem of sedimentation of fluid-solid mixtures at high concentrations in tilted ducts, under different physical conditions using COMSOL Multiphysics with the CFD package. The variables studied were the initial particle concentration, the fluid viscosity and the angle of the duct. A rich phenomenology associated with the dynamics of mixtures at high particle concentrations and at different angles was observed.

The present results showed that the initial particle concentration is a very relevant variable for knowing under what conditions the duct could get obstructed and, in combination with some system angles, they might represent a risk of duct plug. In particular, we have found that viscosity is not as important as the initial concentration of particles and the angle of the system. Additionally, we found a mathematical expression using scaling arguments, formed by three dimensionless groups including the inertial number, particle concentration and the ratio between the sedimentation Grashof number to the Reynolds number to explain the height of the sediment layer in the slope change zone of a duct.

Imposing a condition of obstruction, we have found a combination of initials concentrations of particles and fluid viscosities that shall block the duct in the slope change zone. Finally, we have related and extended these results with a dimensionless expression describing the phenomenon of obstruction. Although the present results are expressive of the effect of solids concentration and duct angles, a more in depth analysis is required to unveil the physics of the particle organization near the zone where the slope change occurs.

To complement the numerical results obtained in this section. Laboratory experiments are being made to understand the process of settling slightly polydisperse particles. In these experiments, we will study the instabilities in the sedimentation process (with special emphasis at the slope change zone). Here, we will try to answer the questions of how and when instabilities growth, in order to know what will be the consequences in engineering transport of mixtures fluid-particles. Preliminary results are shown in next section. We believe that the results presented in this research will represent a small step forward in the understanding of the formation of sediment layers on sloping geometries, and future engineering applications.

Chapter 5

Future work

I would like to show some preliminary experimental results related with the sedimentation process in inclined ducts. The results obtained in this series of experiments will be presented to the scientific community of physics of fluids, as an ISI paper during 2017.

We have made experiments with two types of particles. Glass particles with a diameter $d_1 = 1000 \pm 30$ (μm) and a density of $\rho_1 = 2.50 \pm 0.01$ (g/cm^3) and, resin particles with a diameter $d_2 = 600 \pm 10$ (μm) and a density of $\rho_2 = 1.10 \pm 0.02$ (g/cm^3). The main objective of this experiment is to characterize the height of the sediment layer at the slope change zone as a function of particle concentration (both species) and the inclination angle of the duct. Figure 5.0.1 shows the sedimentation process in a tilted duct as a function of the concentration particle.

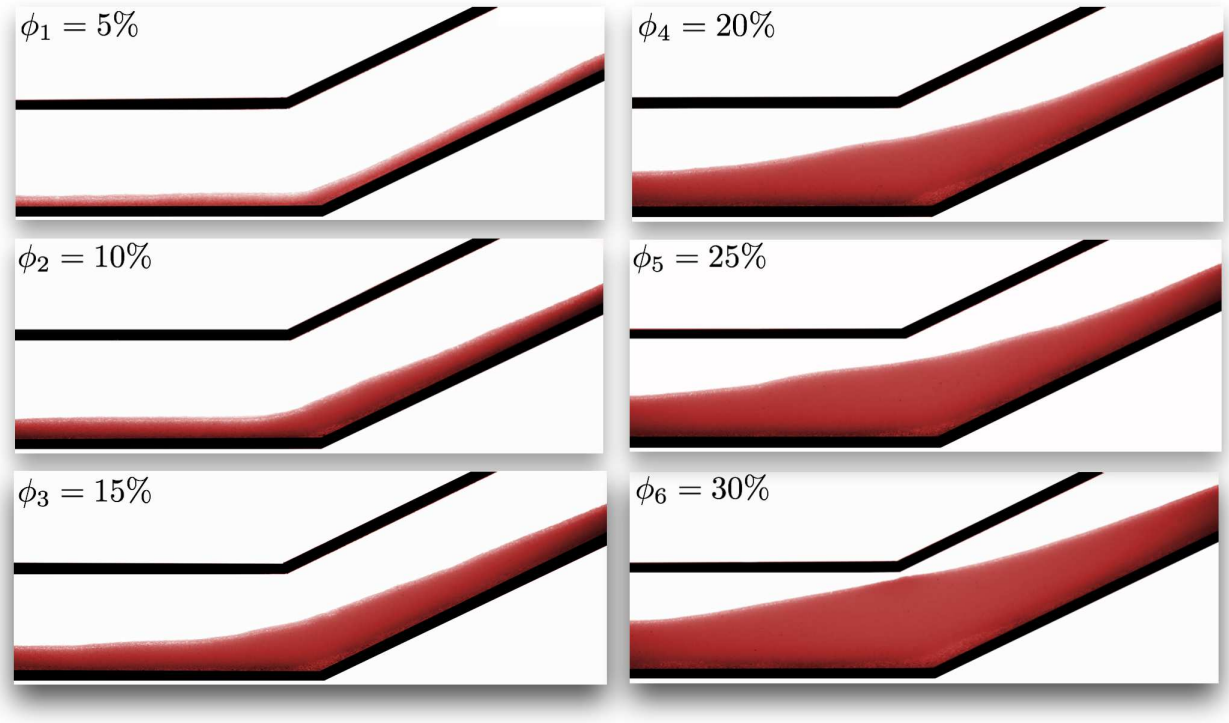

Figure 5.0.1: Sedimentation process in a tilted duct as a function of the concentration particle. Experimental conditions: $\theta_s = 25^\circ$ and particle percentages $d_1 = 7.5\%$ and $d_2 = 92.5\%$. The images correspond to the final time of the sedimentation process.

Additionally, we are interested in studying, characterize and analyze the instabilities that occurs at the interface between the clear fluid layer and the suspension region. Figure 5.0.2 shows the sedimentation process in a tilted duct as a function of time.

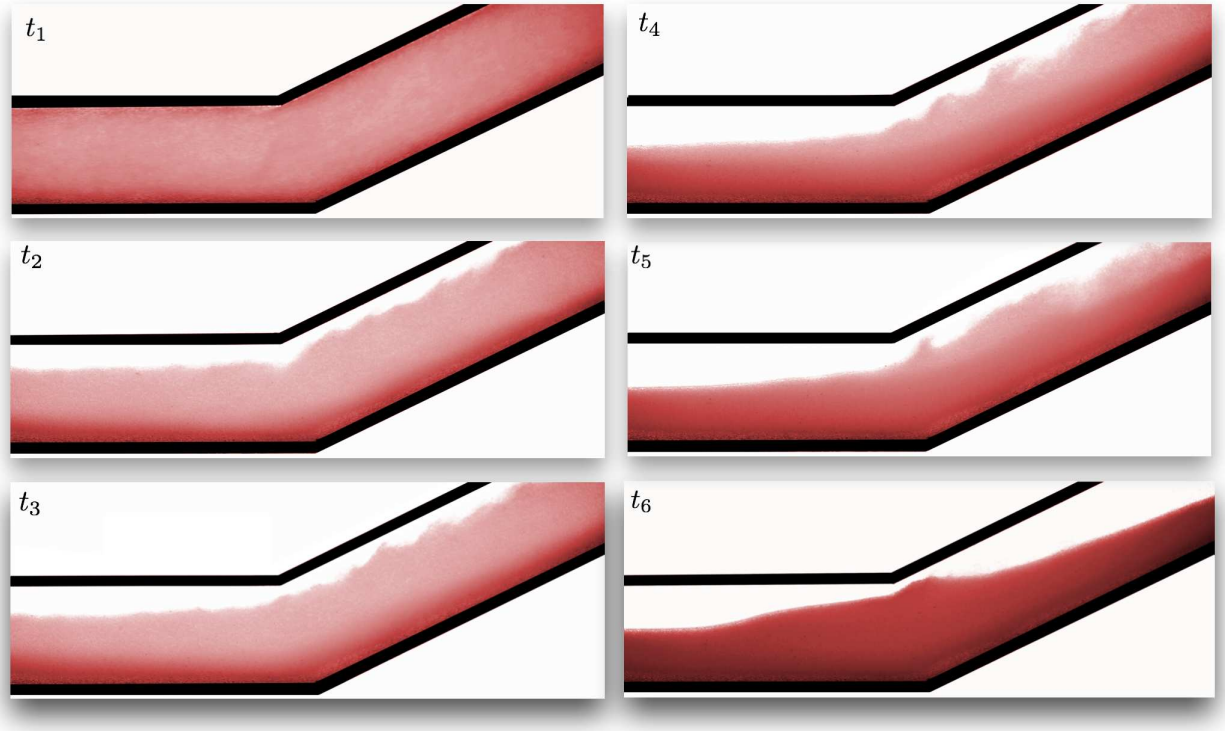

Figure 5.0.2: Sedimentation process in a tilted duct as a function of time. Experimental conditions: $\theta_s = 25°$, $\phi = 0.40$ and particle percentages $d_1 = 7.5\%$ and $d_2 = 92.5\%$.

Finally, we are interested in studying the instabilities due to the resuspension of particles. Figure 5.0.3 shows the resuspension process in a tilted duct as a function of time. Advances in understanding these physical phenomena could bring an endless number of benefits in engineering and applied physics related to particle suspensions.

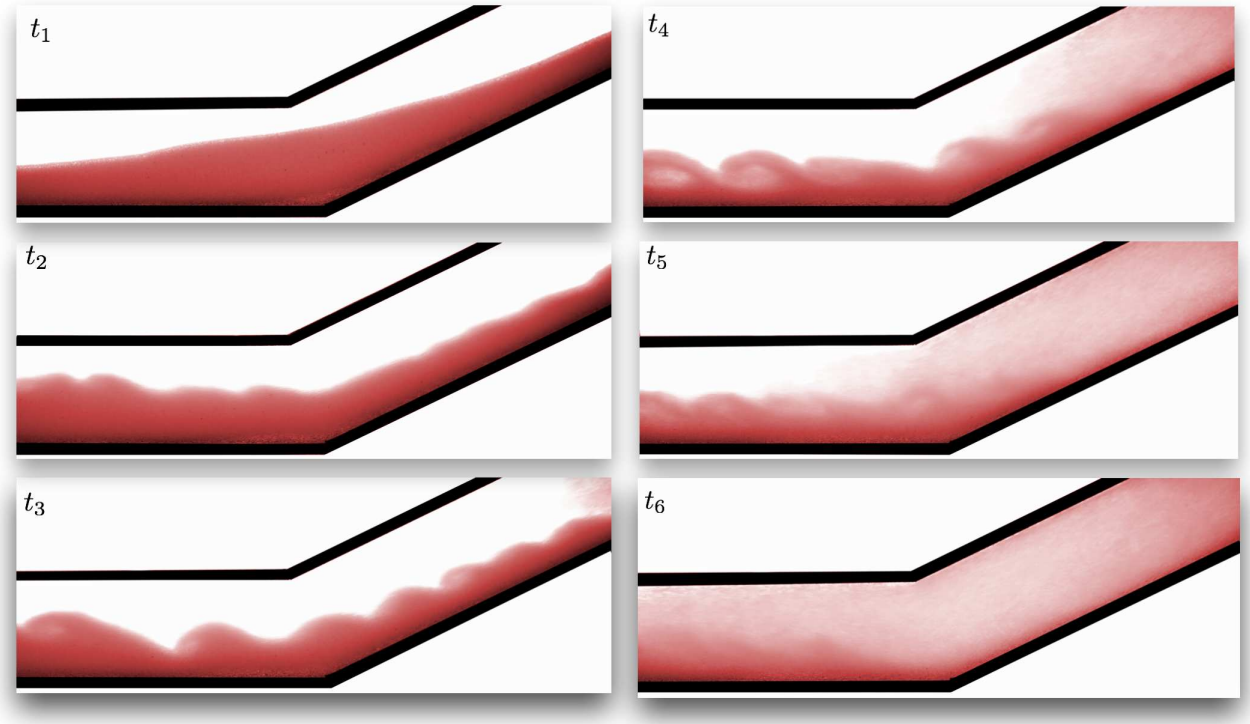

Figure 5.0.3: Resuspension process in a tilted duct as a function of time. Experimental conditions: $\theta_s = 25^\circ$, $\phi = 0.40$ and particle percentages $d_1 = 7.5\%$ and $d_2 = 92.5\%$.

Bibliography

Acrivos, Andreas, & Herbolzheimer, Eric. 1979. Enhanced sedimentation in settling tanks with inclined walls. *Journal of fluid mechanics*, **92**(03), 435–457.

Andreotti, Bruno, Forterre, Yoël, & Pouliquen, Olivier. 2013. *Granular media: between fluid and solid*. Cambridge University Press.

Bagnold, R.A. 1954. Experiments on a gravity-free dispersion of large solid spheres in a Newtonian fluid under shear. *Proceedings of the Royal Society of London. Series A: Mathematical and Physical Sciences*, **225**(1160), 49–63.

Bard, Yonathan. 1974. *Nonlinear parameter estimation*. Vol. 1209. Academic Press New York.

Barnea, E, & Mizrahi, J. 1973. A generalized approach to the fluid dynamics of particulate systems: Part 1. General correlation for fluidization and sedimentation in solid multiparticle systems. *The Chemical Engineering Journal*, **5**(2), 171–189.

Barnes, H A. 2000. *A handbook of elementary rheology*. University of Wales, Institute of Non-Newtonian Fluid Mechanics Aberystyth, England.

Barnes, H A, Hutton, J F, & Walters, K. 1989. *An introduction to rheology*. Vol. 3. Elsevier Science.

Batchelor, GK. 1970. The stress system in a suspension of force-free particles. *Journal of fluid mechanics*, **41**(03), 545–570.

Batchelor, GK. 1972. Sedimentation in a dilute dispersion of spheres. *Journal of fluid mechanics*, **52**(02), 245–268.

Batchelor, GK. 1974. Transport properties of two-phase materials with random structure. *Annual Review of Fluid Mechanics*, **6**(1), 227–255.

Batchelor, GK. 1977. The effect of Brownian motion on the bulk stress in a suspension of spherical particles. *Journal of Fluid Mechanics*, **83**(01), 97–117.

Batchelor, GK. 1982. Sedimentation in a dilute polydisperse system of interacting spheres. Part 1. General theory. *Journal of Fluid Mechanics*, **119**, 379–408.

Batchelor, GK, & Green, J-T_. 1972a. The hydrodynamic interaction of two small freely-moving spheres in a linear flow field. *Journal of Fluid Mechanics*, **56**(02), 375–400.

Batchelor, GK, & Green, JT. 1972b. The determination of the bulk stress in a suspension of spherical particles to order c2. *Journal of Fluid Mechanics*, **56**(03), 401–427.

Boycott, A. E. 1920. Sedimentation of Blood Corpuscles. *Nature*, **104**(2621), 532.

Brady, John F, & Bossis, Georges. 1988. Stokesian dynamics. *Annual review of fluid mechanics*, **20**, 111–157.

Brilliantov, Nikolai V, & Poschel, Thorsten. 2010. *Kinetic theory of granular gases*. Oxford University Press.

Burger, Raimund, Diehl, Stefan, & Nopens, Ingmar. 2011. A consistent modelling methodology for secondary settling tanks in wastewater treatment. *Water Research*, **45**(6), 2247–2260.

Cassar, C, Nicolas, M, & Pouliquen, O. 2005. Submarine granular flows down inclined planes. *Physics of Fluids (1994-present)*, **17**(10), 103301.

Cheng, Nian-Sheng. 2008. Formula for the viscosity of a glycerol-water mixture. *Industrial and engineering chemistry research*, **47**(9), 3285–3288.

Concha, Fernando. 2014. *Solid-Liquid Separation in the Mining Industry*. Springer.

Cortet, P-P, Bonamy, D, Daviaud, F, Dauchot, O, Dubrulle, B, & Renouf, M. 2009. Relevance of visco-plastic theory in a multi-directional inhomogeneous granular flow. *EPL (Europhysics Letters)*, **88**(1), 14001.

Courrech du Pont, Sylvain, Gondret, Philippe, Perrin, Bernard, & Rabaud, Marc. 2003. Granular avalanches in fluids. *Physical Review Letters*, **90**(4), 044301.

Coussot, P., & Ancey, C. 1999. Rheophysical classification of concentrated suspensions and granular pastes. *Physical Review E*, **59**(4), 4445.

Da Cruz, Frédéric, Emam, Sacha, Prochnow, Michaël, Roux, Jean-Noël, & Chevoir, François. 2005. Rheophysics of dense granular materials: Discrete simulation of plane shear flows. *Physical Review E*, **72**(2), 021309.

Dalziel, Stuart B. 2012. *DigiFlow User Guide. Version 3.4*. Dalziel Research Partners.

Davis, R H, & Acrivos, A. 1985. Sedimentation of Noncolloidal Particles at Low Reynolds Numbers. *Annual Review of Fluid Mechanics*, **17**(1), 91–118.

Davis, Robert H. 1984. The rate of coagulation of a dilute polydisperse system of sedimenting spheres. *Journal of Fluid Mechanics*, **145**, 179–199.

Davis, Robert H, Herbolzheimer, Eric, & Acrivos, Andreas. 1983. Wave formation and growth during sedimentation in narrow tilted channels. *Physics of Fluids (1958-1988)*, **26**(8), 2055–2064.

Dixon, DC. 1979. Theory of gravity thickening. *Progress in filtration and separation*, **1**, 113–178.

Duran, Jacques. 2012. *Sands, powders, and grains: an introduction to the physics of granular materials*. Springer Science & Business Media.

Einstein, A. 1906. Eine neue bestimmung der molek{ü}ldimensionen. *Ann. Phys.*, **324**(2), 289–306.

Enwald, H, Peirano, E, & Almstedt, A. E. 1996. Eulerian two-phase flow theory applied to fluidization. *International Journal of Multiphase Flow*, **22**(Dec), 21–66.

Ergun, Sabri. 1952. Fluid Flow through Packed Columns. *Chemical Engineering Progress*, **48**, 89–94.

Ettehadieh, Bozorg, Gidaspow, Dimitri, & Lyczkowski, RW. 1984. Hydrodynamics of fluidization in a semicircular bed with a jet. *AIChE journal*, **30**(4), 529–536.

Feuillebois, FRANCOIS. 1984. Sedimentation in a dispersion with vertical inhomogeneities. *Journal of fluid mechanics*, **139**, 145–71.

Forterre, Yoël, & Pouliquen, Olivier. 2008. Flows of dense granular media. *Annu. Rev. Fluid Mech.*, **40**, 1–24.

Frankel, NA, & Acrivos, Andreas. 1967. On the viscosity of a concentrated suspension of solid spheres. *Chemical Engineering Science*, **22**(6), 847–853.

Garside, John, & Al-Dibouni, Maan R. 1977. Velocity-voidage relationships for fluidization and sedimentation in solid-liquid systems. *Industrial and engineering chemistry process design and development*, **16**(2), 206–214.

Gidaspow, Dimitri. 1994. *Multiphase Flow and Fluidization: Continuum and Kinetic Theory Descriptions*. Academic Press.

Gidaspow, Dimitri, & Ettehadieh, Bozorg. 1983. Fluidization in two-dimensional beds with a jet. 2. Hydrodynamic modeling. *Industrial & Engineering Chemistry Fundamentals*, **22**(2), 193–201.

Gidaspow, Dimitri, Shih, Yang-Tsai, Bouillard, Jacques, & Wasan, Darsh. 1989. Hydrodynamics of a lamella electrosettler. *AIChE journal*, **35**(5), 714–724.

Gondret, P, Lance, M, & Petit, L. 2002. Bouncing motion of spherical particles in fluids. *Phys. Fluids*, **14**(2), 643–652.

Guazzelli, & Morris, Jeffrey F. 2012. *A Physical Introduction to Suspension Dynamics (Cambridge Texts in Applied Mathematics)*. Cambridge University Press.

Guazzelli, Élisabeth, & Hinch, John. 2011. Fluctuations and Instability in Sedimentation. *Annual Review of Fluid Mechanics*, **43**(1), 97–116.

Ham, JM, & Homsy, GM. 1988. Hindered settling and hydrodynamic dispersion in quiescent sedimenting suspensions. *International Journal of Multiphase Flow*, **14**(5), 533–546.

Happel, John. 1958. Viscous flow in multiparticle systems: slow motion of fluids relative to beds of spherical particles. *AIChE Journal*, **4**(2), 197–201.

Hawksley, PGW. 1951. The effect of concentration on the settling of suspensions and flow through porous media. *Some aspects of fluid flow*, 114–135.

Herbolzheimer, Eric. 1983. Stability of the flow during sedimentation in inclined channels. *Physics of Fluids*, **26**(8), 2043.

Herbolzheimer, Eric, & Acrivos, Andreas. 1981. Enhanced sedimentation in narrow tilted channels. *Journal of Fluid Mechanics*, **108**, 485–499.

Hill, William David, Rothfus, RR, & Li, Kun. 1977. Boundary-enhanced sedimentation due to settling convection. *International Journal of Multiphase Flow*, **3**(6), 561–583.

Hinch, EJ. 1977. An averaged-equation approach to particle interactions in a fluid suspension. *Journal of Fluid Mechanics*, **83**(04), 695–720.

Jeffrey, DJ. 1974. Group expansions for the bulk properties of a statistically homogeneous, random suspension. *Pages 503–516 of: Proceedings of the Royal Society of London A: Mathematical, Physical and Engineering Sciences*, vol. 338. The Royal Society.

Johnson, Claes. 1988. *Numerical Solution of Partial Differential Equations by the Finite Element Method*. Cambridge University Press.

Jop, Pierre, Forterre, Yoël, & Pouliquen, Olivier. 2006. A constitutive law for dense granular flows. *Nature*, **441**(7094), 727–730.

Joseph, GG, Zenit, R, Hunt, ML, & Rosenwinkel, AM. 2001. Particle–wall collisions in a viscous fluid. *Journal of Fluid Mechanics*, **433**, 329–346.

Kapoor, B., & Acrivos, A. 1995. Sedimentation and sediment flow in settling tanks with inclined walls. *J. Fluid Mech.*, **290**(-1), 39.

Krieger, I. M., & Dougherty, T. J. 1959. A mechanism for non-Newtonian flow in suspensions of rigid spheres. *T. Soc. Rheol.*, **3**, 137–152.

Krieger, Irvin M. 1972. Rheology of monodisperse latices. *Advances in Colloid and Interface Science*, **3**(2), 111–136.

Kynch, G.J. 1952. A theory of sedimentation. *Transactions of the Faraday Society*, **48**, 166–176.

Lamb, Horace. 1932. *Hydrodynamics*. Cambridge university press.

Leal, LG. 1980. Particle motions in a viscous fluid. *Annual Review of Fluid Mechanics*, **12**(1), 435–476.

Leighton, David, & Acrivos, Andreas. 1987. The shear-induced migration of particles in concentrated suspensions. *J. Fluid Mech.*, **181**(-1), 415.

Leung, Woon Fong. 1983. Lamella and tube settlers. 2. Flow stability. *Ind. Eng. Chem. Proc. Des. Dev.*, **22**(1), 68–73.

Leung, Woon Fong, & Probstein, Ronald F. 1983. Lamella and tube settlers. 1. Model and operation. *Industrial & Engineering Chemistry Process Design and Development*, **22**(1), 58–67.

Lockett, MJ, & Al-Habbooby, HM. 1973. Differential settling by size of two particle species in a liquid. *Trans. Inst. Chem. Eng*, **51**(2), 281.

Lockett, MJ, & Al-Habbooby, HM. 1974. Relative particle velocities in two-species settling. *Powder Technology*, **10**(1-2), 67–71.

Massoudi, M, Rajagopal, KR, Ekmann, JM, & Mathur, MP. 1992. Remarks on the modeling of fluidized systems. *AIChE Journal*, **38**(3), 471–472.

Melik, DH, & Fogler, HS. 1984. Gravity-induced flocculation. *Journal of colloid and interface science*, **101**(1), 72–83.

MiDi, GDR. 2004. On dense granular flows. *The European Physical Journal E*, **14**(4), 341–365.

Mirza, S, & Richardson, JF. 1979. Sedimentation of suspensions of particles of two or more sizes. *Chemical Engineering Science*, **34**(4), 447–454.

More, Jorge J. 1978. *The Levenberg-Marquardt algorithm: implementation and theory*. Springer.

Nakamura, N., & Kuroda, K. 1937. La cause de l'acceleration de la vitesse de sedimentation des suspensions dans les recipients inclines. *Keijo J. Med.*, **8**, 256–296.

Nedderman, Ronald Midgley. 2005. *Statics and kinematics of granular materials*. Cambridge University Press.

Nir, A., & Acrivos, A. 1990. Sedimentation and sediment flow on inclined surfaces. *J. Fluid Mech.*, **212**(-1), 139.

O'Brien, RW. 1979. A method for the calculation of the effective transport properties of suspensions of interacting particles. *Journal of Fluid Mechanics*, **91**(01), 17–39.

Oliver, DR. 1961. The sedimentation of suspensions of closely-sized spherical particles. *Chemical Engineering Science*, **15**(3), 230–242.

Palma, Sergio, Ihle, Christian F, & Tamburrino, Aldo. 2016a. Characterization of a sediment layer of concentrated fluid-solid mixtures in tilted ducts at low Reynolds numbers. *Industrial & Engineering Chemistry Research (under revision)*.

Palma, Sergio, Ihle, Christian F, Tamburrino, Aldo, & Dalziel, Stuart B. 2016b. Particle organization after viscous sedimentation in tilted containers. *Physics of Fluids (1994-present)*, **28**(7), 073304.

Peacock, Tom, Blanchette, F, & Bush, John W. M. 2005. The stratified Boycott effect. *Journal of Fluid Mechanics*, **529**(Apr.), 33–49.

Phillips, Ronald J., Armstrong, Robert C., Brown, Robert A., Graham, Alan L., & Abbott, James R. 1992. A constitutive equation for concentrated suspensions that accounts for shear induced particle migration. *Physics of Fluids A: Fluid Dynamics*, **4**(1), 30–40.

Ponder, Eric. 1926. On Sedimentation and rouleaux formation. *Experimental Physiology*, **16**(2), 173–194.

Poschel, Thorsten, & Schwager, Thomas. 2005. *Computational granular dynamics: models and algorithms*. Springer Science & Business Media.

Pouliquen, O, Cassar, C, Jop, P, Forterre, Y, & Nicolas, M. 2006. Flow of dense granular material: towards simple constitutive laws. *Journal of Statistical Mechanics: Theory and Experiment*, **2006**(07), P07020.

Probstein, Ronald F, & Hicks, R Edwin. 1978. Lamella settlers: a new operating mode for high performance. *Ind. Water Eng.*, **15**, 6–8.

Prosperetti, Andrea, & Tryggvason, Grétar. 2009. *Computational methods for multiphase flow*. Cambridge university press.

Richardson, J.F., & Zaki, W.N. 1954a. Sedimentation and fluidisation: Part I. *Chemical Engineering Research and Design*, **32**(Dec), S82–S100.

Richardson, JF, & Zaki, WN. 1954b. The sedimentation of a suspension of uniform spheres under conditions of viscous flow. *Chemical Engineering Science*, **3**(2), 65–73.

Rubinstein, I. 1980. A steady laminar flow of a suspension in a channel. *International Journal of Multiphase Flow*, **6**(5), 473–490.

Saffman, PG. 1973. On the settling speed of free and fixed suspensions. *Studies in Applied Mathematics*, **52**(2), 115–127.

Sangani, AS, & Acrivos, A. 1982. Slow flow through a periodic array of spheres. *International Journal of Multiphase Flow*, **8**(4), 343–360.

Schowalter, WR. 1984. Stability and coagulation of colloids in shear fields. *Annual Review of Fluid Mechanics*, **16**(1), 245–261.

Shapley, N C, Brown, R A, & Armstrong, R C. 2004. Evaluation of particle migration models based on laser Doppler velocimetry measurements in concentrated suspensions. *J. Rheol. (N. Y. N. Y).*, **48**, 255.

Shaqfeh, Eric Stefan Garrido, & Acrivos, A. 1986. The effects of inertia on the buoyancy-driven convection flow in settling vessels having inclined walls. *Physics of Fluids (1958-1988)*, **29**(12), 3935–3948.

Sierou, A, & Brady, JF. 2002. Rheology and microstructure in concentrated noncolloidal suspensions. *Journal of Rheology (1978-present)*, **46**(5), 1031–1056.

Smith, TN. 1965. The differential sedimentation of particles of two different species. *Trans. Inst. Chem. Eng*, **43**, T69–T73.

Smith, TN. 1966. The sedimentation of particles having a dispersion of sizes. *Trans. Instn. Chem. Engrs*, **44**, T152–T157.

Stamatakis, K, & Tien, Chi. 1988. Dynamics of batch sedimentation of polydispersed suspensions. *Powder technology*, **56**(2), 105–117.

Steinour, Harold H. 1944. Rate of sedimentation. Nonflocculated suspensions of uniform spheres. *Industrial & Engineering Chemistry*, **36**(7), 618–624.

Stickel, Jonathan J, & Powell, Robert L. 2005. Fluid mechanics and rheology of dense suspensions. *Annu. Rev. Fluid Mech.*, **37**, 129–149.

Tanner, R I. 2000. *Engineering rheology*. Vol. 52. Oxford University Press, USA.

Taylor, John R. 1982. An Introduction to Error Analysis: The Study of Uncertainties in Physical Measurements, 327 pp. *Univ. Sci. Books, Mill Valley, Calif.*

Thornton, Colin. 2015. *Granular Dynamics, Contact Mechanics and Particle System Simulations*. Springer.

Weiland, RH, Fessas, YP, & Ramarao, BV. 1984. On instabilities arising during sedimentation of two-component mixtures of solids. *Journal of Fluid Mechanics*, **142**, 383–389.

Wen, C.Y., & Yu, Y.H. 1966. Mechanics of Fluidization. *Chemical Engineering Progress Symposium Series.*, **62**, 100–110.

Whitmore, RL. 1955. The sedimentation of suspensions of spheres. *British Journal of Applied Physics*, **6**(7), 239.

Yeoh, Guan Heng, & Tu, Jiyuan. 2009. *Computational techniques for multiphase flows*. Elsevier.

Zienkiewicz, Olek C, Taylor, Robert L, & Nithiarasu, P. 2013. *The Finite Element Method for Fluid Dynamics, Seventh Edition*. Butterworth-Heinemann.